

5-2007

Remote Assessment of 4-D Phytoplankton Distributions off the Washington Coast

Brandon S. Sackmann

Follow this and additional works at: <http://digitalcommons.library.umaine.edu/etd>

 Part of the [Oceanography Commons](#)

Recommended Citation

Sackmann, Brandon S., "Remote Assessment of 4-D Phytoplankton Distributions off the Washington Coast" (2007). *Electronic Theses and Dissertations*. 165.

<http://digitalcommons.library.umaine.edu/etd/165>

This Open-Access Dissertation is brought to you for free and open access by DigitalCommons@UMaine. It has been accepted for inclusion in Electronic Theses and Dissertations by an authorized administrator of DigitalCommons@UMaine.

**REMOTE ASSESSMENT OF 4-D PHYTOPLANKTON DISTRIBUTIONS
OFF THE WASHINGTON COAST**

By

Brandon S. Sackmann

B.S. University of Washington, 2001

A DISSERTATION

Submitted in Partial Fulfillment of the

Requirements for the Degree of

Doctor of Philosophy

(in Oceanography)

The Graduate School

University of Maine

May, 2007

Advisory Committee:

Mary Jane Perry, Professor of Oceanography, Advisor

Andrew Thomas, Professor of Oceanography

Emmanuel Boss, Associate Professor of Oceanography

Huijie Xue, Associate Professor of Oceanography

Kate Beard-Tisdale, Professor of Spatial Information Science and Engineering

© 2007 Brandon S. Sackmann
All Rights Reserved

LIBRARY RIGHTS STATEMENT

In presenting this dissertation in partial fulfillment of the requirements for the advanced degree at The University of Maine, I agree that the Library shall make it freely available for inspection. I further agree that permission for "fair use" copying of this dissertation for scholarly purposes may be granted by the Librarian. It is understood that any copying or publication of this dissertation for financial gain shall not be allowed without my written permission.

Signature:

A handwritten signature in black ink, consisting of a large, stylized initial 'B' followed by a series of loops and a long horizontal stroke.

Date:

February 23, 2007

**REMOTE ASSESSMENT OF 4-D PHYTOPLANKTON DISTRIBUTIONS
OFF THE WASHINGTON COAST**

By Brandon S. Sackmann

Dissertation Advisor: Dr. Mary Jane Perry

An Abstract of the Dissertation Presented
In Partial Fulfillment of the Requirements for the
Degree of Doctor of Philosophy
(in Oceanography)
May, 2007

Satellite-based optical measurements were coupled with physical and optical measurements from Seaglider – a long-range autonomous glider – to study interactions between biological and physical processes off the coast of Washington, USA, and to evaluate space-time variability of regional phytoplankton and particle distributions. Using satellite ocean color data variability in near-surface chlorophyll *a* was characterized across a range of spatial and temporal scales ranging from 1 – 500 km and from days – years to assess region-wide responses by phytoplankton to changes in environmental conditions. Results from 1998 – 2002 revealed both strong negative and positive anomalies associated with lingering effects of the 1997-98 El Niño and an invasion of Subarctic water into the California Current System in 2002, respectively. Ocean color satellite data were also used to derive ‘spectral signatures’ for waters associated with the Juan de Fuca Eddy to monitor these waters as they moved southwards towards Washington beaches. Episodic southward transport of these waters may play a

role in bloom initiation of the potentially toxigenic pennate diatom *Pseudo-nitzschia* and the ability to track these waters by remote sensing could help determine when to initiate more intensive sampling for domoic acid along the Washington coast. From April 2002 – December 2005 Seaglider conducted highly resolved (~5 km horizontal spacing, ~1 m vertical resolution, ~15 d temporal resolution) surveys across the northern California Current System. A new matchup procedure minimized discrepancies between Seaglider fluorescence and satellite-derived estimates of chlorophyll *a* at the surface ($r = 0.834$) allowing observations from these disparate remote sensing platforms to be fused together to create a quasi-4-dimensional representation of the phytoplankton distribution within a persistent offshore eddy in September and October 2004. Unfortunately daytime fluorescence is quenched at all times of the year in these waters with maximum quenching exceeding 80% during summer making it difficult to compare near-surface fluorescence measurements with satellite-derived estimates of surface phytoplankton biomass. A detailed statistical characterization of mid-day fluorescence quenching in April 2002 and from August 2003 – December 2005 was conducted to constrain the magnitude and variability in mid-day quenching to better use fluorescence as an independent validation for phytoplankton biomass at the surface.

DEDICATION

This dissertation is dedicated to the two most important women in my life – my wife and my mother. Your unwavering love has been the foundation upon which all of my achievements, both personal and academic, have been built. I love you both.

ACKNOWLEDGEMENTS

My advisor, Mary Jane Perry, has been an ideal mentor and friend. She has fostered my development as a scientist and I cannot thank her enough for the support, guidance, and encouragement she has given me over the years. She has helped make these last 5 years in Maine a truly wonderful experience for myself and my family. Thank you!

I appreciate the support that I have received from all of the members, past and present, of the Perry lab (Mary Kay Talbot, Lisa Mack, Rick Reynolds, James Coleman, Remy Luerssen, Emily Kallin, Dave Kallin, Brian Thompson, Andrea Drzewianowski, and Avery Briggs). Mary Kay was the first to show me what it meant to be an ‘Oceanographer’ when she took me under her wing when I was an undergraduate working in Mary Jane’s lab at the University of Washington. She will forever be the ‘gold standard’ that I aspire to when it comes to keeping myself organized in the lab and in the field. Dave Kallin was not only a wonderful friend and lab-mate, he was also an invaluable resource and helped me troubleshoot many of the statistical analyses related to fluorescence quenching that are presented in Chapter 5.

Miles Logsdon helped me develop a solid foundation in satellite remote sensing. His wonderful sense of humor and approachable nature allowed an otherwise timid undergraduate to feel at ease. I will always be grateful.

I thank my committee (Mary Jane Perry, Andrew Thomas, Emmanuel Boss, Huijie Xue, and Kate Beard-Tisdale) for their guidance and constructive criticism throughout this project. I also thank members of NASA’s Ocean Biology Processing

Group and the University of Washington's Seaglider Group for making available much of the data used in this project. In particular, I would like to acknowledge help and support from Charlie Eriksen, Craig Lee, Neil Bogue, and Joe Martin. Funding for this project was provided by Washington State Sea Grant (NA76RG0119), NASA (NAG5-9959 and NAG5-7604), NSF (OCE 9911037), the NSF Graduate Research Fellowship Program, and the University of Maine Graduate Provost Fellowship Program.

I especially want to thank my wife, Katherine. Since moving to Maine she has given me her constant love and support, not to mention two wonderful boys Aidan and Ian. My boys have provided me with pleasant distractions and have made sure that I keep at least somewhat focused on the more important things in life (i.e., them!).

My final thanks are to our families, both Katherine's and mine. It has been much easier for us to move forward knowing that we have been supported on all sides! Thank you all...

TABLE OF CONTENTS

DEDICATION	iii
ACKNOWLEDGEMENTS	iv
LIST OF TABLES	xi
LIST OF FIGURES	xii
Chapter	
1. INTRODUCTORY MATERIALS	1
Project Description.....	4
Region of Interest.....	6
Description of Seaglider	8
2. SEASONAL AND INTER-ANNUAL VARIABILITY OF SEAWIFS-DERIVED CHLOROPHYLL A CONCENTRATIONS IN WATERS OFF THE WASHINGTON AND VANCOUVER ISLAND COASTS, 1998-2002.....	11
Background.....	12
Methods.....	16
Data Selection/Image Processing.....	16
Median Chlorophyll Maps	18
Data Density.....	19
30-day Moving Window Statistics.....	19
Integrated Primary Production Estimates	32
Upwelling Data	38

Results and Discussion	41
Regional Characteristics	41
Data Density.....	41
Inter-annual Chlorophyll Trends (6-month Medians).....	43
Seasonal Chlorophyll Trends (30-day Medians)	44
Chlorophyll Variability.....	47
Primary Production	49
Conclusions.....	51
Acknowledgements.....	54
3. OCEAN COLOR OBSERVATIONS OF A SURFACE WATER TRANSPORT EVENT: IMPLICATIONS FOR <i>PSEUDO-NITZSCHIA</i> ON THE WASHINGTON COAST	55
Introduction.....	56
Materials and Methods.....	58
Satellite Ocean Color and Sea Surface Temperature	58
Meteorological Buoys.....	64
Feature Tracking	67
Results.....	68
Satellite-derived Chlorophyll <i>a</i> Distributions.....	68
Optical Characterization of Water Masses	70
Sea Surface Temperature Distributions	72
Meteorological Observations	73
Feature Tracking.....	74

	Discussion.....	74
	Conclusions.....	81
	Acknowledgements.....	83
4.	MULTI-PLATFORM DATA FUSION: MERGING IN-WATER SEAGLIDER OPTICS AND SATELLITE OCEAN COLOR TO OBSERVE QUASI-4-DIMENSIONAL PHYTOPLANKTON DISTRIBUTIONS OFF THE WASHINGTON COAST	84
	Introduction.....	85
	Data and Methods	88
	Satellite Data Products.....	88
	Sea Level and Geostrophic Velocity Anomalies	88
	Sea Surface Temperature and Ocean Color	89
	Seaglider Data.....	92
	Vehicle Characteristics, Deployment History, and Instrumentation	92
	Optical Data Processing.....	95
	Data Fusion Techniques.....	96
	Regional Temperature/Nitrate/SLA Relationships	103
	Quasi-4-dimensional Visualization.....	103
	Results and Discussion	106
	Surface Satellite Observations of the Eddy	106
	Near-surface Satellite/Seaglider Matchups.....	107
	Seaglider Sections Through the Eddy.....	109
	Fused Satellite/Seaglider Data Products	112

	Summary and Conclusions	115
	Acknowledgements.....	116
5.	USING SEAGLIDER TO QUANTIFY VARIABILITY IN SURFACE MID-DAY FLUORESCENCE QUENCHING	117
	Introduction.....	118
	Data and Methods	120
	Description of Seaglider Deployments	120
	Optical Data Processing.....	123
	Instantaneous Surface PAR from SeaWiFS.....	126
	Quantifying Mid-day Fluorescence Quenching.....	129
	Manual Method.....	129
	Statistical Method	132
	Results and Discussion	141
	Manifestation of Quenching in Seaglider Fluorescence Measurements (April 2002)	141
	‘Correcting’ Fluorescence Profiles for the Effects of Quenching	143
	Seasonal and Inter-annual Patterns of Fluorescence Quenching (August 2003 – December 2005).....	147
	Summary and Conclusions	149
	Acknowledgements.....	151
6.	SUMMARY AND CONCLUSIONS	152
	REFERENCES	155

APPENDICES	173
Appendix A. Maps of monthly and six-month median (50 th percentile) chlorophyll <i>a</i> concentrations with corresponding estimates of data density	174
Appendix B. Statistical Model of Fluorescence Quenching	195
BIOGRAPHY OF THE AUTHOR.....	203

LIST OF TABLES

Table 2.1	Average number of observations per pixel	24
Table 2.2	Median chlorophyll <i>a</i> concentrations.....	31
Table 2.3	Skewness test statistic calculated on log-transformed chlorophyll distributions.....	35
Table 2.4	Median rates of integrated water column production	37
Table 2.5	Correlations between daily shelf chlorophyll and upwelling events	40
Table 3.1	Water mass summary statistics	66

LIST OF FIGURES

Figure 1.1	Schematic of Seaglider’s standard mode of operation.....	9
Figure 1.2	Standard V-shaped Seaglider transect off the Washington coast	10
Figure 2.1	Map of the continental margin off the Washington and Vancouver Island coasts	17
Figure 2.2	Six-month median chlorophyll <i>a</i> concentrations for 1998 and 2002.....	20
Figure 2.3	Maps of median chlorophyll <i>a</i> concentrations and data density for June 2000 and May 2001	22
Figure 2.4	Median shelf chlorophyll <i>a</i> concentrations and daily upwelling indices	27
Figure 2.5	Median slope and oceanic chlorophyll <i>a</i> concentrations	29
Figure 2.6	IQR/Median ratios	33
Figure 2.7	Daily chlorophyll image from Day 251 in 2001	50
Figure 3.1	Map of coastal waters of Washington, USA, and Vancouver Island, Canada.....	59
Figure 3.2	SeaWiFS chlorophyll and sea surface temperature images	61
Figure 3.3	RGB false color composite of SeaWiFS remote sensing reflectance	63
Figure 3.4	Wind speed and direction between 1 May–15 June 1999.....	65
Figure 3.5	Feature tracking	69
Figure 3.6	Schematic of transport event observed in May 1999.....	78
Figure 4.1	Eriksen Seaglider	86
Figure 4.2	Map of Washington coast showing locations of Seaglider/satellite matchups	87
Figure 4.3	Sea level and geostrophic velocity anomalies	90

Figure 4.4	Sea surface temperature and ocean color from 27 September 2003 and 1 October 2004.....	91
Figure 4.5	Satellite-derived chlorophyll estimates compared with Seaglider fluorescence	93
Figure 4.6	Satellite-derived estimates of water leaving radiance at 555 nm compared with Seaglider near-infrared backscatter by particles	94
Figure 4.7	Seaglider/satellite matchups.....	99
Figure 4.8	Depth resolved fluorescence and dissolved oxygen from Seaglider	101
Figure 4.9	Depth resolved near-infrared backscatter by particles and the fluorescence-to-backscatter ratio from Seaglider	102
Figure 4.10	Historical temperature versus nitrate relationship	104
Figure 4.11	Sea level anomaly versus 10° C isotherm depth from 22 August – 31 October of 2003 and 2004.....	105
Figure 4.12	Fused Seaglider/SeaWiFS data product.....	114
Figure 5.1	Map of Washington coast.	122
Figure 5.2	Seaglider fluorescence and backscatter by particles.....	125
Figure 5.3	Near-surface fluorescence and satellite-derived estimates of iPAR.....	128
Figure 5.4	Scatterplots of fluorescence versus backscatter by particles	130
Figure 5.5	Correcting for the bias due to mid-day fluorescence quenching	131
Figure 5.6	Near-surface fluorescence from Seaglider compared with satellite-derived estimates of chlorophyll <i>a</i>	133
Figure 5.7	Near-surface fluorescence from August 2003 – December 2005.....	135
Figure 5.8	Histograms of $1-F_D:F_N$ and $1-b_{bp}(700)_D/b_{bp}(700)_N$ from Seaglider	136
Figure 5.9	Estimates of $1-F_D:F_N$ and iPAR	137
Figure 5.10	Summer and winter values of $1-F_D:F_N$	138
Figure 5.11	Scatterplots of $1-F_D:F_N$ versus iPAR	140

Figure 5.12	Comparison of methods for assessing mid-day fluorescence quenching.....	142
Figure A.1	Maps of monthly and six-month median (50 th percentile) chlorophyll <i>a</i> concentrations for April – September of 1998 – 2002 (panels 1-70, odd) with corresponding estimates of data density (panels 1-70, even)	174
Figure B.1	Model estimates of $1-F_D:F_N$	198
Figure B.2	Modeled versus observed estimates of $1-F_D:F_N$	199
Figure B.3	Model estimates of $1-F_D:F_N$ for a hypothetical 12-hr day	202

Chapter 1

INTRODUCTORY MATERIALS

Phenomena in the ocean are manifested in a turbulent 4-dimensional spatio-temporal domain (i.e., x, y, depth, and time). The ability to integrate, manage, and analyze large spatially and temporally referenced datasets is of great interest to the oceanographic community. For nearly thirty years ocean color satellites have provided routine estimates of phytoplankton biomass at the surface, albeit with a long break between the Coastal Zone Color Scanner and the Sea-viewing Wide Field-of-view Sensor (SeaWiFS). The ability of satellites to make synoptic measurements in the horizontal dimensions (i.e., x and y) revolutionized our understanding of biological variability in the ocean and in this study satellite ocean color data were used to characterize variability in near-surface chlorophyll *a* across a range of spatial and temporal scales ranging from 1 – 500 km and from days – years in waters off the Washington coast.

Seasonal and inter-annual variability in SeaWiFS-derived estimates of near-surface chlorophyll *a* and primary production were examined in three regimes (i.e. shelf, slope and deep oceanic waters) off Washington and Vancouver Island from 1998 – 2002. Shelf concentrations varied from 2 to 10 mg m⁻³ and were generally lower in April and May and maximal in September. Chlorophyll *a* on the slope followed a similar seasonal pattern (ranging from 0.5 to 4 mg m⁻³); however, concentrations were always greater on the Vancouver Island slope compared to the Washington slope for any 30-day period. In oceanic waters chlorophyll concentrations were usually less than 1 mg m⁻³ and averaged approximately 0.3 mg m⁻³. One consequence of the 1997-98 El Niño appeared to be a

reduction in chlorophyll concentration, and inferred rates of primary productivity, in slope and oceanic waters off Vancouver Island in 1998 which may have limited offshore carbon transport and sequestration in this region. In contrast, six-month median chlorophyll concentrations were maximal in 2002 for all subregions off Vancouver Island and for shelf and slope regions off Washington; likely due to increased advection of nutrient-rich Subarctic waters into the California Current System that may have led to a widespread increase in phytoplankton production. A more complete understanding of these kinds of dramatic variations are critical to our understanding of carbon cycling in this dynamic upwelling regime and such analyses would be difficult, if not impossible, to perform without satellite data.

Ocean color measurements from SeaWiFS were also used to define ‘spectral signatures’ to track and monitor water masses off the Washington coast. It has been suggested that episodic southward transport of surface waters from the Juan de Fuca Eddy may play a role in bloom initiation of the potentially toxigenic pennate diatom *Pseudo-nitzschia* along the Washington coast under certain circumstances. Using an eight-day time series of ocean color images from May 1999 it was determined that waters from the Juan de Fuca Eddy can indeed move southward into Washington coastal waters. In this case surface velocities ranged from 8–16 km d⁻¹. In the future the ability to track surface waters from the Juan de Fuca Eddy by remote sensing could be used to help determine when to initiate more intensive sampling for domoic acid along the Washington coast.

In recent years the notion of what constitutes an oceanographic remote sensing platform has grown to include not only satellites, but also a number of autonomous and

Lagrangian platforms and sensors (ALPS). Many of these new platforms have been outfitted with optical sensors and are capable of making highly resolved measurements in the vertical (z) dimension over long distances and/or time spans (e.g., gliders, auvs, drifters, etc.). From April 2002 – present Seaglider – a long-range autonomous glider – has been conducting repeat surveys off the Washington coast along a V-shaped transect that extends 200 km from the continental shelf break, into deep oceanic waters. Highly resolved (~5 km horizontal spacing, ~1 m vertical resolution, ~15 d temporal resolution) sections across the northern California Current System provide measurements of temperature, salinity and dissolved oxygen to 1000 m, and chlorophyll *a* fluorescence (a proxy for phytoplankton concentration) and optical backscattering (a proxy for particle concentration) to 150 m. By combining satellite imagery with subsurface Seaglider observations we can now effectively monitor changes in the distribution of phytoplankton throughout the water column. To illustrate this ability a quasi-4-dimensional representation of the phytoplankton distribution was created for September and October 2004 which coincided with the occurrence of persistent offshore eddy. The application of a new matchup procedure successfully minimized discrepancies between Seaglider fluorescence and SeaWiFS chlorophyll *a* estimates at the surface ($r = 0.834$) and allowed us to fuse observations from these disparate remote sensing platforms. With this new data product it was possible to assess the vertical distribution of phytoplankton biomass in and around the eddy and compare it with conditions from the previous year.

Mid-day quenching of Seaglider fluorescence makes it difficult to quantitatively compare near-surface fluorescence measurements with satellite-derived estimates of surface phytoplankton biomass. Fluorescence during the daytime is quenched at all times

of the year in these waters with maximum quenching exceeding 80% during summer. To avoid the bias due to mid-day fluorescence quenching one must either relate nighttime fluorescence measurements to daytime satellite measurements or be able to constrain (i.e., model) the magnitude and variability in mid-day quenching to use fluorescence as an independent validation for phytoplankton biomass at the surface. While each dataset (i.e., satellite ocean color/Seaglider optics) is useful in its own right the union of these technologies provide a more thorough understanding of how oceanographic processes affect phytoplankton distributions in the ocean.

Project Description

To quantify 4-D phytoplankton distributions in waters off the Washington coast, USA, my dissertation research project integrates satellite observations with data collected with an autonomous underwater glider from April 2002 – present. Satellite products that were used include:

- 1) *ocean color* measurements from the Sea-viewing Wide Field-of-view Sensor (SeaWiFS) and the MODerate-resolution Imaging Spectroradiometer (MODIS Aqua);
- 2) *sea surface temperature* measurements from the Advanced Very High Resolution Radiometer (AVHRR) and MODIS Aqua; and
- 3) *sea surface height anomalies* from the radar altimeter onboard the Jason-1 satellite.

Despite success in resolving some of the patterns of variability, large uncertainties in satellite-based assessments of phytoplankton biomass remain. In particular, synoptic

remotely sensed measurements of ocean color are difficult to obtain in these waters due to a persistence of cloud cover for much of the year. Surface and subsurface observations made with Seaglider, an autonomous underwater glider developed by Dr. C. Eriksen at the University of Washington, provide high spatial and temporal resolution measurements of various physical and optical parameters. These *in-situ* measurements improve our ability to accurately interpret satellite ocean color measurements and allow us to extend our interpretation of these measurements beyond the sea surface. Optical measurements made by Seaglider include chlorophyll fluorescence, a proxy for phytoplankton biomass, and two wavelengths of backscatter, proxies for particle concentration. The results of my research contribute to a greater understanding of the regional oceanography off the Washington coast by:

- 1) describing spatial and temporal scales of variability of phytoplankton biomass and integrated water column production using SeaWiFS data from 1998 – 2002 in waters off the Washington coast (Sackmann *et al.*, 2004; Chapter 2);
- 2) comparing optical characteristics of water masses throughout the region to track water from the Juan de Fuca Eddy which may supply an inoculum of the harmful algae species *Pseudo-nitzschia* to Washington coastal waters under certain circumstances (Sackmann and Perry, 2006; Chapter 3);
- 3) using satellite ocean color and in-water optical measurements from Seaglider to assess changes in total water-column phytoplankton biomass along a repeated transect off the Washington coast (Chapter 4);

- 4) providing a basis for inferring subsurface distributions of optically active materials from surface satellite data (e.g., ocean color, sea surface temperature and sea level anomalies; Chapter 4); and
- 5) characterizing the bias due to mid-day fluorescence quenching to correct *in-situ* estimates of phytoplankton biomass which could be used as ground truth to aid the interpretation of ocean color measurements (Chapter 5).

Region of Interest

Continental margins are of great importance in global carbon and nitrogen biogeochemical cycles (Walsh, 1991). My region of interest is the continental shelf, slope and deep oceanic waters off the northwest coast of the U.S.A. Ocean color measurements have documented large inter-annual differences in the phytoplankton pigment concentrations and the timing of blooms at the surface, presumably in response to variability in environmental forcing (McGowan *et al.*, 1998; Thomas and Strub, 2001; Thomas *et al.*, 2003; Sackmann *et al.*, 2004). This variability could alter the ways in which the ecosystem processes organic carbon and may affect recruitment success, or failure, for certain economically-important fisheries. The presence of harmful algal species in the area is also problematic. Recent blooms of the potentially toxigenic pennate diatom *Pseudo-nitzschia* have resulted in elevated concentrations of domoic acid (DA) in razor clams and closure of clam beds along the Washington coast leading to significant economic losses to shellfish industries (Trainer *et al.*, 2002; Wekell *et al.*, 2002). It is likely that episodic southward transport of surface waters from the Juan de Fuca Eddy may play a role in harmful bloom initiation along the Washington coast under

certain circumstances (MacFadyen *et al.*, 2005; Sackmann and Perry, 2006). Taken together these results suggest that sustained monitoring of these waters is warranted. It is imperative that we develop a more complete understanding of how various physical, chemical, and biological processes can affect local phytoplankton distributions.

The dominant mechanism facilitating nutrient supply to the euphotic zone is seasonally intense wind-driven upwelling. However, episodic wind mixing events, localized topographically-mediated upwelling, and nutrient enriched outflow from the Strait of Juan de Fuca and Columbia River can also be important. Once nutrients are incorporated into surface waters, variable cloud cover and a mid-latitude cycle of solar insolation determine the degree to which conditions are suitable for phytoplankton growth (Perry *et al.*, 1989; Hickey and Banas, 2003).

The large-scale wind driven circulation pattern in the region is modulated by changes in the strength of the Aleutian Low pressure system. The circulation includes the North Pacific Current that bifurcates into the southward flowing California Current System and the northward flowing system that joins the Alaskan Gyre. The strength of the North Pacific Current and the exact location of the bifurcation are variable and changes in its position may determine how much surface water is delivered to the region from the Pacific basin. This variable water supply is likely to influence the horizontal and vertical structure of various physical, chemical and biological parameters and ecosystem-level responses to such perturbations are to be expected (Landry *et al.*, 1989).

Description of Seaglider

Seaglider is an autonomous underwater glider developed by Dr. C. Eriksen (University of Washington) and colleagues (Eriksen *et al.*, 2001). My advisor, Dr. M. J. Perry, collaborated with Dr. Eriksen in the National Ocean Partners Program (NOPP) Seaglider project to miniaturize optical sensors. Seaglider is equipped with wings that provide lift, and moves through the water in a sawtooth pattern by adjusting its buoyancy (Fig. 1.1). The maximum horizontal range is currently 5,500 km at 25 cm s⁻¹ horizontal speed and it is capable of diving 900 times to 1000 m depth over a 7 month period in weakly stratified portions of the ocean. To date, Seaglider has completed 13 deployments off the Washington coast.

Seaglider samples along a 'standard' V-shaped transect off the Washington coast (Fig. 1.2) and measures physical parameters (i.e. conductivity, temperature, and pressure) as well as dissolved oxygen concentrations, chlorophyll fluorescence, and two wavelengths of backscatter (blue and near-infrared). Measures of backscatter and fluorescence are obtained from a single miniaturized sensor, the ECO-BB2F, which was developed by WET Labs specifically for Seaglider. Seaglider is completely autonomous and uses Iridium satellite telephone communication to download data at the end of each dive cycle and to receive new mission instructions when necessary (Eriksen *et al.*, 2001).

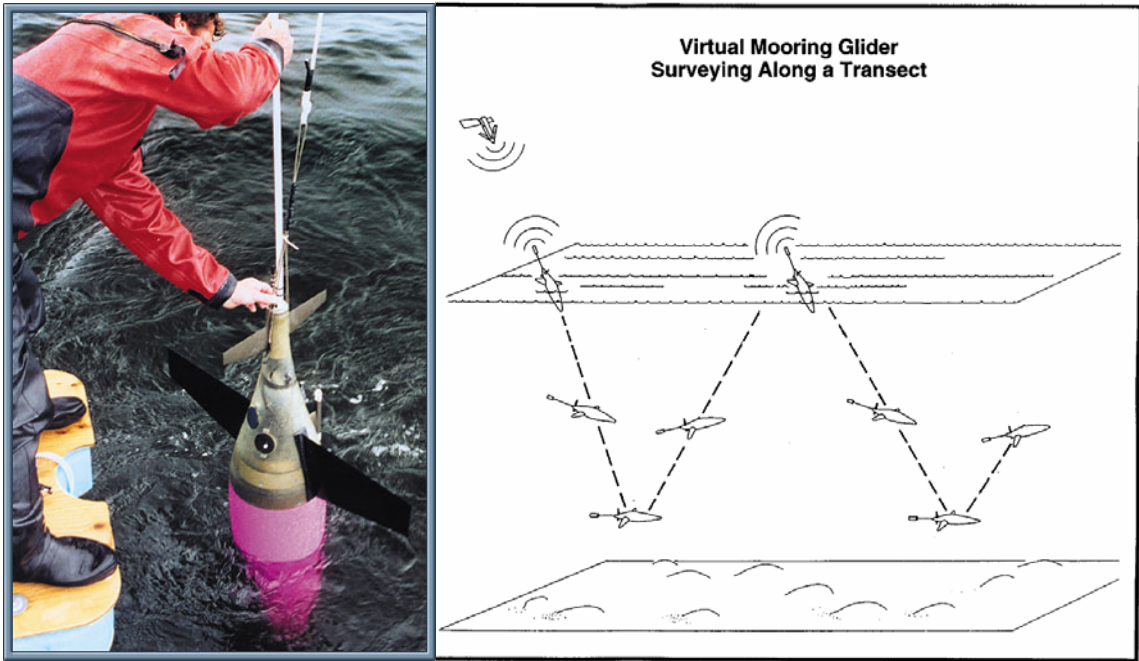


Figure 1.1 Schematic of Seaglider's standard mode of operation.



Figure 1.2 **Standard V-shaped Seaglider transect off the Washington coast.**

Chapter 2

SEASONAL AND INTER-ANNUAL VARIABILITY OF SEAWIFS-DERIVED CHLOROPHYLL A CONCENTRATIONS IN WATERS OFF THE WASHINGTON AND VANCOUVER ISLAND COASTS, 1998-2002

Seasonal and inter-annual variability in satellite-derived estimates of near-surface chlorophyll *a* concentration and primary production were examined in three regimes (i.e. shelf, slope and deep oceanic waters) off Washington and Vancouver Island from 1998-2002. Wind-induced upwelling predominates in late spring and summer, coinciding with the maximum in solar radiation, leading to increased accumulations of phytoplankton biomass. Shelf chlorophyll concentrations varied from 2 to 10 mg m⁻³ and were generally lower in April and May and maximal in September. Chlorophyll concentrations on the slope followed a similar seasonal pattern (ranging from 0.5 to 4 mg m⁻³); however, concentrations were always greater on the Vancouver Island slope compared to the Washington slope for any 30-day period. Oceanic chlorophyll concentrations were generally less than 1 mg m⁻³ and averaged approximately 0.3 mg m⁻³. The Pacific Northwest is often cloud covered; data density maps provide an index of confidence in the 'regional' applicability of the summary statistics. One consequence of the 1997-98 El Niño appears to be a reduction in chlorophyll concentration, and inferred rates of primary productivity, in slope and oceanic waters off Vancouver Island in 1998. An increased frequency in El Niño events may lead to a reduction in offshore carbon transport and sequestration and these results help develop an understanding of the variability in carbon cycling in a dynamic upwelling region. Six-month median chlorophyll concentrations were maximal in 2002 for all subregions off

Vancouver Island and for shelf and slope regions off Washington. The dramatic increases in chlorophyll concentrations seen in 2002 are consistent with hypothesized increased advection of nutrient-rich Subarctic waters into the California Current.

Background

North Pacific waters off the U.S. and Canada's west coast are characterized by high rates of primary production, fueled by upwelling of nutrient-rich water, that support economically important fisheries. Over the last four decades, a number of field programs have explored phytoplankton distributions and rates of primary production in waters overlying the continental margins off the Washington and Vancouver Island coasts (Anderson, 1964; Perry *et al.*, 1989; Boyd and Harrison, 1999). The Sea-viewing Wide Field-of-view Sensor (SeaWiFS), launched in late 1997, provides a way to augment the existing body of knowledge on this region, particularly during periods without field campaigns, as well as to explore seasonal and inter-annual variability in the distribution of surface chlorophyll in greater spatial and temporal detail. Because satellite ocean color measurements can also provide estimates of local rates of primary production (Perry *et al.*, 1989), these remotely-sensed measurements are critical to our understanding of carbon cycling in this dynamic upwelling regime.

Northerly winds begin to dominate the coastal wind field in late spring and persist through the summer, leading to the seasonally intense offshore Ekman transport and coastal upwelling that is common to the west coast of the United States (Smith, 1995). The upwelling of nutrient rich water into the euphotic zone provides the fuel that drives the intense biological production that is observed. Upwelling-favorable winds, variations

in local cloud cover combined with a mid-latitude cycle of solar insolation, and interannual patterns in annual precipitation and subsequent river discharge are a few of the physical processes that work in concert to affect the observed distributions of *in situ* properties (e.g. surface chlorophyll *a* concentrations) in the region (Landry *et al.*, 1989). This complex assortment of processes is superimposed on the large-scale circulation pattern that includes the North Pacific Current or West Wind Drift that bifurcates into the southward flowing California current system and the northward flowing system that joins the Alaskan Gyre. The California current system, which flows equatorward along the eastern edge of the North Pacific (Hickey, 1979), has a well documented network of filaments, meanders, eddies, and jets (Strub *et al.*, 1991) that provide one mechanism for off-shore transport of surface chlorophyll in this region (Ikeda and Emery, 1984; Fang and Hsieh, 1993; Mackas and Yelland, 1999). Buoyancy driven flux from the Strait of Juan de Fuca maybe another (Hickey *et al.*, 1991).

The development and maintenance of an archive of 1-km SeaWiFS imagery has allowed systematic and sustained monitoring of these waters at spatial and temporal resolutions unattainable by traditional field-based sampling programs. Data mining and real time monitoring may prove to be useful tools for important resource management issues. For example, it has been suggested that harmful algal blooms (e.g. *Pseudo-nitzschia* spp.) along the Washington coast may be correlated with a sustained high phytoplankton biomass patch at the mouth of the Strait of Juan de Fuca (Adams *et al.*, 2000; Horner *et al.*, 2000). Tracking the trajectories of such patches maybe useful to initiate intensified conditional sampling for domoic acid outbreaks in the region. Because phytoplankton form the bases of many aquatic food webs, variations in the

spatial and temporal distribution of phytoplankton biomass (as inferred from satellite-derived estimates of surface chlorophyll *a*) are of significant economic importance, as they affect energy transfer to higher trophic levels, including zooplankton and commercially important fish (McFarlane *et al.*, 1997; Bottom *et al.*, 1998). Juvenile salmon are free-swimming when they enter the ocean. Survival conditions near the point of ocean entry likely depend on local upwelling conditions and food availability, in terms of zooplankton stocks (Fisher and Percy, 1988). In May and June, after juvenile salmon have entered the ocean the precise timing of individual phytoplankton bloom events may be crucial in determining whether these young fish survive and the magnitude of the returning fishery yield in subsequent years (Percy, 1992).

The primary goal of this study was to determine multi-year biological variability in the coastal waters off Washington State, USA, and Vancouver Island, Canada, from 1998 to 2002. A secondary goal was to determine if there was a phytoplankton biomass response in the year following the intense El Niño of 1997-98. Along the west coast of North America after a strong El Niño event, an anomalously warm surface layer leads to a deepening of the pycnocline and significantly impedes vertical transport of nutrient rich waters to the surface (Huyer and Smith, 1985; Rienecker and Mooers, 1986; Lynn *et al.*, 1995; Kahru and Mitchell, 2000). Reduced phytoplankton biomass was observed in oceanic waters in 1998. The confinement of high biomass to shallower regions of the continental margin, if this is a typical consequence of El Niño events, suggests a reduction in carbon transport offshore and to the deep ocean.

In contrast to the low chlorophyll concentrations observed in 1998, 6-month median chlorophyll concentrations were maximal in 2002 for all subregions off

Vancouver Island and for shelf and slope regions off Washington. Observations of an anomalously cool, fresh, and potentially nutrient-rich subsurface layer off Vancouver Island, approximately 100 m thick, combined with dramatic increases in chlorophyll concentrations in this region are consistent with a hypothesized invasion of nutrient-rich Subarctic water into the California Current (Freeland *et al.*, 2003; Thomas *et al.*, 2003). The biological response to this invasion of Subarctic water does not appear to be limited to waters off Washington and Vancouver Island, as similar positive chlorophyll anomalies were documented by Thomas *et al.* (2003) for much of the California Current system and a 2-3 fold increase in primary production and a 2-5 fold increase in chlorophyll fluorescence (over similar measurements made in summer 2001 and 2000) were observed in 2002 off Oregon (Wheeler *et al.*, 2003).

It is difficult to develop summary statistics that are meaningful over large spatio-temporal domains, yet we often try to develop a single number to represent a given region and/or a given period of time. One important issue that is sometimes neglected in dealing with large, remotely-sensed datasets relates to how the observations are distributed in space and time and the problems that can arise if the observations are not evenly distributed. Data densities are presented throughout this work to clearly identify when these spatial and temporal biases may be affecting our summary statistics. We urge the reader to consult these data densities (the complete set of monthly data densities are given in Appendix A) in conjunction with the various summary statistics and, more importantly, the inferences that we draw from them.

Methods

Data Selection/Image Processing

The study region off the U.S. west coast extends from 46°N to 50°N and seaward from the coast to 128°W. Locations within coastal estuaries and the Strait of Juan de Fuca were excluded from the analysis. Three subregions, corresponding to the continental shelf, slope and deep-ocean, were determined objectively based upon a gradient analysis of local bathymetry. The 250-m and 2200-m isobaths represent the division between the continental shelf/slope and slope/oceanic waters, respectively. The bathymetrically delineated subregions were further divided to separate waters off the Washington and Vancouver Island coasts (Fig. 2.1).

Daily images (n = 389) of chlorophyll *a* concentration were processed from Level 1a local-area-coverage (LAC) SeaWiFS data, obtained at full 1.1-km² nadir resolution, for spring, summer, and early autumn (April-September) of 1998-2002. The remaining 6 months of data from each year were not included in the dataset due to increased atmospheric effects during these periods of low seasonal sun angle (thought to degrade the accuracy of derived chlorophyll *a* estimates) and a predominance of cloud cover over the region of interest. Data were collected by the Monterey Bay Aquarium Research Institute, the Institute of Ocean Sciences in Sydney, British Columbia, Canada and the University of California at Santa Barbara and distributed by NASA's GSFC Earth Science Distributed Active Archive Center (DAAC). Thumbnail images with 8.8 km resolution were examined to determine if the center of the study region was within +/- 45° (+/- 700 km) of nadir and whether at least 15% (approximately) of the study region

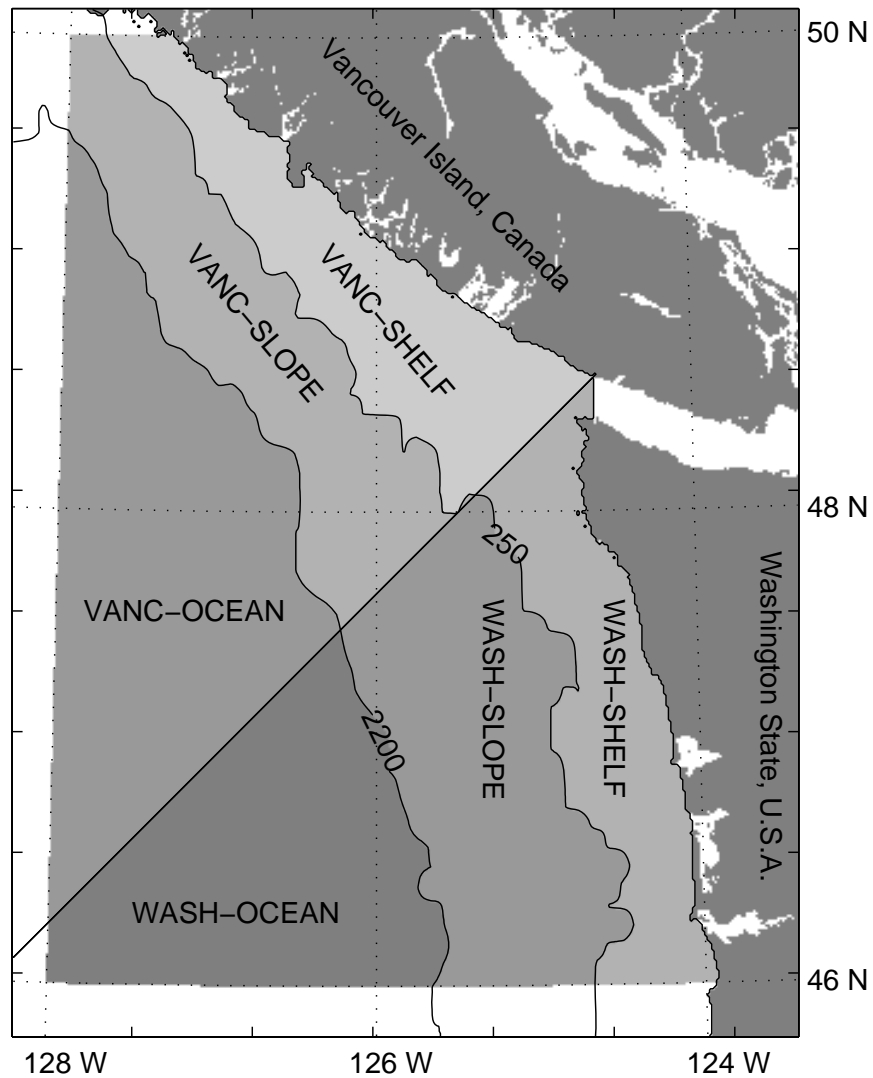


Figure 2.1 **Map of the continental margin off the Washington and Vancouver Island coasts.** The 250-m and 2200-m isobaths represent the division between the continental shelf/slope and slope/oceanic waters, respectively. These subregions were further divided to separate waters off the Washington (WASH) and Vancouver Island (VANC) coasts.

was cloud and/or haze free. Daily images meeting both selection criteria were obtained from the DAAC and included in the dataset. Images coincident with the major dust event in April of 2001 (Naval Research Laboratory, 2001) were not used, as the dust plume was visible over the region of interest and the chlorophyll retrievals were thought to be suspect.

Standard Level 2 products, consistent with the fourth SeaWiFS data reprocessing, were computed using the default parameter values implemented in SeaDAS v. 4.3p3. The Level 2 'chlor_a' (chlorophyll *a* concentration in mg m^{-3}) product was mapped to a standard isotropic transverse mercator projection with an average pixel size of 1.1 km^2 . Daily mapped images of the Level 2 'chlor_a' product were imported into Matlab v. 6.5 (The MathWorks Company) for additional statistical exploration. Anomalous chlorophyll *a* retrievals were often observed adjacent to cloud and land edges. To mediate the impact of these retrievals on subsequent statistical analysis, masked areas (i.e. clouds/land) were uniformly dilated by one pixel in all directions. The effluent from the Columbia River during the spring and summer was primarily directed southward and out of the region of interest, thereby reducing the impact of suspended sediment on chlorophyll retrievals in the shelf and slope regions off the southern Washington coast.

Median Chlorophyll Maps

Maps of monthly and 6-month median (50th percentile) chlorophyll *a* concentrations (Figs. 2.2-2.3; Appendix A) were constructed to explore the spatial distribution of biomass across the region of interest. The median was calculated for each pixel from all observations available for the given time period. To facilitate data

summary, ‘high’, ‘intermediate’, and ‘low’ chlorophyll *a* concentrations have been defined as $> 2.0 \text{ mg m}^{-3}$, $0.5 - 2.0 \text{ mg m}^{-3}$, and $< 0.5 \text{ mg m}^{-3}$, respectively. These concentrations are indicated as vertical lines on the color bar in Figure 2.2.

Data Density

Maps of monthly data density were generated to illustrate the spatial distribution of observations on a pixel-by-pixel basis (Fig. 2.3; Appendix A). Table 2.1 presents the average number of observations per pixel after observations were pooled over a given region for a 30-day temporal window that matched traditional calendar months (see below). All spatial information is lost in the tabular representation; however, it provides a condensed summary of the number of observations used to calculate the various descriptive statistics and it quantitatively describes the temporal distribution of the data. This additional piece of information may indicate time periods where insufficient data are available to adequately calculate representative summary statistics.

30-day Moving Window Statistics

Quantile-based statistics were used exclusively to describe the location and dispersion characteristics of chlorophyll *a* distributions and observations were pooled over discrete space/time domains (e.g. Region 1/Month 1, Region 1/Month 2, etc.).

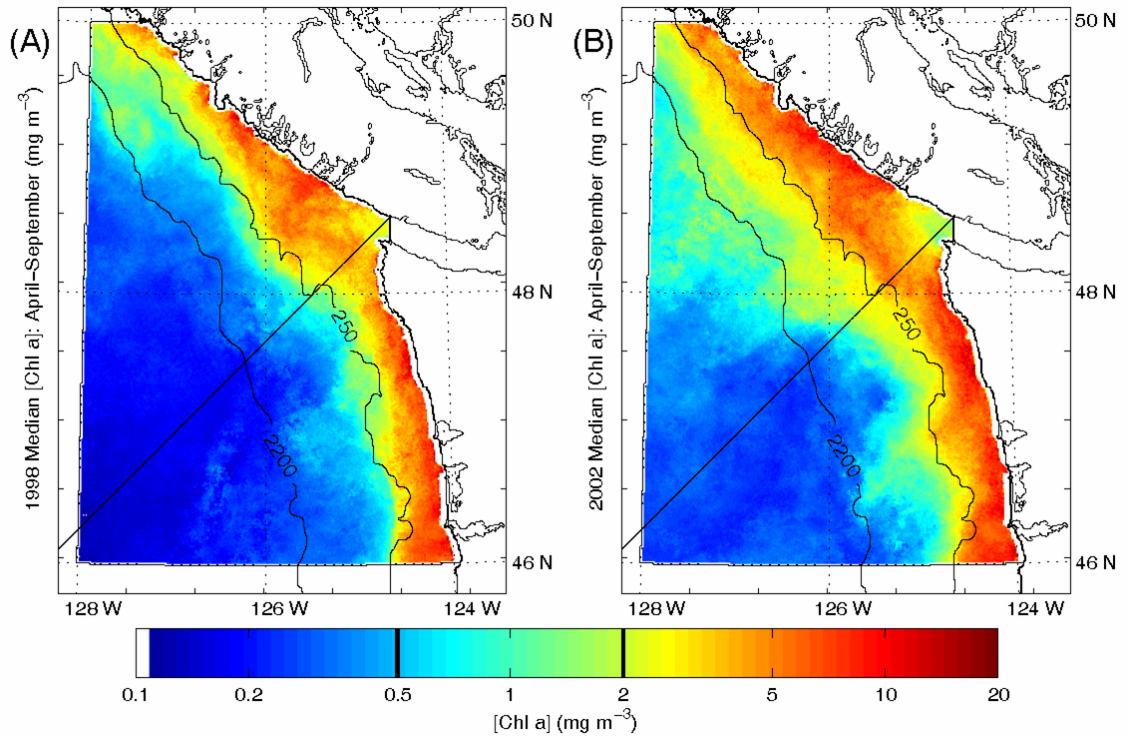


Figure 2.2 **Six-month median chlorophyll *a* concentrations for 1998 and 2002.** Maps of median chlorophyll *a* concentrations for April-September of 1998 (A) and 2002 (B). The median was calculated for each pixel from all observations available for the given 6-month period and ‘high’, ‘intermediate’, and ‘low’ chlorophyll *a* concentrations are defined as $> 2.0 \text{ mg m}^{-3}$, $0.5 - 2.0 \text{ mg m}^{-3}$, and $< 0.5 \text{ mg m}^{-3}$, respectively. Additional maps of median chlorophyll are provided in Appendix A.

Figure 2.3 **Maps of median chlorophyll *a* concentrations and data density for June 2000 and May 2001.** Representative maps of median chlorophyll *a* concentrations for June 2000 (A) and May 2001 (C), with corresponding maps of data density (B, D). Data densities reflect the number of valid chlorophyll *a* retrievals for each pixel for the given month. Additional maps of median chlorophyll and data density are provided in Appendix A.

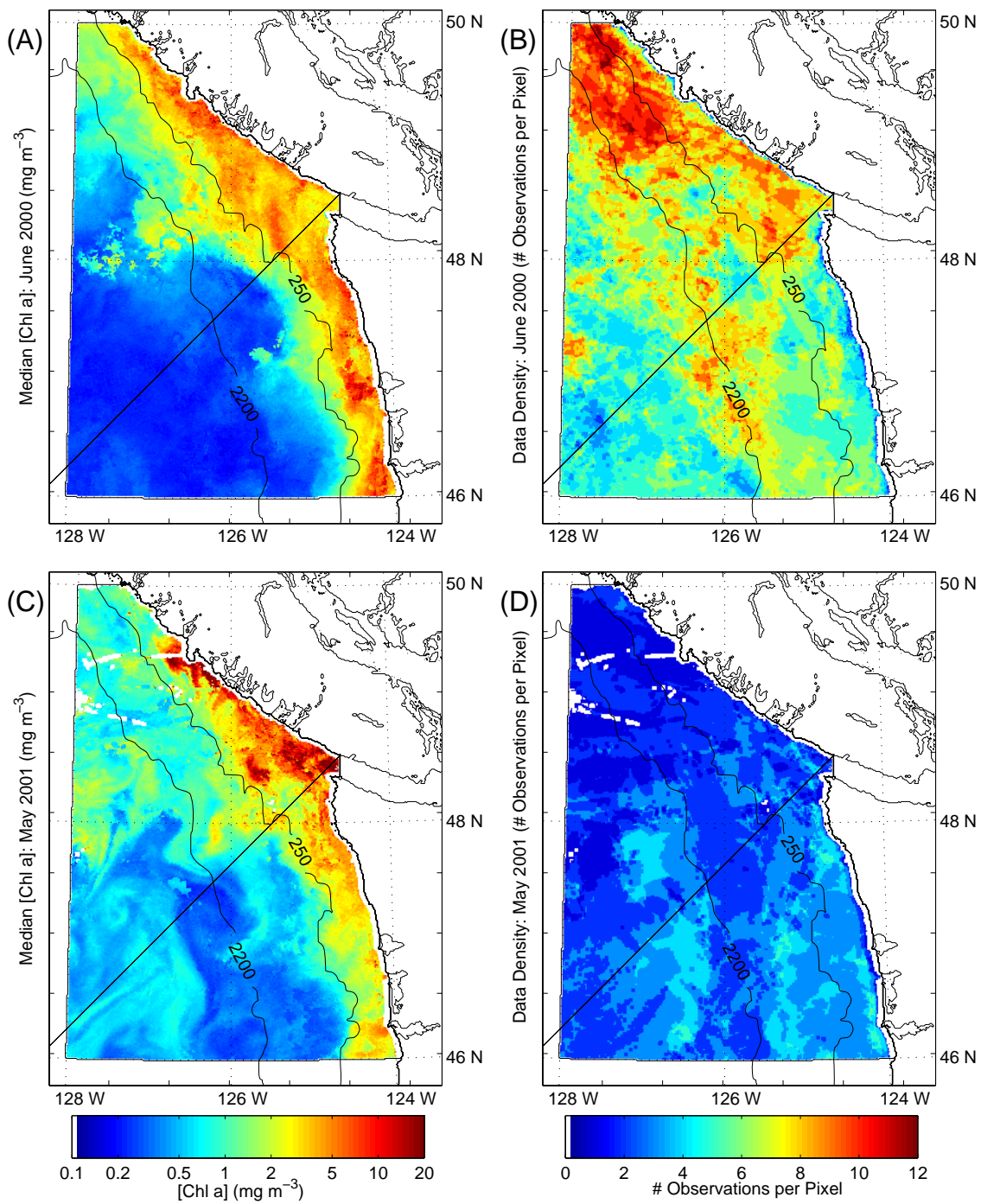


Table 2.1 **Average number of observations per pixel.** Values for the average number of observations per pixel corresponding to traditional calendar months (30-day temporal windows) for each of the six subregions. Five-year monthly averages and 6-month annual averages are also provided. The number in parenthesis associated with each month is the year-day upon which the 30-day temporal window was centered. The number in parenthesis associated with each subregion is the areal extent of the subregion in number of pixels.

		April (105)	May (135)	June (166)	July (196)	August (227)	September (258)	6-Month	
<i>Washington Coast</i>	Shelf (9160)	1998	2.31	2.43	2.09	0.69	4.10	6.80	3.12
		1999	4.14	2.69	2.00	3.51	2.98	8.02	3.89
		2000	2.69	1.86	4.74	4.86	4.11	5.18	3.93
		2001	3.18	2.65	2.30	2.67	2.46	4.59	2.99
		2002	2.50	2.28	2.20	5.32	3.83	6.14	3.88
		5-Yr	2.96	2.38	2.67	3.41	3.49	6.15	3.56
	Slope (13793)	1998	1.96	2.71	1.52	1.31	2.86	6.79	2.86
		1999	4.51	2.44	1.37	3.27	2.17	7.63	3.57
		2000	3.01	2.80	6.30	3.84	3.59	6.14	4.29
		2001	3.06	2.89	1.97	2.30	3.26	4.72	3.03
		2002	1.89	1.37	3.01	5.64	3.66	6.88	3.90
		5-Yr	2.88	2.44	2.83	3.27	3.11	6.43	3.53
	Oceanic (14722)	1998	1.28	1.99	0.54	1.21	2.45	4.03	1.93
		1999	4.07	2.31	0.86	1.74	1.13	5.63	2.62
		2000	3.18	2.46	5.25	1.98	2.05	4.72	3.28
2001		2.71	2.76	1.42	0.83	3.30	2.64	2.28	
2002		1.63	0.98	2.76	4.54	3.91	6.00	3.36	
5-Yr		2.57	2.10	2.17	2.06	2.57	4.60	2.69	

		April (105)	May (135)	June (166)	July (196)	August (227)	September (258)	6-Month	
<i>Vancouver Island Coast</i>	Shelf (9942)	1998	3.01	4.54	3.39	4.23	5.19	5.44	4.49
		1999	4.78	4.17	1.95	5.39	3.27	8.47	4.67
		2000	2.99	4.16	7.34	4.98	4.19	5.11	4.93
		2001	3.23	1.72	4.09	4.11	2.41	4.60	3.37
		2002	3.55	5.08	3.64	6.82	5.81	8.21	5.77
		5-Yr	3.51	3.93	4.08	5.11	4.17	6.37	4.65
	Slope (11818)	1998	2.99	4.59	3.09	4.77	4.35	6.65	4.63
		1999	4.09	3.24	1.10	3.53	2.85	9.00	3.97
		2000	3.36	4.71	7.92	4.68	5.66	5.53	5.41
		2001	3.19	1.70	4.09	3.74	2.88	4.71	3.39
		2002	4.01	3.20	3.67	7.34	6.98	9.05	5.98
		5-Yr	3.53	3.49	3.98	4.81	4.54	6.99	4.67
	Oceanic (20042)	1998	1.44	2.26	1.13	2.71	2.60	3.93	2.46
		1999	3.00	2.15	0.55	0.70	1.74	6.81	2.49
		2000	3.41	2.87	5.92	1.93	2.84	5.06	3.68
2001		2.34	2.03	1.46	0.66	1.91	2.19	1.77	
2002		2.37	2.04	2.53	4.45	6.15	5.63	4.03	
5-Yr		2.51	2.27	2.32	2.09	3.05	4.72	2.89	

We calculated our descriptive statistics over discrete spatial domains and allowed our 30-day temporal domains to overlap (i.e. moving window statistics). A 30-day temporal window was thought to be of sufficient length so that short timescale variability would be attenuated, thus allowing for comparison of seasonal and inter-annual patterns within and among subregions.

The median was used to summarize the average value of each distribution (Figs. 2.4-2.5). Chlorophyll *a* retrievals are often log-normally distributed (Campbell, 1995). When the assumption of log-normality is fulfilled, the median approximates the geometric mean of the distribution. The median has the added advantage, over the geometric mean, of being robust to anomalously high or low chlorophyll retrievals that may be present. Medians from 30-day temporal windows matching traditional calendar months have been extracted from Figures 2.4-2.5 and are compiled in Table 2.2. Daily medians (discrete data points in Figs. 2.4-2.5) were more likely to be spatially biased since clouds could occlude various portions of a region on any particular day. Pooling observations from a given region over a 30-day period minimized (although did not eliminate) the likelihood that our summary statistics would be spatially biased due to locally variable patterns of cloud cover.

The difference between the 75th and 25th percentiles, also known as the interquartile range (IQR), was used as a measure of dispersion (i.e. variability) for each distribution and is analogous to the standard deviation (Zar, 1999). To facilitate the comparison of variability within and among subregions, the IQR from each distribution was scaled by its corresponding median (Fig. 2.6). The spread of a distribution relative to

Figure 2.4 **Median shelf chlorophyll *a* concentrations and daily upwelling indices.** Median shelf chlorophyll *a* concentrations, both 30-day and individual daily medians, for 1998 (A), 1999 (B), 2000 (C), 2001 (D), and 2002 (E). Daily upwelling indices (and a 30-day running mean) were obtained from the NOAA Pacific Fisheries Environmental Laboratory (PFEL) for 48°N, 125°W for 1998-2002 (F, G, H, I, J).

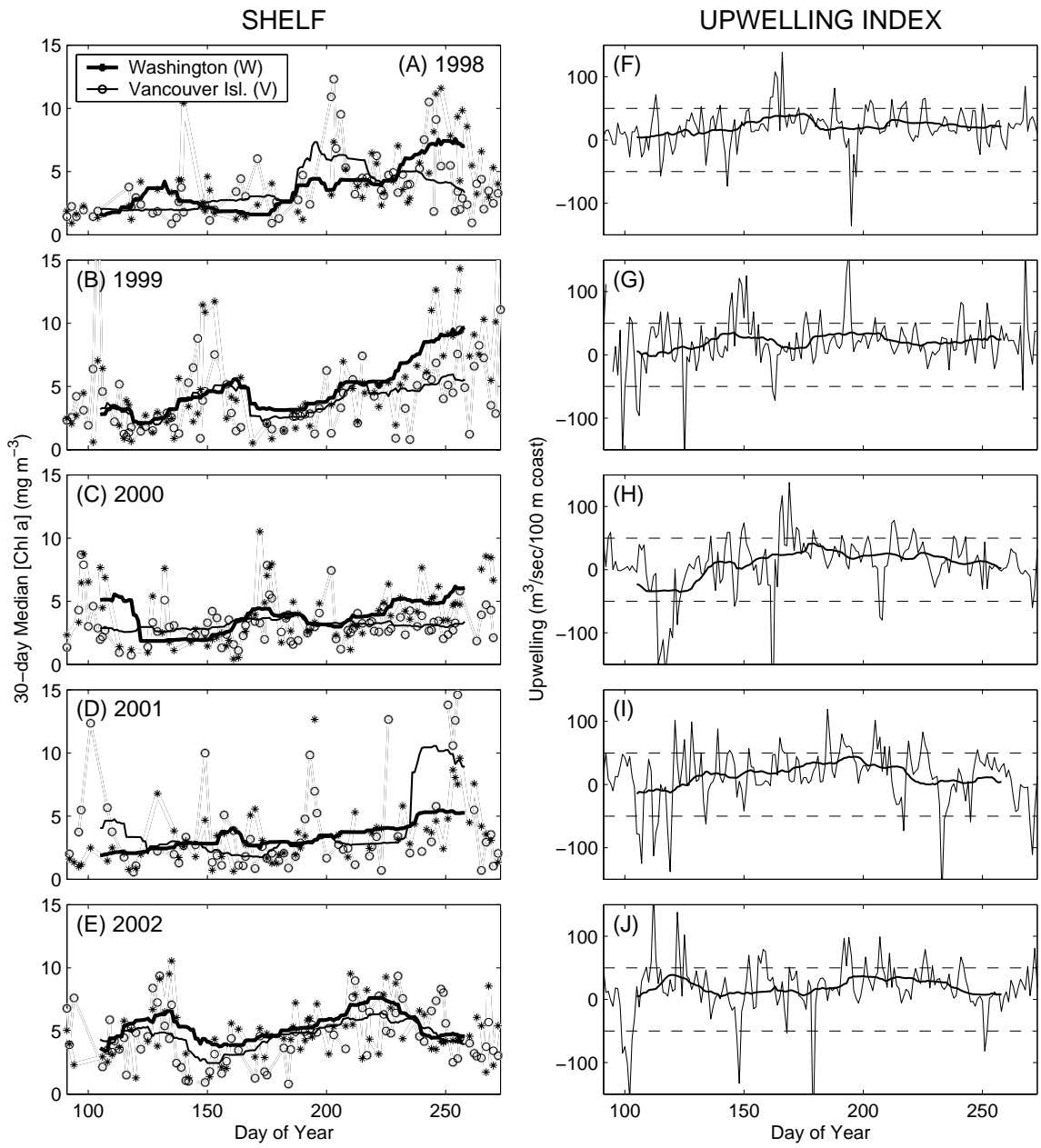


Figure 2.5 **Median slope and oceanic chlorophyll *a* concentrations.** Median slope and oceanic chlorophyll *a* concentrations, both 30-day and individual daily medians, for 1998 (A/F), 1999 (B/G), 2000 (C/H), 2001 (D/I), and 2002 (E/J).

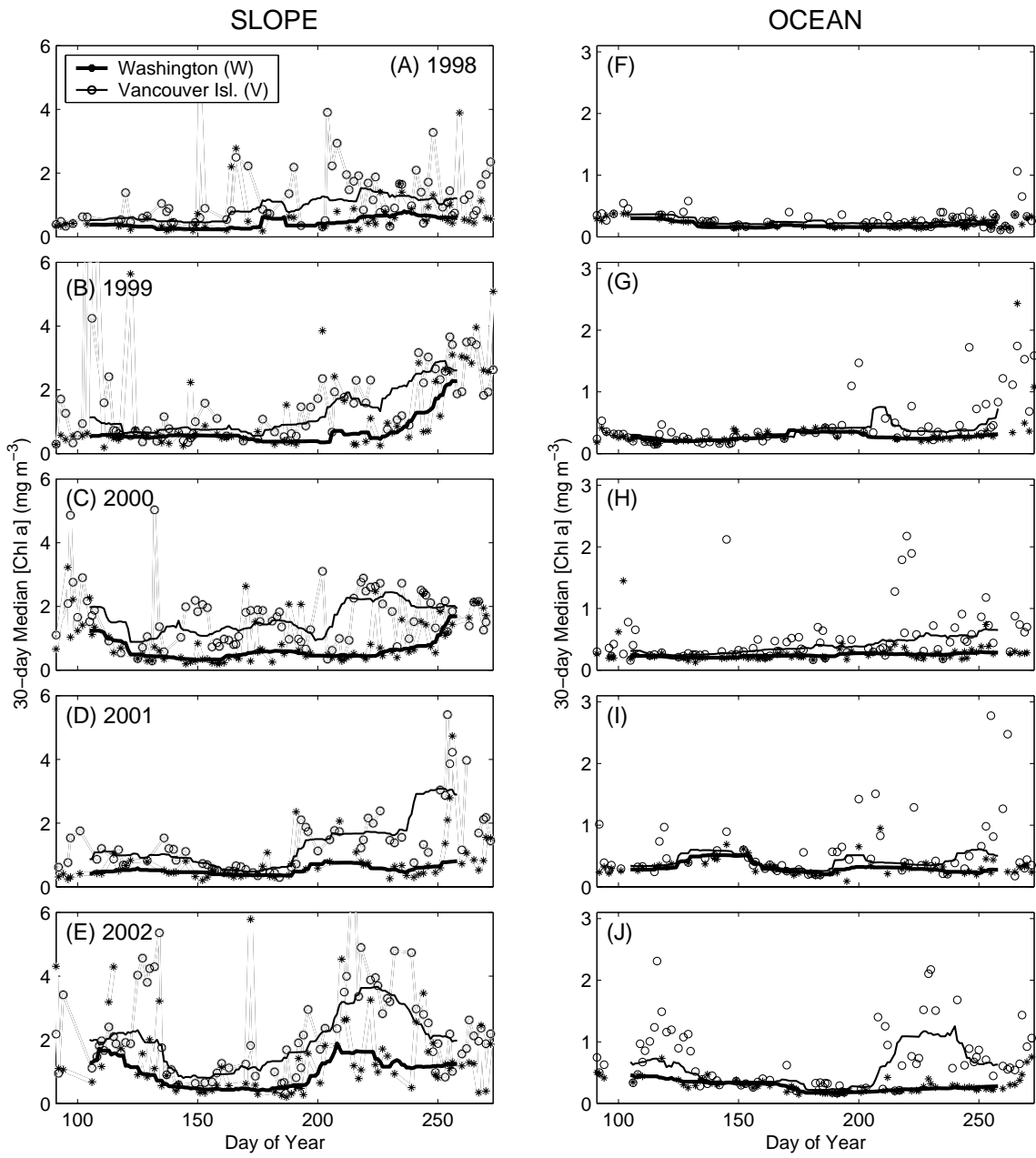


Table 2.2 **Median chlorophyll *a* concentrations.** Median chlorophyll *a* concentrations (mg m^{-3}) corresponding to traditional calendar months (30-day temporal windows) for each of the six subregions. Five-year monthly medians and 6-month annual medians are also provided. The number in parenthesis associated with each month is the year-day upon which the 30-day temporal window was centered. The number in parenthesis associated with each subregion is the areal extent of the subregion in number of pixels.

		April (105)	May (135)	June (166)	July (196)	August (227)	September (258)	6-Month	
<i>Washington Coast</i>	Shelf (9160)	1998	1.67	3.38	1.67	4.44	4.28	7.03	4.07
		1999	2.78	3.21	4.91	3.76	5.61	9.68	5.13
		2000	5.10	1.92	3.51	3.20	4.58	6.08	4.11
		2001	1.90	2.51	2.97	3.12	4.04	5.26	3.29
		2002	3.65	6.57	4.24	5.45	7.26	4.58	5.18
		5-Yr	2.79	3.09	3.30	3.92	5.01	6.39	4.36
	Slope (13793)	1998	0.38	0.25	0.27	0.35	0.66	0.59	0.46
		1999	0.53	0.53	0.56	0.39	0.54	2.28	0.62
		2000	1.24	0.43	0.45	0.46	0.55	1.69	0.65
		2001	0.41	0.52	0.38	0.56	0.57	0.80	0.50
		2002	1.29	0.72	0.46	0.66	1.15	1.24	0.99
		5-Yr	0.56	0.46	0.44	0.47	0.67	1.17	0.61
	Oceanic (14722)	1998	0.30	0.16	0.17	0.16	0.16	0.24	0.18
		1999	0.24	0.21	0.30	0.35	0.24	0.31	0.28
		2000	0.24	0.20	0.23	0.27	0.26	0.28	0.24
2001		0.28	0.51	0.28	0.29	0.29	0.28	0.30	
2002		0.46	0.36	0.32	0.18	0.24	0.28	0.26	
5-Yr		0.28	0.24	0.25	0.21	0.24	0.29	0.26	

		April (105)	May (135)	June (166)	July (196)	August (227)	September (258)	6-Month	
<i>Vancouver Island Coast</i>	Shelf (9942)	1998	2.04	2.02	2.83	7.33	4.46	3.34	3.46
		1999	3.21	3.13	5.06	3.19	4.63	5.55	4.06
		2000	2.84	2.64	3.67	3.03	3.41	3.38	3.19
		2001	4.05	3.01	1.80	3.07	2.90	8.91	3.53
		2002	4.34	4.78	3.40	5.03	5.65	3.97	4.64
		5-Yr	3.21	2.92	3.22	4.00	4.25	4.51	3.77
	Slope (11818)	1998	0.52	0.49	0.80	1.03	1.40	1.20	0.79
		1999	1.13	0.75	0.76	1.01	1.73	2.61	1.55
		2000	1.97	1.20	1.29	1.19	2.30	1.93	1.65
		2001	0.86	1.03	0.51	1.46	1.69	2.90	1.21
		2002	2.00	1.82	1.07	1.79	3.54	1.97	2.03
		5-Yr	1.36	0.83	0.89	1.37	2.34	2.03	1.48
	Oceanic (20042)	1998	0.36	0.22	0.24	0.22	0.22	0.26	0.24
		1999	0.30	0.23	0.26	0.42	0.36	0.73	0.35
		2000	0.31	0.25	0.33	0.37	0.55	0.65	0.40
2001		0.34	0.59	0.31	0.51	0.36	0.50	0.42	
2002		0.67	0.41	0.36	0.25	1.17	0.63	0.50	
5-Yr		0.36	0.30	0.33	0.28	0.43	0.53	0.38	

its location provides a unitless measure of relative variability, similar in interpretation to the coefficient of variation (standard deviation/mean). Quantile-based estimates of skewness (Equation 2.1) were calculated for the log-transformed distributions (Table 2.3) to assess the underlying assumption of log-normality (Zar, 1999):

$$\text{skewness} = (P_{75} + P_{25} - 2P_{50}) / (P_{75} - P_{25}) \quad \text{Equation 2.1}$$

where subscripts represent percentiles from the distribution under consideration. Values of skewness range from -1 for extreme left skewness, to 0 for a symmetric distribution, to 1 for extreme right skewness. The quantile-based measures of dispersion and skewness also have the advantage of being robust to anomalous chlorophyll *a* retrievals in the tails of the distributions.

Integrated Primary Production Estimates

Satellite derived surface chlorophyll concentrations (Table 2.2) were used to estimate integrated water column primary production (Table 2.4) based upon a local relationship published by Perry *et al.* (1989). Data used to derive the relationship were collected from 17 cruises conducted between 1974 and 1982 in shelf and slope waters off the Washington coast (Equation 2.2):

$$\text{Primary Production (mg C m}^{-2} \text{ d}^{-1}) = 1177 * [chl_{surf}]^{0.3735} \quad \text{Equation 2.2}$$

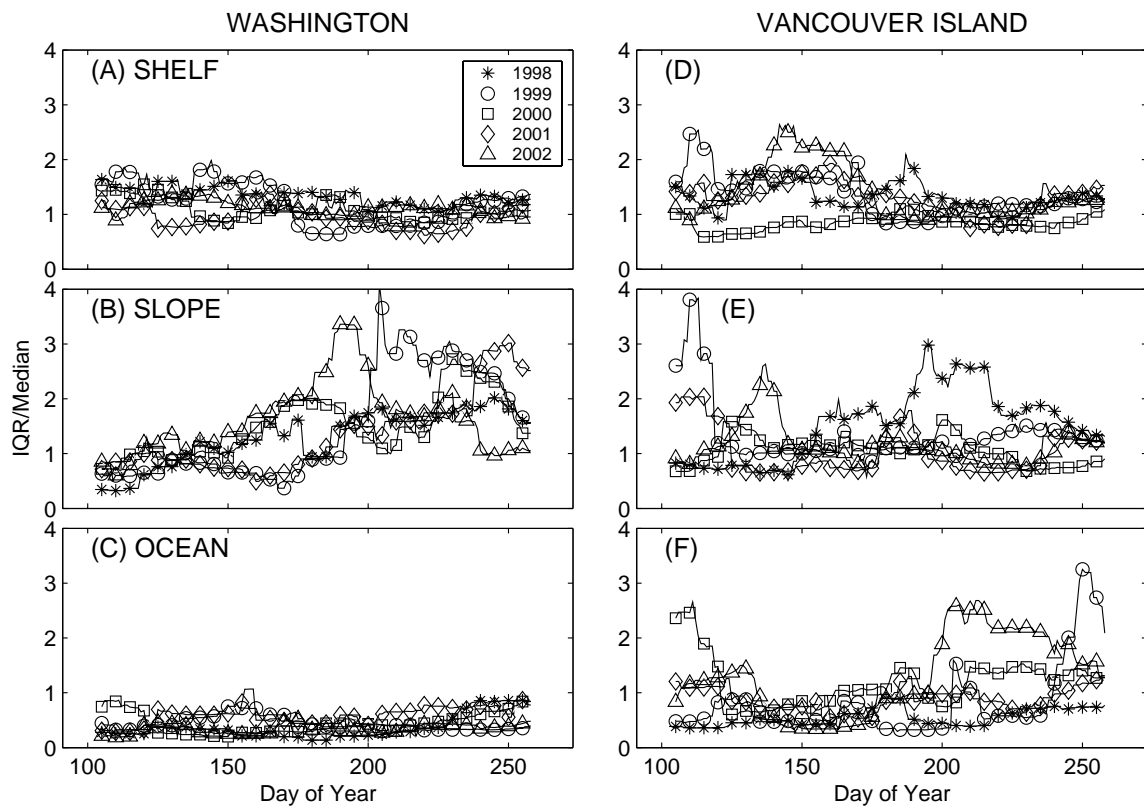


Figure 2.6 **IQR/Median ratios.** IQR/Median ratios for the six subregions (A-F). The IQR from each 30-day distribution of chlorophyll observations was scaled by its corresponding median to provide a unitless measure of relative variability (similar to a coefficient of variation).

Table 2.3 **Skewness test statistic calculated on log-transformed chlorophyll distributions.** Skewness test statistic calculated on log-transformed distributions of chlorophyll corresponding to traditional calendar months (30-day temporal windows) for each of the six subregions. Five-year monthly values and 6-month annual values are also provided. Significant departures from log-normality were assessed as skewness values in excess of +/- 0.2. Values outside this range correspond to distributions where the difference between the 75th and 50th percentile is 1.5 times as large as the difference between the 25th and 50th percentile (and vice versa). The number in parenthesis associated with each month is the year-day upon which the 30-day temporal window was centered. The number in parenthesis associated with each subregion is the areal extent of the subregion in number of pixels.

		April (105)	May (135)	June (166)	July (196)	August (227)	September (258)	6-Month	
<i>Washington Coast</i>	Shelf (9160)	1998	0.01	-0.12	0.00	0.05	0.12	-0.08	-0.04
		1999	-0.17	0.13	-0.12	0.06	0.07	0.02	0.06
		2000	0.03	0.09	-0.04	0.10	0.12	0.04	0.04
		2001	-0.01	0.00	-0.10	-0.06	-0.08	0.03	-0.04
		2002	0.11	0.00	-0.09	0.05	0.00	0.06	0.02
		5-Yr	0.02	0.07	-0.06	0.05	0.05	0.03	0.02
	Slope (13793)	1998	0.02	0.33	0.38	0.24	0.23	0.35	0.21
		1999	-0.04	0.14	0.08	0.65	0.30	-0.42	0.44
		2000	-0.23	0.12	0.19	0.38	0.49	-0.29	0.25
		2001	0.09	0.11	0.23	0.13	0.36	0.20	0.33
		2002	-0.22	0.15	0.23	0.18	0.01	-0.19	-0.15
		5-Yr	0.30	0.07	0.15	0.43	0.27	-0.06	0.28
	Oceanic (14722)	1998	0.05	0.26	0.06	0.06	0.27	-0.17	0.29
		1999	0.01	0.15	0.13	0.01	-0.06	0.19	-0.01
		2000	0.40	0.14	-0.01	-0.23	-0.12	-0.07	0.10
2001		0.10	-0.30	0.05	-0.21	0.39	0.09	0.31	
2002		0.03	0.09	-0.15	-0.01	0.14	0.09	0.04	
5-Yr		0.10	0.26	0.09	0.18	-0.01	-0.05	-0.01	

		April (105)	May (135)	June (166)	July (196)	August (227)	September (258)	6-Month	
<i>Vancouver Island Coast</i>	Shelf (9942)	1998	0.15	0.06	0.09	-0.10	-0.03	-0.05	0.04
		1999	0.08	0.17	-0.18	0.00	0.16	0.09	0.08
		2000	0.30	0.15	0.11	0.07	0.11	0.13	0.12
		2001	-0.18	0.12	0.15	0.12	0.25	0.00	0.10
		2002	-0.05	-0.06	0.18	0.13	-0.05	0.19	0.04
		5-Yr	0.09	0.15	0.04	0.04	0.07	0.09	0.08
	Slope (11818)	1998	0.28	0.18	-0.05	0.02	-0.15	-0.22	0.16
		1999	0.12	0.08	0.43	-0.07	-0.17	0.09	-0.09
		2000	0.09	-0.14	-0.08	-0.25	-0.39	-0.26	-0.25
		2001	0.38	-0.01	0.09	-0.22	-0.13	-0.21	0.01
		2002	-0.03	0.09	-0.27	-0.38	-0.02	-0.16	-0.11
		5-Yr	-0.11	0.13	0.00	-0.27	-0.24	-0.12	-0.14
	Oceanic (20042)	1998	-0.07	-0.12	0.39	0.24	0.24	-0.01	0.18
		1999	-0.01	-0.13	0.42	-0.02	0.06	0.05	0.48
		2000	0.46	0.19	0.26	-0.05	0.30	0.12	0.15
2001		0.47	0.19	0.13	0.29	0.25	0.08	0.18	
2002		0.14	0.41	0.26	0.35	-0.13	0.27	0.31	
5-Yr		0.31	0.18	0.12	0.15	0.38	0.21	0.26	

Table 2.4 **Median rates of integrated water column production.** Median rates of integrated water column production (mg C/m²/d) corresponding to traditional calendar months (30-day temporal windows) for each of the six subregions. Five-year monthly medians and 6-month annual medians are also provided. The number in parenthesis associated with each month is the year-day upon which the 30-day temporal window was centered. The number in parenthesis associated with each subregion is the areal extent of the subregion in number of pixels (1.1-km² nadir resolution).

		April (105)	May (135)	June (166)	July (196)	August (227)	September (258)	6-Month	
<i>Washington Coast</i>	Shelf (9160)	1998	1424	1854	1426	2053	2026	2438	1988
		1999	1724	1819	2132	1931	2241	2748	2168
		2000	2163	1503	1881	1816	2077	2309	1996
		2001	1496	1661	1768	1801	1983	2188	1836
		2002	1908	2378	2018	2217	2467	2078	2176
		5-Yr	1726	1794	1837	1960	2149	2353	2040
	Slope (13793)	1998	818	698	723	798	1009	969	883
		1999	926	931	949	826	935	1601	984
		2000	1274	860	873	879	945	1432	1000
		2001	844	919	819	949	954	1085	911
		2002	1293	1040	881	1009	1241	1275	1171
		5-Yr	950	884	863	888	1012	1247	977
	Oceanic (14222)	1998	752	594	613	594	597	695	626
		1999	695	662	747	797	691	762	733
		2000	685	643	679	719	710	735	686
2001		733	912	732	742	740	728	753	
2002		880	801	768	623	689	729	716	
5-Yr		731	686	705	655	691	739	711	

		April (105)	May (135)	June (166)	July (196)	August (227)	September (258)	6-Month	
<i>Vancouver Island Coast</i>	Shelf (9942)	1998	1535	1529	1735	2477	2057	1846	1872
		1999	1819	1803	2157	1815	2086	2232	1986
		2000	1737	1691	1913	1781	1862	1855	1815
		2001	1985	1775	1466	1790	1751	2665	1886
		2002	2036	2112	1859	2151	2247	1969	2088
		5-Yr	1820	1756	1822	1976	2021	2067	1932
	Slope (11818)	1998	923	900	1082	1191	1334	1261	1076
		1999	1233	1055	1063	1179	1444	1684	1388
		2000	1517	1261	1295	1254	1606	1506	1420
		2001	1114	1189	916	1357	1433	1751	1263
		2002	1524	1473	1205	1464	1887	1518	1532
		5-Yr	1321	1096	1126	1324	1617	1534	1361
	Oceanic (20042)	1998	807	667	692	668	667	710	695
		1999	754	677	712	849	807	1045	798
		2000	759	705	782	816	942	1002	837
2001		786	969	757	916	800	911	851	
2002		1015	845	806	700	1248	990	910	
5-Yr		808	748	780	735	862	928	817	

In the absence of recent concurrent *in situ* data, this relationship was used to provide a first order approximation for rates of primary production.

Upwelling Data

To characterize inter-annual differences in large-scale wind forcing, daily upwelling indices were obtained from the NOAA Pacific Fisheries Environmental Laboratory (PFEL) for 48°N, 125°W (Fig. 2.4). Their indices were calculated according to Ekman's theory of mass transport due to wind stress; values for wind stress were derived from mean surface atmospheric pressure fields obtained from the U.S. Navy Fleet Numerical Meteorological and Oceanographic Center (FNMOC). Positive values for the upwelling index are typically associated with an offshore advection of surface waters resulting from equatorward wind stress and suggest an increased supply of nutrients to the euphotic zone. Daily upwelling indices were summarized with a running mean rather than a median so that extreme, short-timescale events would have some influence on the summary statistic. Upwelling 'events' were defined as daily upwelling indices in excess of +/- 50 m³/sec/100 m coastline. Correlations between upwelling events and daily shelf chlorophyll concentrations, at lag distances ranging from 0 to 6 days, were performed to assess the strength and statistical significance (p-value < 0.1) of a linear relationship between the two datasets (Table 2.5). Table 2.5 also presents correlations between daily Washington and Vancouver Island shelf chlorophyll concentrations.

Table 2.5

Correlations between daily shelf chlorophyll and upwelling events.

Correlations between daily shelf chlorophyll and upwelling events, at lag distances ranging from 0 to 6 days. Upwelling 'events' were defined as daily upwelling indices in excess of +/- 50 m³/sec/100 m coastline. Statistically significant correlations have been shaded and were defined as having a p-value < 0.1. Correlations between daily Washington and Vancouver Island shelf chlorophyll concentrations are also presented.

	<u>Lag</u>	<u>Correlation</u>	<u>Count</u>	<u>P-Value</u>	<u>Correlation</u>	<u>Count</u>	<u>P-Value</u>
		<i>Washington Shelf [Ch]</i>			<i>Vancouver Island Shelf [Ch]</i>		
1998	0	-0.59	8	0.12	-0.31	12	0.32
	1	-0.51	6	0.30	-0.27	8	0.51
	2	0.03	10	0.94	-0.04	11	0.90
	3	0.19	8	0.65	0.27	10	0.45
	4	-0.50	9	0.17	0.16	9	0.68
	5	0.07	12	0.84	-0.09	16	0.73
	6	-0.27	8	0.53	-0.50	8	0.21
1999	0	0.07	15	0.80	0.15	16	0.58
	1	-0.01	15	0.98	0.06	17	0.83
	2	0.58	15	0.02	0.19	16	0.48
	3	0.44	11	0.18	-0.31	13	0.30
	4	0.29	16	0.29	-0.16	16	0.54
	5	0.54	6	0.27	-0.39	9	0.30
	6	-0.22	12	0.50	-0.12	14	0.67
2000	0	0.23	12	0.46	0.40	14	0.16
	1	0.68	14	0.01	0.80	14	0.00
	2	0.42	17	0.09	0.44	17	0.08
	3	0.75	13	0.00	0.61	14	0.02
	4	0.54	15	0.04	0.30	17	0.24
	5	0.33	14	0.26	0.12	17	0.66
	6	0.61	15	0.02	0.28	18	0.27
2001	0	-0.04	9	0.92	0.30	15	0.27
	1	0.38	19	0.11	0.28	22	0.21
	2	0.28	17	0.28	0.26	18	0.30
	3	0.46	15	0.08	0.12	14	0.68
	4	0.25	16	0.35	0.06	13	0.86
	5	0.35	14	0.22	0.18	15	0.53
	6	0.24	10	0.50	0.12	13	0.71
2002	0	-0.37	16	0.16	-0.20	19	0.41
	1	0.16	15	0.58	0.36	17	0.16
	2	0.28	17	0.28	0.71	18	0.00
	3	0.51	16	0.05	0.40	17	0.12
	4	0.37	19	0.12	0.34	21	0.14
	5	0.60	14	0.02	0.65	17	0.01
	6	0.34	15	0.21	0.34	16	0.20

	<u>Year</u>	<u>Correlation</u>	<u>Count</u>	<u>P-Value</u>
<i>Washington Shelf [Ch] vs. Vancouver Island Shelf [Ch]</i>	1998	0.25	57	0.07
	1999	0.51	65	0.00
	2000	0.54	71	0.00
	2001	0.58	53	0.00
	2002	0.35	70	0.00

Results and Discussion

Regional Characteristics

The width of the Washington shelf was more uniform (approx. 50 km throughout) than the Vancouver Island shelf, which was approximately 80 km wide in the southeast portion of the region and narrowed to approximately 25 km in the northwest (Fig. 2.1). The continental slope regions were uniform in width although the Washington slope was wider than the Vancouver Island slope. The width of the combined Vancouver Island shelf plus slope region was narrower than off Washington; hence, the oceanic waters (i.e. waters deeper than 2200 m) off Vancouver Island were located closer to land (especially in the northwest portion of the study region) than oceanic waters off Washington. The areal extent of each subregion (in numbers of pixels) is provided in Table 2.1.

Data Density

The Pacific Northwest is often cloud covered. Table 2.1 gives the average number of cloud free observations per pixel in each of the six subregions. The minimum number of cloud free observations per pixel was 0.55 for Vancouver Island oceanic waters in June 1999, while the maximum was 9.05 for Vancouver Island slope waters in September 2002. There was considerable inter-annual variability in the total number of chlorophyll *a* retrievals. In each of the subregions off Vancouver Island, the year 2002 had the greatest and 2001 the least number of observations. Waters off Washington had the largest number of observations recorded in 2000 for the shelf and slope regions and in 2002 for oceanic regions. The least number of observations were recorded for the slope and oceanic regions in 1998 and for the shelf region in 2001. In general, there was an

increase in the average number of observations per pixel in September of each year; however, more detailed patterns of seasonal variability were inconsistent among the five years of data (Table 2.1). There were a number of instances of very low data densities (i.e. high cloud cover) that persisted for long periods of time (> 30 days). During these times summary statistics may be biased; based on satellite observations alone it is difficult to determine if these values are representative of the entire region over the 30-day period.

Data densities on the slope followed a pattern similar to what was observed on the shelf, although the average number of observations was typically less than on the shelf (Table 2.1). In all oceanic waters data densities were less than 3 observations per pixel throughout large portions of 1998, 1999, and 2001. In 2000 and 2002 there was an increase in the average number of observations in oceanic waters and typical data densities were in excess of 3 observations per pixel for any given 30-day period.

Chlorophyll retrievals pooled and summarized statistically over a given spatio-temporal domain are not necessarily randomly sampled within that domain. Data densities are presented in conjunction with summary statistics as an index of confidence in the regional statistic. Examples of monthly data density maps are shown in Figure 2.3 (all are provided in Appendix A). Despite qualitatively similar monthly median composites in June 2000 and May 2001 (Fig. 2.3), average data densities in May 2001 are < 3 observations per pixel over much of the scene, whereas data densities in June 2000 are often > 6 observations per pixel. Cloud patterns associated with weather systems moving through the region tend to obscure many of the sequential images, resulting in a temporal bias.

Although low data densities and spatial biases in the sampling of a given spatio-temporal domain (e.g. distribution of samples in Vancouver Island shelf and slope regions) should raise suspicion as to the ‘regional’ applicability of any summary statistics that are calculated, in this paper we did assume that our summary statistics for a given region over a 30-day period can be used as a valid index of the entire region. However, the data density maps in Figure 2.3 and the summary values in Table 2.1 help illustrate and call attention to situations where this assumption is weak or invalid.

Inter-annual Chlorophyll Trends (6-month Medians)

In all five years ‘high’ chlorophyll concentrations ($> 2.0 \text{ mg m}^{-3}$) were found on the continental shelf (Fig. 2.2; Appendix A). With the exception of 2001, the 6-month median concentrations of chlorophyll were higher on the Washington shelf than on the Vancouver Island shelf (Table 2.2). The greatest difference between the two shelf regions occurred in 2000, when the Washington shelf median chlorophyll concentration was 30% greater than that observed on the Vancouver Island shelf. On average, 6-month median chlorophyll concentrations for the Vancouver Island slope were 2 times higher than those observed for the Washington slope (Table 2.2). Six-month median oceanic chlorophyll concentrations off of Vancouver Island were greater than those off of Washington for all 5 years. The smallest observed difference between the two oceanic regions was in 1998, the year following El Niño, when offshore advection of higher chlorophyll waters from the Vancouver Island slope was minimal. Six-month median chlorophyll concentrations were maximal in 2002 for all subregions off Vancouver Island and for shelf and slope regions off Washington.

The spatial extent of 'intermediate' chlorophyll ($0.5 - 2.0 \text{ mg m}^{-3}$) water was variable among the five years. In 1998, the year following the intense 1997-98 El Niño event, 'intermediate' chlorophyll waters were primarily confined to the continental slope and rarely extended into oceanic regions. In 1999-2002 'intermediate' chlorophyll waters extended farther over the slope and into deeper oceanic waters (Fig. 2.2; Appendix A). The offshore extent of 'intermediate' chlorophyll water was typically greater off the Vancouver Island coast than off the Washington coast. Generally, 'low' chlorophyll ($< 0.5 \text{ mg m}^{-3}$) waters were found in oceanic waters off Washington and Vancouver Island, although significant regions of 'low' chlorophyll water were also observed on the Washington slope (Fig. 2.2; Appendix A).

Seasonal Chlorophyll Trends (30-day Medians)

On average, 30-day median chlorophyll concentrations on the shelf varied from 2 to 10 mg m^{-3} (Fig. 2.4). In 1998-2001 concentrations were generally lower in April and May and maximal in September of each year. In 2002 two distinct peaks in median chlorophyll concentrations were observed in May and August, respectively. Observations of early blooms (defined as regions with concentrations $> 3 \text{ mg m}^{-3}$ in April) were observed in 1999, 2001, and 2002 on the Vancouver Island shelf and in 2000 and 2002 on the Washington shelf. Median chlorophyll concentrations in excess of 6 mg m^{-3} were only observed in September 1998-2000 and in May and August 2002 on the Washington shelf and in July 1998 and September 2001 on the Vancouver Island shelf. In 2000 Vancouver Island shelf chlorophyll concentrations were low, averaging 3.19 mg m^{-3} , and exhibited very little dynamic range throughout the year.

We have used the same regional upwelling index to describe the large-scale wind forcing for waters off Washington and Vancouver Island. The expected pattern of increased surface chlorophyll concentration following upwelling events was often observed. For example, in 1999 a peak in the median chlorophyll concentrations followed the upwelling event around day 145 while the downwelling event at day 160 was followed by a decrease in shelf chlorophyll (Fig. 2.4B, G). Similarly, the downwelling event at day 120 and the upwelling event at day 170 in 2000 are associated with a decrease and increase in median chlorophyll concentrations, respectively (Fig. 2.4C, H). Conversely, not all upwelling or downwelling events were associated with increased or decreased chlorophyll concentrations. For example, the strong downwelling events at day 190 in 1998 and at day 235 in 2001 are associated with large increases in median chlorophyll concentrations (Fig. 2.4A, D, F, I). These conflicting observations suggest that dynamics predicted from winds alone are insufficient to explain all of the patterns in surface chlorophyll. The number of upwelling ‘events’ in each year was 26, 36, 36, 45, and 42 for 1998-2002, respectively. Significant correlations between daily median shelf chlorophyll and upwelling event strength (with lags from 0-6 days) ranged from 0.42 to 0.80 (Table 2.5). All 14 of the statistically significant correlations were positive. No significant positive correlations were observed in 1998. In 1999, Washington shelf chlorophyll showed a relationship with upwelling event strength at a lag of 2 days. Despite the significant correlation ($r = 0.51$) between Washington and Vancouver Island shelf chlorophyll concentrations, Vancouver Island shelf chlorophyll did not reveal a significant linear relationship to upwelling event strength at any lag. Strong correlations were observed in 2000 with a 1-day lag. Vancouver Island and

Washington shelf chlorophyll concentrations had correlations with upwelling event strength of 0.80 and 0.68, respectively. Strong correlations between the strength of the 30-day mean upwelling index and the 30-day median chlorophyll concentrations were not evident. Because no in-water measurements were collected, we cannot assess the role of nutrient concentration or subsurface phytoplankton distributions on events that do not behave as textbooks predict.

Chlorophyll concentrations were always greater on the Vancouver Island slope compared to the Washington slope for any given 30-day period (Fig. 2.5). Typical values of median chlorophyll ranged from 0.5 to 4 mg m⁻³. Around day 220 in 2000 the difference between concentrations off of the Washington coast and the Vancouver Island coast was maximal and exceeded a factor of 4 (Fig. 2.5C). Qualitatively the seasonal pattern was similar over the slope as it was over the shelf in each year (i.e., low values in April-May with maximal values in September of each year). The Vancouver Island slope in 2000 was a notable exception to this pattern and chlorophyll concentrations were approximately equal in April and September (Table 2.2). In 2000 median slope and oceanic concentrations off Vancouver were high despite relatively low median shelf concentrations.

Median chlorophyll concentrations in oceanic waters were typically less than 1 mg m⁻³ (Fig. 2.5) and averaged approximately 0.3 mg m⁻³ (Table 2.2). No obvious seasonal pattern was consistent among the five years of data. In 1998 seasonal variations in median chlorophyll were minimal and median concentrations averaged 0.24 mg m⁻³ off Vancouver Island and 0.18 mg m⁻³ off Washington. In contrast, seasonal variability was greatest in 2002 where median oceanic concentrations fluctuated by nearly a factor of 5

off Vancouver Island and distinct peaks in median chlorophyll were observed around days 120 and 230. Interestingly, median oceanic concentrations off Washington in 2002 averaged 0.26 mg m^{-3} and exhibited very little dynamic range. In 2000 median chlorophyll concentrations appeared to rise steadily throughout the season in Vancouver Island oceanic waters.

Chlorophyll Variability

Estimates of normalized variability for waters off the Washington coast show the greatest variability in waters overlying the slope (Fig. 2.6). Off the Washington coast slope variability was similar to that observed in deeper oceanic waters in April of each year and rose steadily throughout the summer season. Values for the ratio of IQR/Median typically exceeded 1.5 in September of each year and short excursions to values greater than 3 were observed in 1999, 2001, and 2002. In general, variability was minimal over deeper oceanic waters and very little seasonal variation was seen in the IQR/Median ratio for either the shelf or oceanic regions off Washington.

Levels of variability for the Vancouver Island shelf were comparable to those seen off the Washington coast. There was greater inter-annual variability over the slope and oceanic waters off of Vancouver Island; however, no consistent seasonal increase was seen for these slope waters in contrast to the Washington slope. High variability was seen in April and May of 1999 and 2001 for slope waters and in April and May 2000 and August 2002 for oceanic waters off the Vancouver Island coast, a pattern that was not seen in corresponding areas off of Washington. After day 150 in 1998, variability on the Vancouver Island slope was greater than was typically seen in any of the other 4 years.

Estimates of skewness for each of the 30-day log-normalized distributions of chlorophyll were used to assess the assumption of log-normality, and are also used as an additional measure of variability (Table 2.3). Skewness values in excess of +/- 0.2 correspond to distributions where the difference between the 75th and 50th percentile is 1.5 times as large as the difference between the 25th and 50th percentile (and vice versa). The continental shelves off Washington and Vancouver Island had relatively few instances of skewness in excess of the +/- 0.2 range, suggesting minimal departures from log-normality (to the extent that log-normality can be assessed by the skewness test statistic alone). On the Washington slope departures from log-normality were more common in July-September of each year. On the Vancouver Island slope there was a tendency for the distributions to be negatively skewed after July in each of the 5 years, a reversal of the pattern observed on the Washington slope. In Vancouver Island oceanic waters positive skewness was prevalent.

On the Washington slope waters an increase in the IQR/Median ratio was observed as the season progressed (Fig. 2.6). If we assume that sufficient data density was obtained to assure that the summary statistics calculated were representative of the entire spatio-temporal domain, one interpretation for this increase in the IQR/Median ratio is an increase in the offshore transport of higher chlorophyll concentrations from the shelf onto the slope. As relatively high shelf concentrations are advected offshore they mix with the lower biomass waters more typical of slope and oceanic regions. Where these higher chlorophyll filaments extend out into lower chlorophyll waters, a zone of increased variability would develop.

The skewness test statistic (Table 2.3) can be used to gauge the relative location of this zone of increased variability. Positive skewness values indicate distributions dominated by low chlorophyll concentrations and intrusions of higher chlorophyll would be manifested as elongated tails in the high chlorophyll regions of the distributions, and vice versa. On the Washington slope we observed a tendency for the distributions to be positively skewed, suggesting that overall the region is oceanic in nature and parcels of high chlorophyll water develop within, or move through the region. Conversely, in Vancouver Island slope waters we observed a tendency for the distributions to be skewed negatively, suggesting that this region is more coastal in nature and that parcels of lower chlorophyll water were occasionally observed in the region. In Vancouver Island oceanic waters the tendency for positive skewness is consistent with the hypothesis that higher chlorophyll waters can be advected farther offshore into this deep-ocean regime. The northward flowing buoyant discharge from the Strait of Juan de Fuca may also be involved in seaward displacement of high chlorophyll shelf waters (Fig. 2.7).

Primary Production

The linear relationship between integrated water column primary production and surface chlorophyll concentration (Equation 2.2; Perry *et al.*, 1989) was applied directly to median chlorophyll concentrations (Table 2.2) to provide an estimate of regional production in g carbon m⁻² d⁻¹ (Table 2.4). Calculated values of integrated production were consistent with the more recent estimates of Boyd and Harrison (1999). Using median chlorophyll concentrations (from observations pooled over all 5 years of data) for each of the six subregions, we calculated an average 6-month rate of carbon production

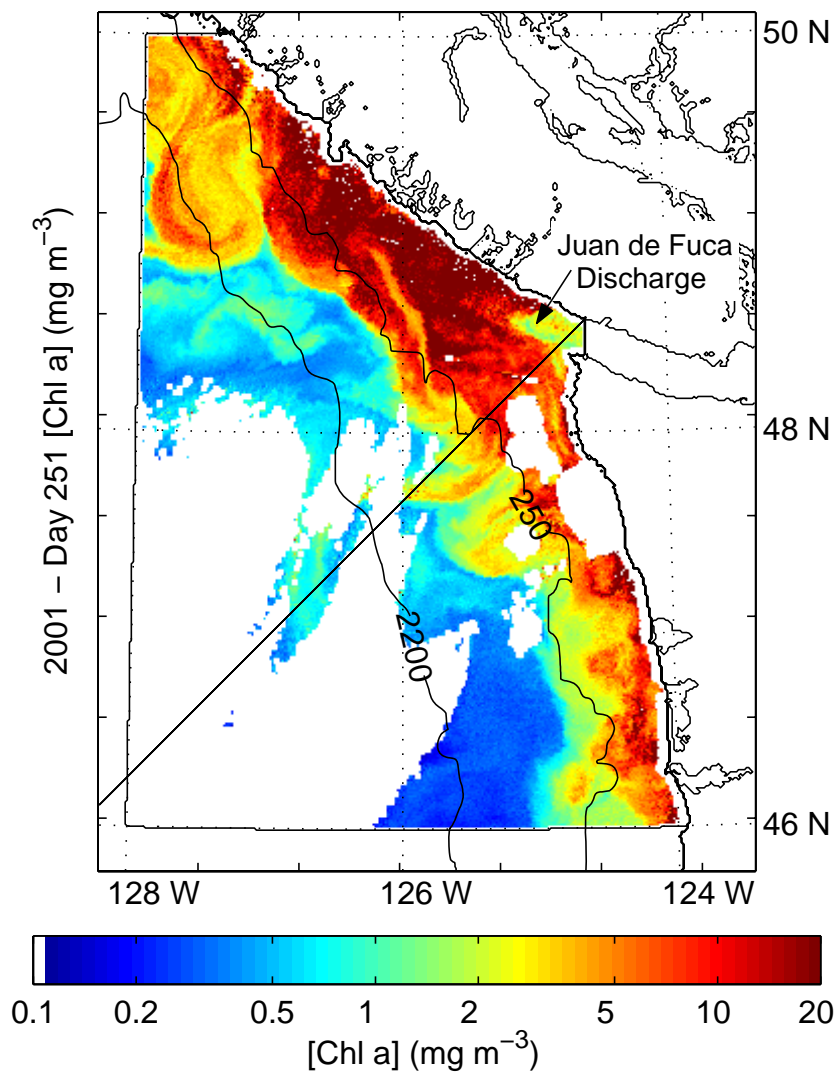


Figure 2.7 **Daily chlorophyll image from Day 251 in 2001.** Image illustrates how discharge of low chlorophyll water from the Strait of Juan de Fuca may also play a role in offshore biomass transport as material is forced off the shelf into deeper waters to accommodate the intrusion.

for waters adjacent to Vancouver Island and Washington. Off Washington the estimated regional rate of carbon production was 9.33×10^{12} g C 6-months⁻¹; off Vancouver Island 11.41×10^{12} g C 6-months⁻¹. The observed difference is due, in part, to the greater areal extent of the subregions off Vancouver Island.

Conclusions

Historical patterns of the cross-shelf variability of phytoplankton biomass, derived from the Coastal Zone Color Scanner dataset, have been well documented for the entire California Current (Strub *et al.*, 1990; Tomas and Strub, 2001). In part, our dataset extends this work and clearly illustrates significant inter-annual variations in surface biomass over the entire region of interest, especially with regard to the offshore extent of ‘intermediate’ chlorophyll waters in 1998 compared to the remaining 4 years of data (Fig. 2.2). Sea surface temperature anomalies in April and May of 1998 reveal an anomalously warm (1-2 °C) surface layer, suggesting that the intense El Niño in 1997 had pronounced effects well into 1998. This lingering effect of El Niño, manifested in a region-wide warm surface layer, was not observed in any of the other months throughout the 5-year period (NOAA/NESDIS CoastWatch, 2003). Most of the surface biological production in 1998 appeared to be confined to the shelf with very little extension of high phytoplankton biomass into offshore oceanic surface waters. These observations support the hypothesis that biological production was suppressed following the strong El Niño event, particularly in oceanic waters and in Vancouver Island slope waters.

In 1999- 2002 extensions of ‘intermediate’ chlorophyll waters into deep-oceanic waters were more common off Vancouver Island. The observed difference in the

offshore extent of 'intermediate' chlorophyll waters off Vancouver Island versus Washington (Fig. 2.2) could be due, in part, to the orientations of the coasts relative to the dominant modes of physical forcing or differences in the activity and efficiency of various offshore transport mechanisms. In the daily image shown in Figure 2.7 one can see the offshore extension of high biomass waters from the Vancouver Island shelf onto the slope. Figure 2.7 also suggests that the effluent from the Strait of Juan de Fuca may play an important role in the offshore transport of biomass off the Vancouver Island shelf. Waters within the Strait appear to be low in chlorophyll; as they displace higher biomass waters on the shelf material may be forced onto the slope to accommodate the intrusion. The 2200-m isobath off Vancouver Island is relatively close to shore. As a consequence offshore advection can occur over a shorter distance, facilitating transport of material into deep-oceanic water. The close proximity of the Vancouver shelf to the deep ocean may be important in terms of net carbon flux to the deep sea. Alternatively, the apparent extensions of 'intermediate' chlorophyll water could also be manifestations of increased *in situ* production in offshore waters. With the present dataset we cannot resolve which mechanism is responsible for the observed patterns, nor are we able to discern the subsurface patterns of biomass distribution from remotely-sensed satellite data.

Freeland *et al.* (2003) observed a difference in spiciness for waters at the shelf-break off Oregon and along Line-P (a section extending from the mouth of the Strait of Juan de Fuca to Station Papa at 50°N, 145°W in the Gulf of Alaska) of about -0.25 when observations from 2002 were compared with more 'typical' hydrographic conditions at the same locations in previous years. Waters that were cooler and fresher were defined as

less 'spicy' and are thought to be associated with the intrusion of nutrient-rich Subarctic water into the California Current (alternate hypotheses are discussed by Freeland *et al.* (2003) and Thomas *et al.* (2003) but will not be addressed here). The observed decrease in spiciness was approximately the same magnitude, but opposite sign, as the change observed during the 1997-98 El Niño (i.e. warmer and saltier hydrographic conditions were associated with the 1997-98 El Niño). In sharp contrast to patterns observed in 1998, 6-month median chlorophyll concentrations in 2002 were maximal and pronounced seasonal variability, with distinct peaks in median chlorophyll around days 120 and 230, was observed for all subregions off Vancouver Island and for shelf and slope regions off Washington. The general relationship between local hydrography and satellite-derived estimates of surface chlorophyll is useful to define the first-order causal mechanisms that may explain observed spatio-temporal patterns in surface phytoplankton biomass. Given the intensities of the hydrographic and chlorophyll anomalies observed in 1998 (i.e. El Niño) and 2002 (Subarctic water intrusion) we have begun to constrain the range in which our physical and biological observations lie. With the upper and lower bounds better defined we can more accurately formulate models of 'typical' oceanographic conditions in the Pacific Northwest and determine the relative importance of anomalous situations that may occur in the future.

The magnitude of and pathways for carbon sequestration in the deep ocean remain major questions relevant to the role of the ocean carbon cycle in climate change. Net carbon sequestration depends on the transfer of primary productivity from the euphotic zone to the deep ocean. Efficient offshore transport mechanisms that remove carbon from regions of high productivity to deep-water oceanic regions may play a critical role

in carbon sequestration (Walsh, 1991). One consequence of the 1997-98 El Niño appears to be a reduction in surface chlorophyll concentrations, and by inference, rates of primary productivity, in slope and oceanic waters off Vancouver Island. We speculate that the increased frequency of El Niño events may lead to a reduction in offshore carbon transport and sequestration. Conversely, the apparent invasion of Subarctic water into the California Current in 2002 is correlated with increased chlorophyll concentrations throughout the region of interest. Such episodic intrusions, if shown to be common in the Pacific Northwest, may lead to increased offshore carbon production and sequestration.

Acknowledgements

This work was supported by Washington State Sea Grant (NA76RG0119) and NASA (NAG5-9959 and NAG5-7604).

Chapter 3

OCEAN COLOR OBSERVATIONS OF A SURFACE WATER TRANSPORT EVENT: IMPLICATIONS FOR *PSEUDO-NITZSCHIA* ON THE WASHINGTON COAST

A persistent patch of high biomass water, associated with the Juan de Fuca Eddy, is often observed in surface chlorophyll *a* images off the southwest coast of Vancouver Island, Canada. Outbreaks of toxic *Pseudo-nitzschia* spp. along the Washington, USA, coast are believed to correlate with the transport of waters from Juan de Fuca Eddy southward to Washington beaches. A time series of SeaWiFS satellite ocean color images from late May 1999 of coastal waters off Washington and Vancouver Island, processed for surface chlorophyll *a* concentration and spectral remote sensing reflectance, captured a transport event where water from the Juan de Fuca Eddy was transported onto the Washington shelf. Strong upwelling-favorable winds appeared to deform the patch over an eight-day period and move it southward into Washington coastal waters with surface velocities of approximately 8–16 km d⁻¹. SeaWiFS and sea surface temperature imagery showed the local phytoplankton response to wind-driven coastal upwelling restricted to a narrow (10–15 km) region along the Washington coast. Although we did not observe transport of high biomass water originating in the Juan de Fuca Eddy to Washington beaches in May 1999, transport of *Pseudo-nitzschia* cells could occur following a rapid shift to downwelling-favorable conditions. Tracking the trajectory of surface waters from the Juan de Fuca Eddy by remote sensing could be used to trigger conditional sampling for domoic acid along the Washington coast.

Introduction

High concentrations of the potentially toxigenic pennate diatom in the genus *Pseudo-nitzschia* have been reported to occur within a sustained, high biomass, phytoplankton patch associated with the Juan de Fuca Eddy (Mackas and Sefton, 1982; Horner et al., 2000; Trainer et al., 2002). This semi-permanent cyclonic eddy develops annually following the spring transition at the coastal terminus of the Strait of Juan de Fuca (Tully, 1942; Freeland and Denman, 1982). Trainer et al. (2002) and Marchetti et al. (2004) postulate that episodic southward transport of surface waters from the eddy may play a role in harmful bloom initiation along the Washington coast. The 1998 *Pseudo-nitzschia* blooms responsible for the elevated concentrations of the neurotoxin domoic acid (DA) in razor clams and closure of the clam beds on Kalaloch Beach, Washington, were thought to originate in the Juan de Fuca Eddy where environmental conditions favoring toxin production have been observed (Trainer et al., 2002; Marchetti et al., 2004). Elevated concentrations of DA in razor clams can lead to immediate closure of coastal clamming beaches, often for an entire season, due to the slow depuration of DA in razor clam tissue (Trainer et al., 2002; Wekell et al., 2002). In addition to the significant economic losses to shellfish industries, blooms of *Pseudo-nitzschia* have detrimental effects on marine mammal and bird populations on the west coast of North America (Fritz et al., 1992; Horner et al., 1997; Scholin et al., 2000; Trainer et al., 2000).

While the eddy populations are not the only inoculum for *Pseudo-nitzschia* blooms, transport of surface waters from the eddy into Washington coastal waters may be an important mechanism for bloom initiation under certain conditions. We used sequences of SeaWiFS (Sea-viewing Wide Field-of-view Sensor) ocean color satellite

images and AVHRR (Advanced Very High Resolution Radiometer) sea surface temperature (SST) images from late May 1999 to test the hypothesis that the Juan de Fuca Eddy can supply inoculum of *Pseudo-nitzschia* to Washington coastal waters. The high chlorophyll *a* concentration (chl *a*) and low spectral remote sensing reflectance ($R_{rs}(\lambda)$) of the Juan de Fuca Eddy allowed us to monitor its surface expression over an eight-day period. Buoy wind data and sea surface temperature patterns confirm that this was a period of strong upwelling-favorable conditions.

Although the patch itself did not appear to intersect the shore, our observations are relevant to the potential delivery of *Pseudo-nitzschia*. As conditions shift from upwelling to downwelling-favorable, surface currents could transport cells from offshore waters to the coast (Roegner et al., 2002; Trainer et al., 2002; McGillicuddy et al., 2003, MacFadyen et al., 2005). Alternatively, under upwelling-favorable conditions, ‘reseeded’ of toxic cells near the coast could result from offshore populations sinking from the surface into deeper onshore-flowing waters that are ultimately brought back to the surface near the coast (Brink et al., 1981; Smith et al., 1983). Trainer and Suddleson (2005) describe recent efforts to develop an integrated harmful algal bloom forecasting system for Washington State that will depend on near real-time data obtained from a number of *in situ* and satellite-based sensors. Our observations suggest that spectral reflectance patterns, obtained historically from SeaWiFS and currently from MODIS (Moderate-resolution Imaging Spectroradiometer), could be used to track trajectories of water masses associated with the Juan de Fuca Eddy and to provide a diagnostic to initiate intensified conditional sampling for DA along the coast.

Materials and Methods

Satellite Ocean Color and Sea Surface Temperature

The Juan de Fuca Eddy, also known as the Tully Eddy (Tully, 1942), is typically located near the mouth of the Strait of Juan de Fuca at the Canada–United States border (Fig. 3.1), although the precise location of the eddy can vary with local hydrographic and wind conditions (Fig. 3.2A–B). A sequence of SeaWiFS images for 22–29 May 1999 captures the deformation and southward transport of surface waters from the eddy (Fig. 3.2B–F); although the sequence is gappy due to cloud cover and/or poor sensor viewing geometry on missing days, the imagery captures the main features of the event.

Chlorophyll *a* concentration and $R_{rs}(\lambda)$ were processed from Level 1a local-area-coverage (LAC) data, obtained at full 1.1-km² nadir resolution from NASA’s GSFC Earth Science Distributed Active Archive Center. Standard Level 2 products, consistent with the fourth SeaWiFS data reprocessing, were computed using the default parameter values implemented in SeaDAS v. 4.3p3. The Level 2 'chlor_a' (chl *a* concentration in mg m⁻³) and $R_{rs}(\lambda)$ products were mapped to transverse Mercator projections with an average pixel size of 1.1 km². Remote sensing reflectance at 555, 510 and 443 nm were used to generate standard RGB false color composite images for 22 May (Day 1; Fig. 3.3A) and 26 May (Day 5; Fig. 3.3B). For each optically-distinctive water mass, an area clearly inside its borders was selected (boxes in Fig. 3.3A–B) and an average remote

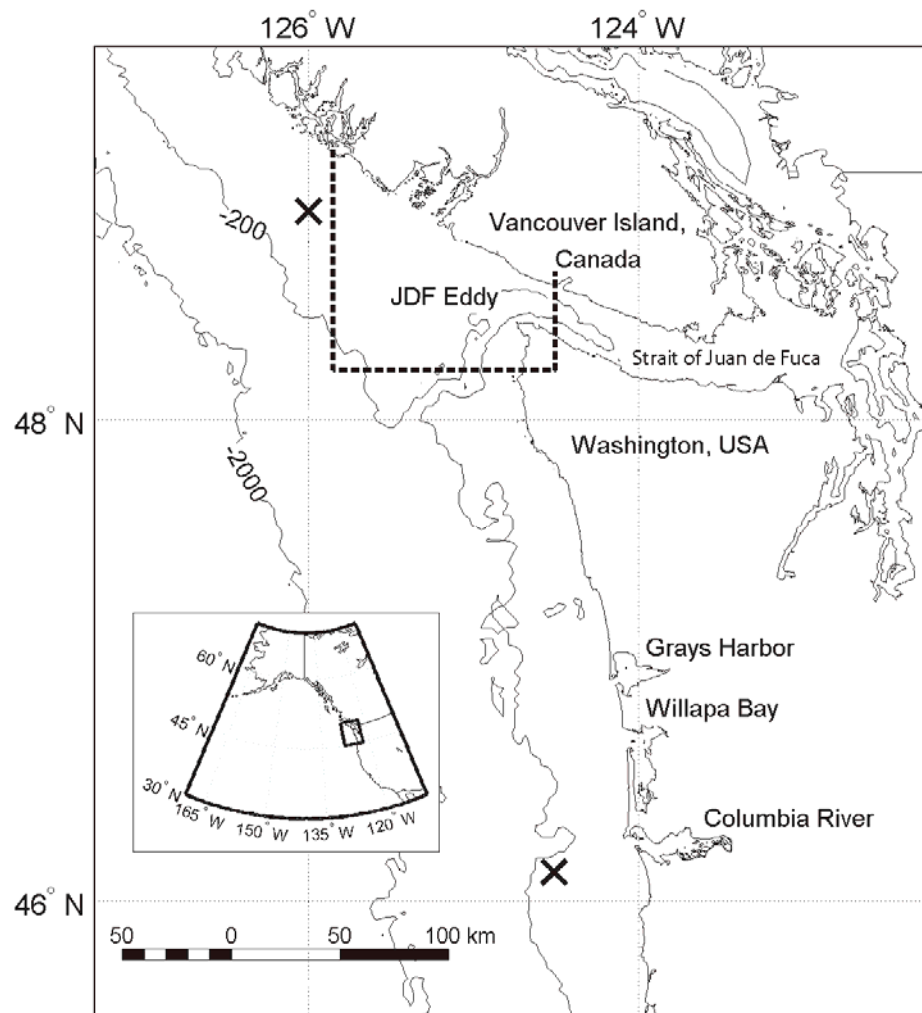


Figure 3.1 **Map of coastal waters of Washington, USA, and Vancouver Island, Canada.** Pacific Northwest (insert) and coastal waters of Washington, USA, and Vancouver Island, Canada. X denotes location of meteorological buoys at La Perouse Bank ($48^{\circ}50'24''$ N, $126^{\circ}00'00''$ W) and Columbia River Bar ($46^{\circ}07'12''$ N, $124^{\circ}30'36''$ W). The area typically occupied by the Juan de Fuca Eddy is redrawn from Tully (1942).

Figure 3.2 **SeaWiFS chlorophyll and sea surface temperature images.** SeaWiFS surface chlorophyll and sea surface temperature (SST) images; coordinates are given in (A) only. SeaWiFS image for 31 May 2002 shows clearly defined Juan de Fuca Eddy (A). SeaWiFS images for 22, 25, 26, 28 and 29 May 1999 (B–F) show transport event; color bar units are mg chl m^{-3} . SST images for 22, 25, and 28 May 1999 (G–I) are overlain with 5 mg chl m^{-3} contour lines generated from the co-located SeaWiFS images; SST color bar units are $^{\circ}\text{C}$.

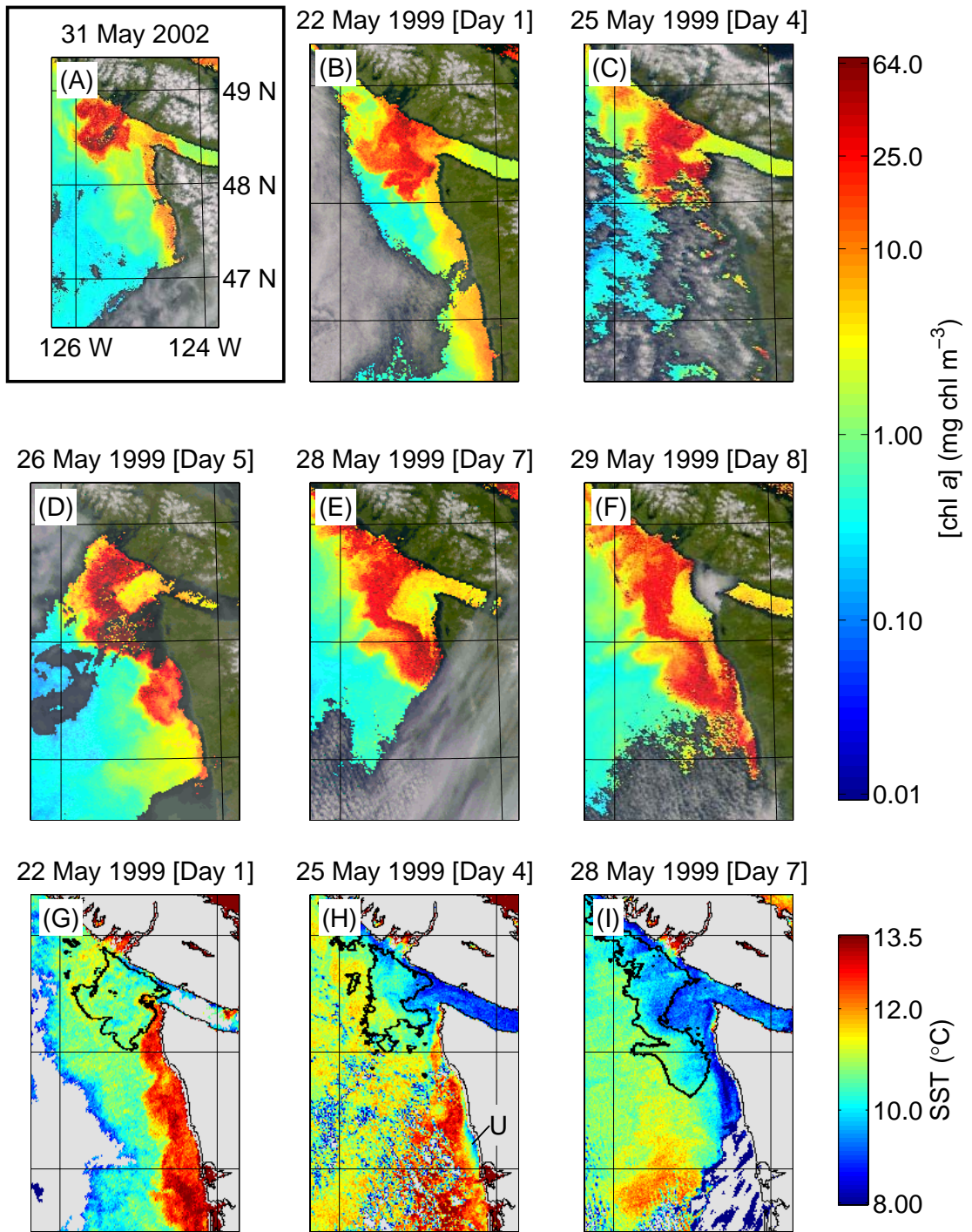
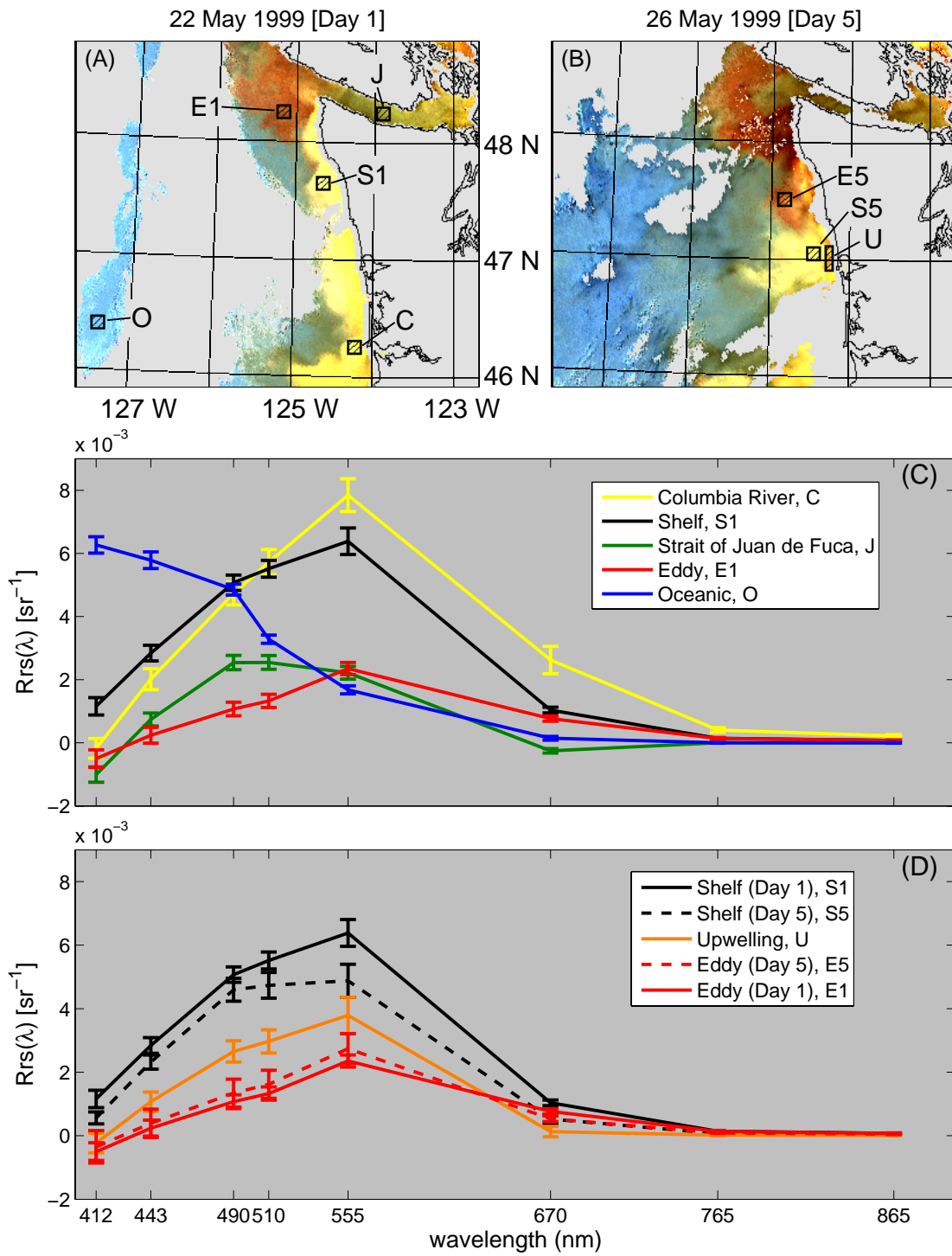


Figure 3.3 **RGB false color composite of SeaWiFS remote sensing reflectance.** RGB false color composites of SeaWiFS remote sensing reflectance ($R_{rs}(\lambda)$) at 555, 510, and 443 nm for 22 May (A) and 26 May 1999 (B). Remote sensing reflectance spectra were extracted from each optically-distinctive water mass (boxes in A–B); average spectra with error bars (± 1 standard deviation) are shown for 22 May (C) and 26 May (D).



sensing reflectance spectrum was determined by averaging 100 pixels (Fig. 3.3C–D). Chlorophyll *a* distributions were summarized using a geometric mean and geometric standard deviation (Table 3.1) because chl *a* is usually distributed log-normally (Campbell, 1995).

Corresponding infrared AVHRR images from the polar-orbiting weather satellite NOAA 14 were obtained at full 1.1-km² nadir resolution from NOAA's Comprehensive Large Array-data Stewardship System. Infrared measurements from Band 4 (10.3–11.3 μm) were converted to SST, mapped to transverse Mercator projections with an average pixel size of 1.1 km², and cloud/land masked (Fig. 3.2G–I). A simple cloud masking algorithm was applied where a pixel was defined as a cloud if the following two conditions were satisfied: 1) Band 4 was below freezing or Band 2 exceeded a reflectance threshold of 10% and 2) the difference between Band 3 and Band 4 exceeded 15°C.

Meteorological Buoys

Meteorological buoys, located at La Perouse Bank in the north and Columbia River Bar in the south (Fig. 3.1), provided wind speed and direction data (1 May–15 June 1999; Fig. 3.4). No observations were recorded at La Perouse Bank between 21–24 May. Data sources were Canadian Department of Fisheries and Ocean's Marine Environmental Data Service and NOAA's National Data Buoy Center. Observations were recorded hourly and decomposed into north-south and east-west components. Each component was smoothed independently using a 1-day median filter and subsampled at 6-h intervals.

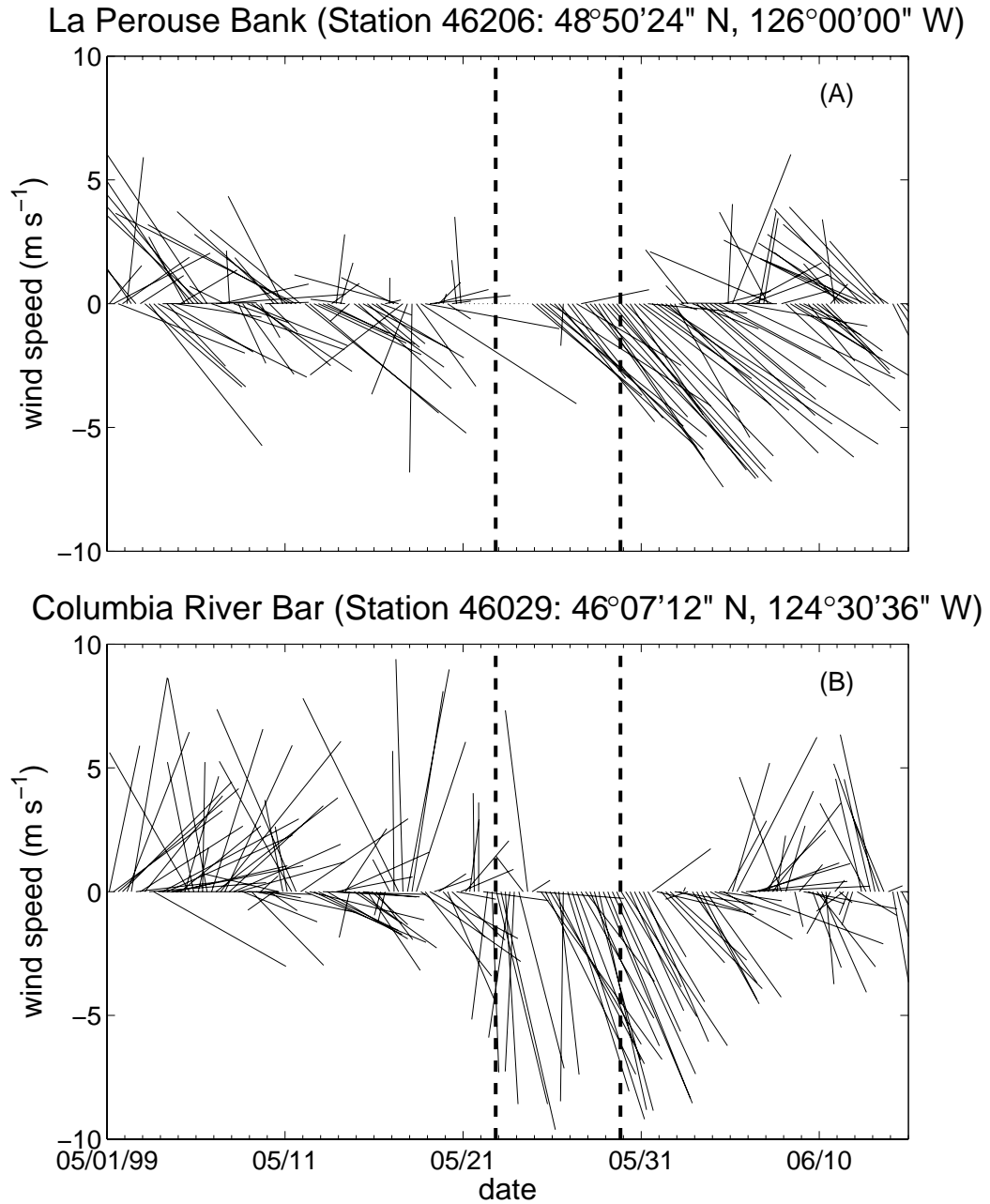


Figure 3.4 **Wind speed and direction between 1 May–15 June 1999.** Wind speed and direction between 1 May–15 June 1999 from meteorological buoys located at La Perouse Bank (A) and Columbia River Bar (B); buoy locations in Fig. 3.1. Dotted lines define the times of the transport event in Fig. 3.2. Positive numbers indicate winds are from the south; negative, from the north.

<u>Region</u>	<u>mean (μ)</u>	<u>mean – std ($\mu - \sigma$)</u>	<u>mean + std ($\mu + \sigma$)</u>
Columbia River, C	6.60	6.04	7.22
Shelf (Day 1), S1	3.69	3.27	4.17
Shelf (Day 5), S5	2.54	2.29	2.81
Strait of Juan de Fuca, J	1.52	1.42	1.63
Eddy (Day 1), E1	17.71	12.24	25.61
Eddy (Day 5), E5	15.90	9.54	26.50
Oceanic, O	0.18	0.16	0.20
Upwelling, U	5.11	3.82	6.41

Table 3.1 **Water mass summary statistics.** Geometric mean and geometric standard deviation (std) for satellite-derived chlorophyll *a* concentrations (mg chl m⁻³) within the eight optically-distinctive water masses described in the text.

Feature Tracking

Sequential gray-scale images of Rrs(555 nm) from 28 and 29 May were used to estimate surface advection speeds and directions (Fig. 3.5) because this wavelength has the greatest penetration in coastal waters, has a high signal-to-noise ratio, and was less affected by errors associated with atmospheric correction. We assumed that at spatial scales of variability ranging from 50–100 km, optically-active suspended material could serve as passive tracers over the 1–day interval separating the two images (Denman and Abbott, 1988; Denman and Abbott, 1994). The adaptive, least-squares image matching technique was patterned after Gruen (1985) to match pixels by establishing a correspondence that minimizes the squared sum of the differences of their gray values. A template, approximately 75 km x 75 km, was chosen from the image collected on 28 May (bounding box in Fig. 3.5A); corresponding coordinates for each pixel were then estimated for the image collected on 29 May. The method differs from traditional cross-correlation techniques (e.g., Emery et al., 1986) in that the coordinates of the two images are related through a six-parameter affine transformation and can therefore accommodate translation, rotation, scaling and/or shearing of the template from one image to the next (Equations 3.1 and 3.2). Each pixel's coordinates in the image from 29 May ($x_{\text{Day2}}, y_{\text{Day2}}$) correspond to a pixel's coordinates in the image from 28 May ($x_{\text{Day1}}, y_{\text{Day1}}$) according to

$$x_{\text{Day2}} = a_1 + a_2 x_{\text{Day1}} + a_3 y_{\text{Day1}} \quad \text{Equation 3.1}$$

$$y_{\text{Day2}} = b_1 + b_2 x_{\text{Day1}} + b_3 y_{\text{Day1}} \quad \text{Equation 3.2}$$

where a_{1-3} and b_{1-3} are the six affine transformation parameters. The vectors overlaid on both images in Fig. 3.5 illustrate the motion defined by the transformation parameters obtained from the final least-squares solution.

Results

Satellite-derived Chlorophyll *a* Distributions

As presented below, winds prior to 22 May 1999 were unfavorable to upwelling and switched, becoming more upwelling-favorable, after 22 May (Fig. 3.4). During the period after 22 May surface chlorophyll concentrations within the Juan de Fuca Eddy ranged from 10 to 25 mg m⁻³ (Table 3.1). Elevated chl *a* concentrations in the eddy, relative to ambient shelf concentrations, can be observed in many other SeaWiFS images during the period after the spring transition. However, in late summer when ambient shelf concentrations increase, it becomes more difficult to clearly distinguish the eddy from ambient shelf waters (Sackmann et al., 2004). In spring and early summer the high-chl *a* waters often appear centered in the region identified by Tully (1942) as cohesive and symmetric features with limited spatial extent (e.g., Fig. 3.2A–B). While Tully (1942) delineated the most probable location of the Juan de Fuca Eddy, its precise location is not constant, but varies with local wind forcing and/or buoyant discharge from the Strait of Juan de Fuca. Figure 3.2A shows a satellite ocean color image from another year (31 May 2002) with the high biomass of the eddy clearly defined, although its location is displaced to the northwest compared to the image from 22 May 1999 (Fig. 3.2B). Other SeaWiFS images observed between 1998–2004 resemble the later phase of

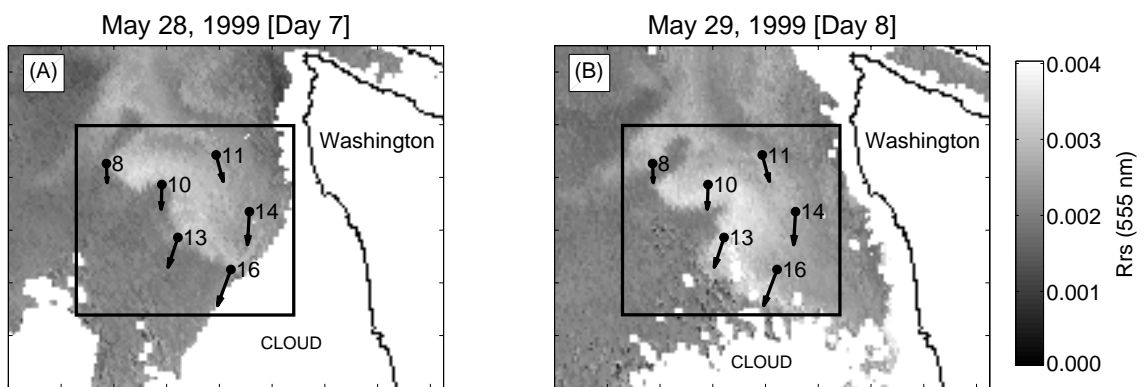


Figure 3.5 **Feature tracking.** Gray-scale images of $R_{rs}(555 \text{ nm})$ from 28 May (A) and 29 May 1999 (B). Arrows indicate trajectory of features and numbers indicate distance traveled (km) over 24 h.

our sequence (e.g., Fig. 3.2C–F) and depict features that are larger, more filamentous and asymmetric, extending southward into Washington coastal waters. The eight-day sequence in May 1999, in which we were able to track the movement of water from the eddy, is unique because it was an exceptionally clear period that appeared to capture an entire transport event.

Optical Characterization of Water Masses

Four optically-distinctive water masses, each with a unique remote sensing reflectance spectrum, were identified in the RGB composite for 22 May (Day 1; Fig. 3.3A): the Columbia River (C) and Washington shelf (S1), Strait of Juan de Fuca (J), Juan de Fuca Eddy (E1), and offshore oceanic waters (O). Spectral remote sensing reflectance is primarily determined by scattering and absorption of light by pure water, phytoplankton, suspended mineral particles, and other colored dissolved material (CDM). In coastal waters concentrations of each substance can vary independently and $Rrs(\lambda)$ can be expressed as a proportionality using the total backscattering ($b_b(\lambda)$) and absorption ($a(\lambda)$) coefficients for a given water mass (Equation 3.3; Gordon et al., 1988; Sathyendranath et al., 2000):

$$Rrs(\lambda) \propto \frac{b_b(\lambda)}{a(\lambda) + b_b(\lambda)} \quad \text{Equation 3.3}$$

In productive and/or turbid waters $Rrs(\lambda)$ will be underestimated due to difficulties with atmospheric correction, with increasing severity at shorter wavelengths (Siegel et al.,

2000; Stumpf et al., 2003). The magnitude of error is difficult to quantify and may lead to negative values of SeaWiFS-derived $R_{rs}(\lambda)$ at blue wavelengths and inaccuracies in calculation of absolute pigment concentration. Possible adjacency or proximity effects may also introduce errors in $R_{rs}(\lambda)$ for water pixels located very close to land and/or clouds. Despite these limitations, the remote sensing reflectance spectra is diagnostic of individual water masses.

The eddy had low values of $R_{rs}(\lambda)$ typically associated with high concentrations of strongly absorbing phytoplankton. The average spectrum of waters in the Strait was similar to the eddy's, but significantly different at 490 and 510 nm (see error bars associated with each average spectrum in Fig. 3.3C), most likely due to lower concentrations of blue-absorbing material (both phytoplankton and CDM). The spectra of Columbia River and Washington shelf waters were very different from the eddy's. The high values of $R_{rs}(\lambda)$ are consistent with high concentrations of non-absorbing, suspended mineral particles, with a high index of refraction relative to phytoplankton (Twardowski et al., 2001, Slawomir and Stramski, 2004). Measurements of spectral backscattering made with an underwater autonomous glider in April 2002 confirm the presence of non-absorbing particles throughout the entire water column on the shelf, at the mouth of the Strait (Eriksen and Perry, unpub.). Offshore, the spectrum was typical of clear blue ocean waters with low phytoplankton biomass (Sathyendranath et al., 2000).

By 26 May (Day 5) higher biomass water was observed along the northern Washington coast, extending seaward as far as 45 km (Fig. 3.2D). This water mass had a spectral signature identical to that of the eddy (orange water mass in Fig. 3.3B; spectrum E5 in Fig. 3.3D) and appeared to have displaced the original shelf water mass to the

south. In the south, the shelf water retained the high reflectance spectrum similar to that on Day 1 (yellow water mass in Fig. 3.3B; spectrum S5 in Fig. 3.3D).

Sea Surface Temperature Distributions

Waters on the Washington shelf on 22 May (Day 1) were approximately 2°C warmer than oceanic waters farther offshore (Fig. 3.2G), reflecting the preceding period of downwelling-favorable winds (see below, *Meteorological observations*). The spatial pattern of this warm, coastal water mass matched that of the highly reflective Columbia River and Washington shelf water masses identified in the RGB composite image (Fig. 3.3A). Although though no *in situ* observations were collected as part of our study, between 23 and 25 May 1999 Roegner et al. (2002) conducted a ship-based survey from 46°30' to 47°00' N and seaward from the coast to 125°00' W. During their survey, the Columbia River plume was clearly evident in both the temperature and salinity measurements and manifested as a region of warm, fresh water that extended from the coast to at least 60 km offshore (their furthest offshore sample). Within the Columbia River plume *in situ* temperatures near the surface were approximately 13°C, in good agreement with the AVHRR SST values obtained on 22 May (Fig. 3.2G).

Unfortunately, a cloud-free image of SST could not be obtained for 26 May (Day 5), therefore, the SST image for 25 May (Day 4) was used to define the temperature characteristics of newly upwelled water along the Washington coast. A narrow band of very cold water was observed close to the coast (Fig. 3.2H); the spectrum of this newly-upwelled water was intermediate between the eddy and original shelf waters (spectrum U in Fig. 3.3D). Over the next few days, upwelling of cold water continued (28 May, Fig.

3.2I), although much of the high biomass water remained seaward of the primary temperature front (Fig. 3.2F).

Meteorological Observations

Between 1–21 May 1999, the period preceding the transport event, wind speed and direction were primarily favorable to downwelling at the Columbia River Bar on the Washington shelf but were more variable at La Perouse Bank on the Vancouver Island shelf (Fig. 3.4). Available wind data suggest that between 22 May and early June moderate to strong upwelling-favorable conditions (i.e., winds towards the south) persisted from La Perouse Bank to Columbia River Bar. The gap in the data record for La Perouse Bank between 21–24 May is unfortunate (as is the lack of data from the Cape Elizabeth buoy, just south of the eddy), but given the strength of the upwelling winds observed at Columbia River Bar and the degree to which the two wind records appear correlated thereafter, upwelling-favorable conditions were most likely present at La Perouse Bank during this time period. Theoretical near-surface flow is oriented 45° to the right of the surface windstress under stationary conditions and constant eddy viscosity (Ekman, 1905, Krauss, 1993). Numerous attempts to verify Ekman theory have been made, but quantitative agreement is difficult to obtain in the field. In general, surface current deflections to the right of the windstress are observed; however, the angle of deflection can vary over a large range (Krauss, 1993). A gradient in wind direction was observed between the two meteorological stations, with winds oriented alongshore at each location. Given the orientation of the Vancouver Island coast relative to the

Washington coast, alongshore windstress off Vancouver Island should result in a generally southward near-surface flow.

Feature Tracking

Estimates of surface currents were determined from a SeaWiFS image sequence for 28 and 29 May (Days 7 and 8). The average surface currents speeds derived from feature tracking ranged between 8 and 16 km d⁻¹, oriented in a southward direction (Fig. 3.5). The magnitude of the estimated surface currents was sufficient to transport the high biomass waters from the Juan de Fuca Eddy to the Washington shelf between 22 and 26 May (Days 1 to 5).

Discussion

The large-scale regional circulation is dominated by the North Pacific Current or West Wind Drift that bifurcates into the southward flowing California current system and the northward flowing system that joins the Alaskan Gyre (Hickey, 1989). Northerly winds begin to dominate the coastal wind field in late spring and persist through the summer, leading to the seasonally intense offshore Ekman transport and coastal upwelling that is common to the west coast of the United States (Smith, 1995). The Strait of Juan de Fuca is approximately 20 km wide along its length and behaves like a large estuary, wherein freshwater outflow at the surface is provided primarily by discharge from the Fraser River during spring and summer months (Hickey et al., 1991). Tully (1942) described the Juan de Fuca Eddy as being formed through the interaction of the Strait outflow, flowing north along the coast of Vancouver Island as a buoyant plume

(Hickey et al., 1991), and southward flowing wind-induced currents farther offshore that develop after the spring transition (Huyer et al., 1979). The eddy, in conjunction with the underlying bathymetry, results in the localized upwelling of extremely deep (approximately 450 m) and dense ($\sigma_t = 26.6$) water onto the continental shelf (Freeland and Denman, 1982).

High primary productivity and diatom-dominated phytoplankton biomass have been observed within the Juan de Fuca Eddy (Trainer et al., 2002, Marchetti et al. 2004). The eddy can often be distinguished in ocean color satellite images as a coherent patch of high-chl *a* (Fig. 3.2) with low reflectance (Fig. 3.3C–D). The large difference in the remote sensing reflectance spectra (Fig. 3.3) that we observed in May 1999 between the low-reflectance waters of the eddy and the high-reflectance waters of the Washington shelf is due to high concentrations of phytoplankton in the eddy (high absorption of light) and the presence of suspended mineral particles in the shelf waters (enhanced backscattering of light). Monitoring the location and movement of water from the Juan de Fuca Eddy could be an important public health management tool, due to the large numbers of *Pseudo-nitzschia* spp. that are often found within the eddy (Trainer et al., 2002).

The nearshore distribution of *Pseudo-nitzschia* is of key importance in terms of DA and its potential impacts on shellfish fisheries along the Washington coast. Even though water from the eddy did not appear to intersect the shore during this transport event in May 1999, except perhaps north of 48° N on 25–26 May (Fig. 3.2C–D), our observations retain a general relevance to the potential delivery of *Pseudo-nitzschia* to the Washington coast. If similar transport events are followed by episodic shifts from

upwelling to downwelling-favorable conditions, phytoplankton cells may be delivered directly to northern Washington beaches by the onshore-flowing surface currents that develop (Roegner et al., 2002; Trainer et al., 2002; McGillicuddy et al., 2003, MacFadyen et al., 2005). Northern Washington beaches tend to have higher levels of DA and more frequent beach closures. During downwelling-favorable conditions the rapid northward advection of the Columbia River plume could act as a barrier to the transport of offshore phytoplankton blooms to southern Washington beaches, perhaps keeping them somewhat protected (Hickey et al., 2005). Even under persistent upwelling-favorable conditions, cells that sink from the surface into deeper onshore-flowing waters may provide an inoculum for *Pseudo-nitzschia* that ultimately are upwelled nearshore (Brink et al., 1981; Smith et al., 1983). The ability to detect and track this water mass, even when it remains offshore, could improve the prediction of outbreaks of toxic *Pseudo-nitzschia* spp. along the Washington coast (Trainer and Suddleson, 2005).

Under most conditions the fresher water exiting the Strait of Juan de Fuca (Fig. 3.2G-I) flows north along the Vancouver Island coast as a buoyant plume. However, the discharge from the Strait of Juan de Fuca, when associated with upwelling-favorable conditions, has been observed to turn and flow southward during periods of strong forcing (Hickey, 1991). Ikeda and Emery (1984) used a series of thermal images to follow changes in SST associated with a continental shelf upwelling event off of Vancouver Island in the summer of 1980. Analogous to the results presented here, they noted that wind-driven upwelling could dramatically influence the surface expression of the Juan de Fuca Eddy, extending the cold water boundary of the eddy to the shelf break. Venkatesh and Crawford (1993), using observations of oil leaked from a fishing vessel

that sank off the western entrance to the Strait of Juan de Fuca and a series of numerical simulations, demonstrated southward transport of surface water from the eddy. Surface drifters deployed in the Juan de Fuca Eddy in June 1985 were observed to leave the eddy and travel in a southeasterly direction towards the Washington coast (Emery et al., 1986). More recently, MacFadyen et al. (2005) tracked surface drifters that escaped the eddy; these drifters traveled southeast at velocities of 8–26 km d⁻¹ and had maximum velocities approaching 34 km d⁻¹ near the coast, well in excess of the velocities of 8–16 km d⁻¹ that we obtained through feature tracking. The southward displacement of the patch from 22 to 26 May was between 60–85 km. Velocities estimated from the image sequence obtained on 28 and 29 (Days 7 and 8) appeared to increase towards the coast with velocities in the central portion of the patch ranging from 13–16 km d⁻¹. Assuming these velocities are representative of those experienced from 22 to 26 May (Days 1 to 5), the corresponding displacement estimate is between 52–64 km, with larger displacements possible near the coast. Therefore, it is likely that the high biomass observed on the Washington shelf on 26 May originated in region occupied by the Juan de Fuca Eddy on 22 May.

The sequence of SeaWiFS and AVHRR images in May 1999 (Fig. 3.2) documents the southward transport of high biomass waters from the Juan de Fuca Eddy into waters overlying the Washington shelf. Figure 3.6 outlines the main features of the transport event as it was observed, and illustrates the potential importance of relaxation events (i.e., a switch from upwelling to downwelling-favorable conditions) as a mechanism that could allow the offshore patch of high biomass from the Juan de Fuca Eddy to interact with Washington beaches. The SeaWiFS image on 22 May (Fig. 3.2B)

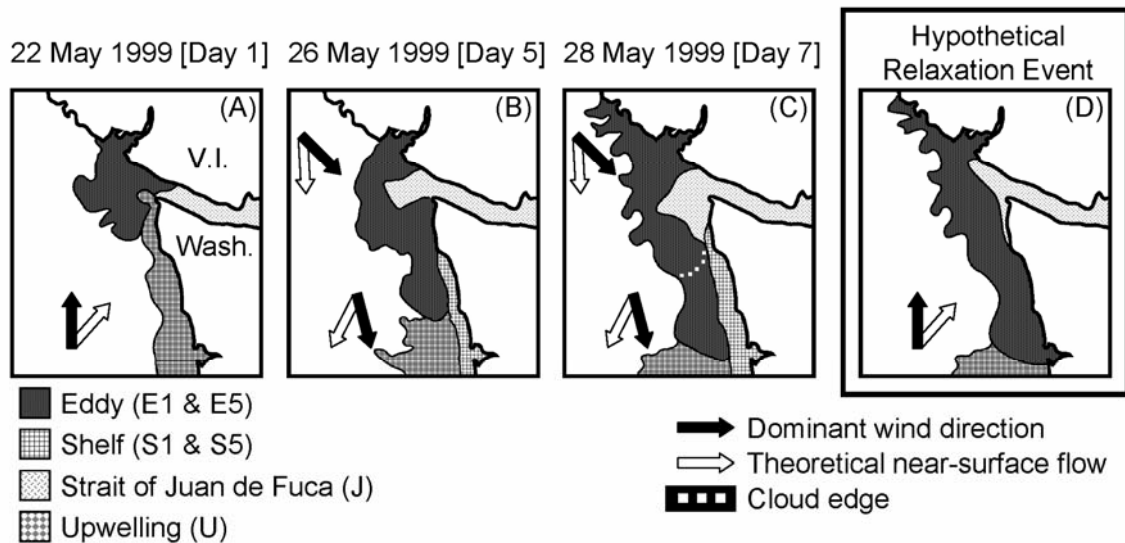


Figure 3.6 **Schematic of transport event observed in May 1999.** Schematic outline of the transport event as it was observed in May 1999 (A–C). Water mass boundaries were approximated from images of surface chlorophyll (Fig. 3.2B–F), remote sensing reflectance (Fig. 3.3A–B), and sea surface temperature (Fig. 3.2G–I). A *Hypothetical Relaxation Event* (i.e., a shift from upwelling to downwelling-favorable conditions), although not observed as part of our study, could allow the offshore patch of high biomass from the Juan de Fuca Eddy to interact with Washington beaches (D).

shows a fairly cohesive eddy within the region described by Tully (1942; redrawn in our Fig. 3.1) with the characteristic high chl *a* and low remote sensing reflectance (Figs. 3.3A, C and 3.6A). By 26 May (Fig. 3.2D) the waters from the eddy appear less cohesive, extending further to the south. Cooler, lower-chl *a* surface waters discharged from the Strait of Juan de Fuca had moved offshore and southward, perhaps deforming the surface expression of the eddy and contributing to its southward transport (Fig. 3.6B). The chl *a* concentrations observed on the northern Washington shelf (box E5 in Fig. 3.3B) remained high and the remote sensing reflectance remained low (spectrum in Fig. 3.3D), similar to the eddy at the beginning of the sequence. This water was very different from the water immediately to its south (box S5 in Fig. 3.3B) in both chl *a* (Table 3.1) and reflectance spectrum (Figs. 3.3D and 3.6B). On 28 May (Fig. 3.2E), the outflow from the Strait is clearly visible as low-chl *a* water and the more filamentous region of high-chl *a* water from the eddy remained seaward of the primary temperature front (Figs. 3.2G and 3.6C). Cloud cover patterns on 28–29 May were unfortunate, since it is likely that the high chl *a* water continued moving southward but cloud occlusion hindered further resolution (Figs. 3.2E–F and 3.6C). The end of the sequence on 29 May (Fig. 3.2F) shows a broad band of high-chl *a* water occupying most of the shelf and extending as far south as 47° N. A relaxation event was not observed in early June 1999 and the high biomass from the Juan de Fuca Eddy likely remained offshore. However, had the upwelling favorable winds relaxed or switched to downwelling-favorable winds, offshore phytoplankton cells could have been delivered to Washington beaches (Fig. 3.6D).

We considered, as an alternative explanation to a transport event, the development of a separate, independent bloom on the Washington shelf as conditions became more

suitable for phytoplankton growth. Prior to 22 May, wind conditions were unfavorable to upwelling; on 22 May the winds switched, becoming more favorable to upwelling (Fig. 3.4). Upwelling-favorable conditions typically result in southward and offshore flow of surface waters with replacement by colder, nutrient-rich waters near the coast (Hickey, 1989). By 25 May (Fig. 3.2H) a narrow band of cold, presumably freshly-upwelled water was visible in the AVHRR image; by 28 May a broad band of cold water was present on the entire shelf. Could the high biomass waters observed on the northern Washington shelf on 26 May (box E5 in Fig. 3.3B) been produced locally, following the switch to upwelling-favorable winds?

On 22 May the remote sensing reflectance spectrum for Washington shelf waters was similar along the entire Washington coast (yellow-colored region in Fig. 3.3C); the spectrum for box S1 in Fig. 3.3A was very similar to the spectrum for waters at the mouth of the Columbia River (box C). The waters overlying the shelf during the downwelling-favorable conditions that had persisted since 1 May (Fig. 3.4) most likely originated in the Columbia River and had moved northward along the coast (Hickey, 1989). SeaWiFS chl *a* (Table 3.1) and fluorescence-based estimates of chlorophyll concentrations collected south of 47° N during the cruise of Roegner et al. (2002) between 23–25 May 1999 indicated that waters with these reflectance spectra contained relatively low concentrations of phytoplankton (Fig. 3.6A).

On 25 May, three days after the initiation of upwelling-favorable winds, a thin band of cold water was observed near the coast; however, the offshore extent of this water mass was limited to <15 km (for example, area U in Fig. 3.2H). A corresponding thin band of high-chl *a* water was observed near the coast on 26 May (Fig. 3.2D) with a

reflectance spectrum (U in Fig. 3.3D) intermediate between the high-biomass eddy (E1 and E5) and the reflective waters of the shelf (S1 and S5). We interpret these patterns to indicate local production of phytoplankton in this narrow band of nutrient-rich, freshly-upwelled water adjacent to the coast. In contrast, in waters approximately 25–45 km off the coast chl *a* concentrations were very different on the northern Washington shelf vs. the southern Washington shelf. North of 47°30' N, average pigment concentration was >15.9 mg chl m⁻³ while to the south, it was <2.5 mg chl m⁻³ (Fig. 3.2D and Table 3.1). The remote sensing reflectance spectra also differed in the north vs. south (Fig. 3.3B, D). North of 47°30' N, the spectrum (E5) was similar to that of the original eddy (E1), while south of 47°30' N, the spectrum (S5) was similar to the original shelf water (S1). We interpret these patterns to indicate transport of phytoplankton from the eddy as far south as 47°30' N by 26 May (reddish-colored region in Fig. 3.3B) and displacement of Columbia River plume waters (yellow-colored regions) further south (Fig. 3.6B).

Conclusions

Over an 8-day period in May 1999 we observed the southward transport of water from the Juan de Fuca Eddy onto the Washington shelf with surface velocities of approximately 8-16 km d⁻¹. Spectral characteristics of the patch were different from waters on the Washington shelf and support the hypothesized southward transport of surface water from the eddy during this event. Ocean color and AVHRR SST data indicate that the biological response to wind-driven coastal upwelling was restricted to a narrow (10-15 km) region along the Washington coast, making it unlikely that the entire region of high biomass observed off the Washington coast was produced locally.

Specifically, we believe that,

- 1) by using a *time series* of remotely sensed images, both ocean color and SST, we have strengthened the case that productive waters from the Juan de Fuca Eddy can be transported southward, and thereby influence the distribution of potentially toxic *Pseudo-nitzschia* off the Washington coast; and that,
- 2) the image sequence provides a basis for interpreting isolated images that resemble those in Fig. 3.2D–F.

Extended time series of ocean color satellite images are rare in the Pacific Northwest because of the frequent cloud cover, but a number of isolated SeaWiFS images from 1998 to 2004 do show large, asymmetric features that extend southward into Washington coastal waters. The complete sequence capturing the transport event in May 1999 suggests that many of these isolated images document the final stages of similar, southward transport events. Data mining of near real-time ocean color datasets, such as those provided historically by SeaWiFS and currently by MODIS, allow for the systematic and sustained monitoring of Washington coastal waters at spatial and temporal resolutions unattainable by traditional field-based sampling programs. Using $Rrs(\lambda)$ to track trajectories of water masses that may be associated with potentially harmful algal species could be used as an important public health management tool to initiate

intensified conditional sampling for marine biotoxins, including domoic acid, along the Washington coast.

Acknowledgements

This work was supported by Washington State Sea Grant (NA76RG0119), NASA (NAG5-9959 and NAG5-7604), and the National Science Foundation Graduate Research Fellowship Program.

Chapter 4

MULTI-PLATFORM DATA FUSION: MERGING IN-WATER SEAGLIDER OPTICS AND SATELLITE OCEAN COLOR TO OBSERVE QUASI-4-DIMENSIONAL PHYTOPLANKTON DISTRIBUTIONS OFF THE WASHINGTON COAST

From August 2003 – present, Seaglider – a long-range autonomous glider – has been conducting repeat surveys off the Washington coast along a V-shaped transect that extends 200 km seaward from the continental shelf break into deep oceanic waters. Highly resolved (~5 km horizontal spacing, ~1 m vertical resolution, ~15 d temporal resolution) sections across the northern California Current System (CCS) provide measurements of temperature, salinity and dissolved oxygen to 1000 m, and chlorophyll *a* fluorescence (proxy for phytoplankton concentration) and optical backscattering (proxy for particle concentration) to 150 m. The standard V-shaped transect occupied by Seaglider spans a dynamic transitional region that links a highly productive shelf environment with the open ocean. In-water optical measurements allowed us to build a quasi-4-dimensional representation of the phytoplankton distribution within a large scale (~150 km) meander of the California Current System that formed a detached cyclonic eddy off the Washington coast, USA, in September and October 2004. Satellite assessment of total water column biomass within this feature, compared to surrounding oceanic waters, is problematic because subsurface phytoplankton maxima are hidden from satellite view. Glider observations provide a particularly efficient and cost-effective way of supplying a vertical context to satellite data, and are unique in their ability to revisit features of interest, such as eddies, once they have been detected. Gliders can also

provide measurements under persistently cloudy conditions when synoptic time series of satellite ocean color measurements are difficult to obtain. The addition of Seaglider to our measurement program has improved our ability to accurately interpret satellite ocean color measurements and allowed us to extend our interpretation of these measurements beyond the sea surface.

Introduction

Gliders represent a new class of ocean remote sensing platform that can be used as efficient and cost-effective tools to provide a vertical context to satellite data (Rudnick and Perry, 2003; Rudnick *et al.*, 2004). By combining near-surface measurements from these disparate platforms one can ensure a seamless transition between *in-situ*, glider-based measurements and measurements obtained using satellites. Here we have merged ocean color satellite imagery of the surface with subsurface optical observations from Seaglider – a long-range autonomous glider (Fig. 4.1; Eriksen *et al.*, 2001) – to produce a quasi-4-dimensional representation of phytoplankton distributions in September and October 2004 within a detached eddy that formed off the Washington coast (Fig. 4.2). Historical observations show that towards the end of August shorter scale meanders (~75-80 km) of the California Current System (CCS) off Washington and Vancouver Island, Canada can be engulfed by larger scale meanders (~150 km) which have been observed to shed large, persistent, cyclonic eddies in the fall (Ikeda *et al.*, 1984a; Ikeda *et al.*, 1984b). These eddies can then lead to episodic enhancement of offshore primary production seaward of the shelf-slope break (Mackas and Yelland, 1999).

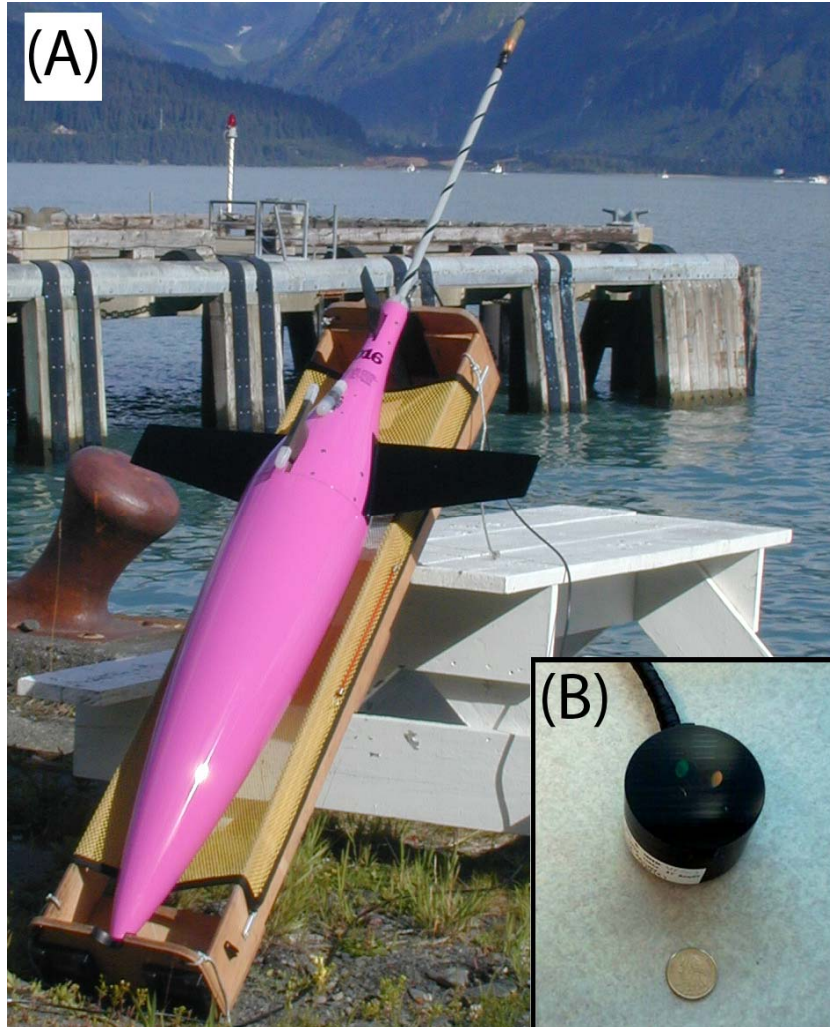


Figure 4.1 **Eriksen Seaglider.** Eriksen Seaglider developed at University of Washington (A). WET Labs ECO-BB2F shown with a quarter for scale (B).

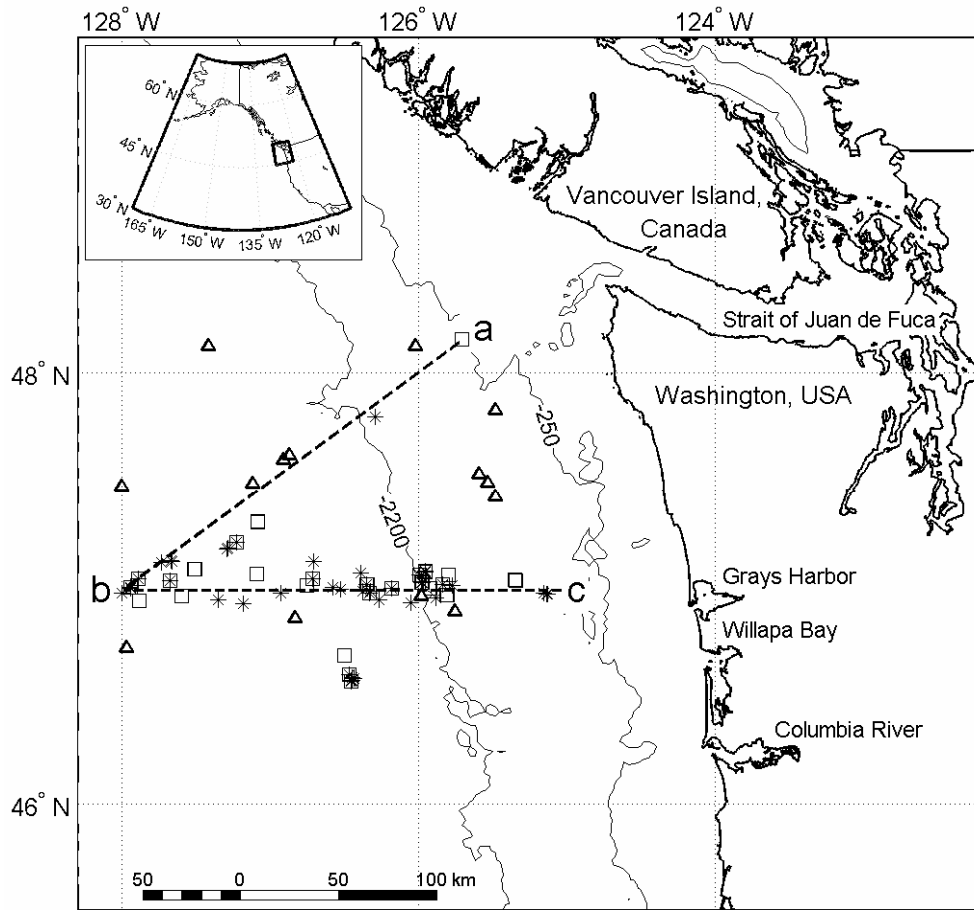


Figure 4.2 **Map of Washington coast showing locations of Seaglider/satellite matchups.** Map of Washington coast. Seaglider/satellite matchups are denoted with squares (SeaWiFS) and asterisks (MODIS Aqua). Triangles denote locations of historical nutrient profiles obtained from the World Ocean Database. Lower-case letters ‘a-c’ serve as spatial references defining the V-shaped transect used by Seaglider (dotted line).

The strength of Seaglider lies not in the ability of a single glider to synoptically sample an entire region of interest, but instead, the eventual use of multiple gliders (possibly of differing type) deployed simultaneously in a distributed network. The fusion of data from this sort of ‘glider-based’ remote sensing platform with more conventional technologies (e.g., satellites, drifters, moorings, etc.) could help to resolve oceanographic patterns and processes over an adaptable range of spatial and temporal scales. Since gliders can easily receive new mission instructions without being recovered they can evolve in the way they sample the ocean (even during a single mission) and are unique in their ability to revisit features of interest once they have been detected. This makes gliders particularly well suited for studying episodic mesoscale phenomena such as eddies. Without Seaglider an assessment of total water column biomass for waters in and around this eddy would have been problematic because subsurface phytoplankton maxima are hidden from satellite view. It is also difficult to obtain synoptic time series of satellite ocean color measurements due to regional persistence of cloud cover for much of the year (Sackmann *et al.*, 2004). Seaglider has given us a sustained presence in these waters and allowed us to remotely assess the vertical distribution of phytoplankton biomass within this offshore cyclonic eddy and compare it with surrounding water masses and conditions from different years.

Data and Methods

Satellite Data Products

Sea Level and Geostrophic Velocity Anomalies. Bi-weekly maps of sea level anomaly (SLA) and geostrophic velocity anomaly were derived from measurements collected

using the radar altimeter onboard the Jason-1 satellite from 27 September 2003 and from 4 September – 30 October 2004 (Fig. 4.3). These gridded data products are distributed by Aviso through a Live Access Server available from their website (<http://www.aviso.oceanobs.com>). Anomalies were computed relative to a seven-year mean (1993 – 1999) and gridded to a $1/3^\circ \times 1/3^\circ$ Mercator grid. Detailed processing methodologies can be found on the Aviso website.

Sea Surface Temperature and Ocean Color. A collection of sea surface temperature (SST) and ocean color measurements was obtained for waters off the Washington coast ($44\text{-}52^\circ \text{ N}$, $120\text{-}132^\circ \text{ W}$) from April 2002 – present. Seaglider has been operating almost continuously in this region since August 2003, however, two earlier deployments were conducted in April and September 2002. This database includes a standard suite of SST and ocean color products from the MODerate Resolution Imaging Spectroradiometer onboard NASA's Aqua satellite (MODIS Aqua) and ocean color measurements from the Sea-viewing Wide Field-of-View Sensor (SeaWiFS). All SST and ocean color data was obtained as processed Level 2 local-area-coverage files at full 1.1 km^2 nadir resolution from NASA's OceanColor WEB (<http://oceancolor.gsfc.nasa.gov>). The data are consistent with MODIS Aqua reprocessing v.1.1 and SeaWiFS reprocessing v.5.1. A complete list of the Level 2 (L2) products included in each file and processing methodologies can be found on NASA's OceanColor WEB website.

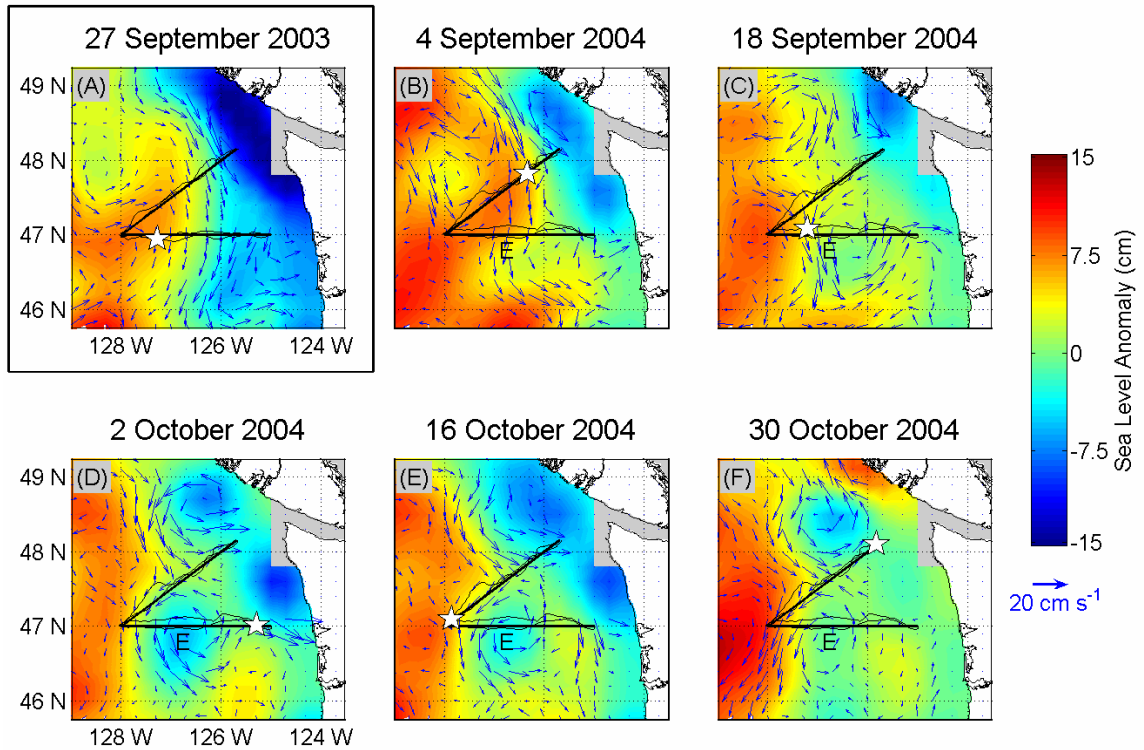


Figure 4.3 **Sea level and geostrophic velocity anomalies.** Satellite-derived sea level and geostrophic velocity anomalies from 27 September 2003 (A) and 4 September – 30 October 2004 (B-F). Seaglider track is overlaid; star denotes point of coincidence with Seaglider. The approximate location of the cyclonic eddy observed in September and October 2004 is denoted as ‘E’.

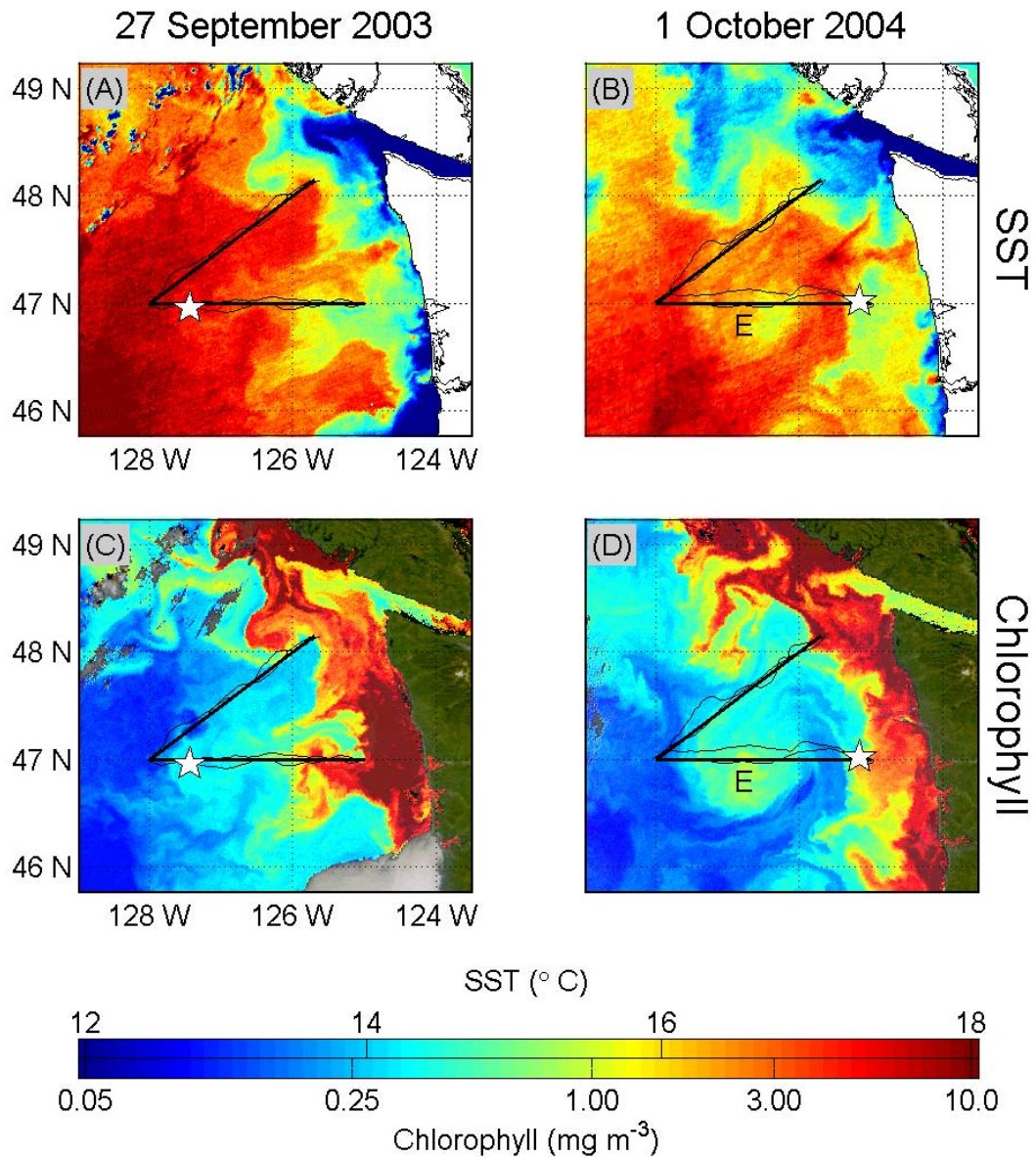


Figure 4.4 **Sea surface temperature and ocean color from 27 September 2003 and 1 October 2004.** Satellite-derived sea surface temperature (MODIS Aqua) and ocean color (SeaWiFS) from 27 September 2003 (A and C) and 1 October 2004 (B and D). Seaglider track is overlaid; star denotes point of coincidence with Seaglider. The approximate location of the cyclonic eddy as observed on 1 October 2004 is denoted as 'E'.

From this collection MODIS Aqua SST measurements from 27 September 2003 and 1 October 2004 were chosen as representative of conditions observed in fall 2003 and 2004 (Fig. 4.4A-B). Corresponding measurements of surface chlorophyll *a* concentration (chl *a*) and water leaving radiance at 555 nm (nLw(555)) were obtained from SeaWiFS. (Figs. 4.4C-D, 4.5A-B, 4.6A-B). This collection of satellite data was also used for the matchup analyses and data density calculations presented below (Figs. 4.5-4.7).

Seaglider Data

Vehicle Characteristics, Deployment History, and Instrumentation. Seaglider is an autonomous underwater glider developed by Dr. C. Eriksen (University of Washington) and colleagues. Seaglider is equipped with wings that provide lift, and moves through the water in a sawtooth pattern by adjusting its buoyancy. Buoyancy is controlled by pumping oil from an external bladder into (glider becomes more dense), or out of (glider becomes less dense), the pressurized hull. Pitch and roll are adjusted by shifting the location of the high-voltage battery packs within the vehicle. The maximum horizontal range is currently 5,500 km at 25 cm s⁻¹ horizontal speed and it is capable of diving 900 times to 1000 m depth over a 7 month period in weakly stratified portions of the ocean. To date, Seaglider has completed 12 deployments off the Washington coast and performed other missions in the Gulf of Alaska, Davis Strait/Labrador Sea, and subtropical Pacific near the Hawaii Ocean Time-series (HOT) station. Seaglider is completely autonomous and uses Iridium satellite telephone communication to download

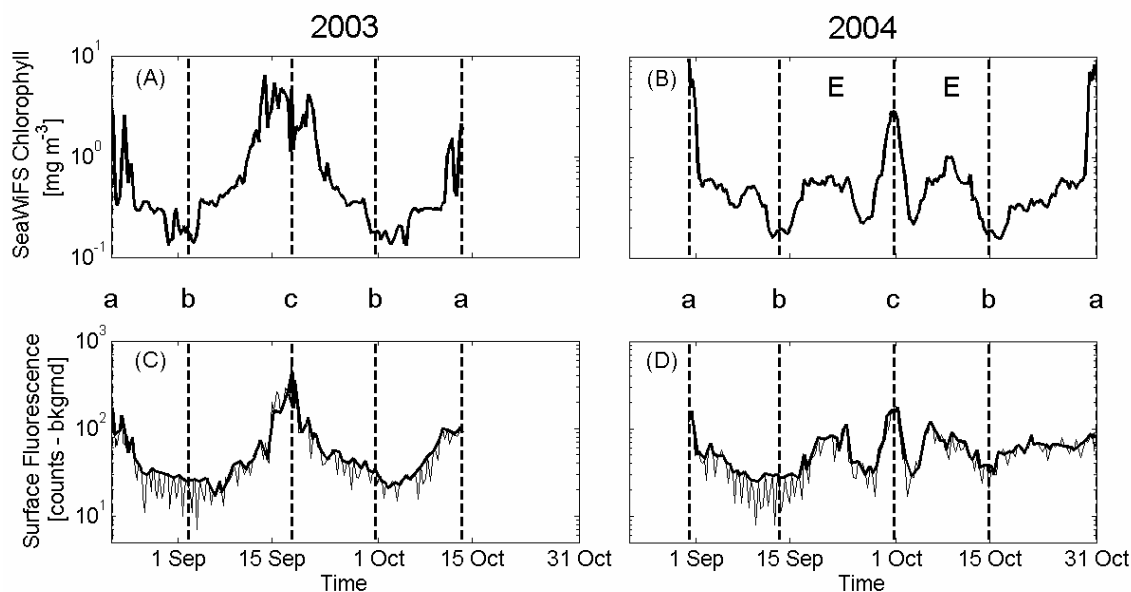


Figure 4.5 **Satellite-derived chlorophyll estimates compared with Seaglider fluorescence.** Satellite-derived chlorophyll estimates from 27 September 2003 (A) and 1 October 2004 (B) along the Seaglider transects shown in Figs. 4C-D and surface Seaglider fluorescence (C-D) plotted as a function of Seaglider time. The bold line in C-D traces fluorescence measurements made at night to help identify variability associated mid-day fluorescence quenching. Lower-case letters ‘a-c’ serve as spatial references as in Fig 4.2. The approximate location of the cyclonic eddy as observed in September and October 2004 is denoted as ‘E’.

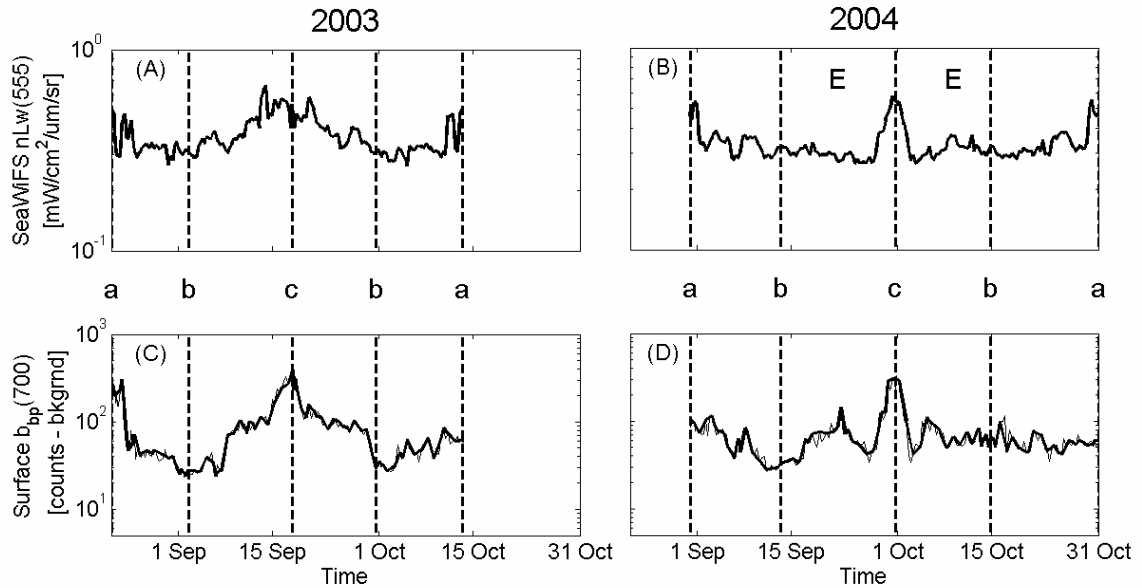


Figure 4.6 **Satellite-derived estimates of water leaving radiance at 555 nm compared with Seaglider near-infrared backscatter by particles.** Satellite-derived estimates of the water leaving radiance (nLw) at 555 nm from 27 September 2003 (A) and 1 October 2004 (B) along the Seaglider transects shown in Figs. 4C-D and surface Seaglider near-infrared backscatter by particles ($b_{bp}(700)$); C-D) plotted as a function of Seaglider time. Satellite-derived nLw(555) is used as a proxy to illustrate spatial variability in near-surface b_{bp} in this region. The bold line in C-D traces measurements made at night to help contrast the pattern of variability observed in $b_{bp}(700)$ with those of fluorescence shown in Figs. 4.7C-D. Lower-case letters ‘a-c’ serve as spatial references as in Fig 4.2. The approximate location of the cyclonic eddy as observed in September and October 2004 is denoted as ‘E’.

data at the end of each dive cycle and to receive new mission instructions when necessary (Eriksen *et al.*, 2001; Rudnick *et al.*, 2004).

Since August 2003 Seaglider has been sampling along a ‘standard’ V-shaped transect off the Washington coast (Fig. 4.2) measuring a suite of parameters that includes conductivity (Sea-Bird Electronics SBE 4), temperature (Sea-Bird Electronics SBE 3), pressure (Paine Corporation 211-75-710-05 1500PSIA), dissolved oxygen (DO; Sea-Bird Electronics 43F Clark-type oxygen electrode), chlorophyll *a* fluorescence (proxy for phytoplankton concentration), two wavelengths of optical backscatter by particles ($b_{bp}(470)$ and $b_{bp}(700)$; proxies for particle concentration), and GPS position.

Measurements of $b_{bp}(\lambda)$ and fluorescence are obtained from a single miniaturized instrument, the ECO-BB2F, which was developed by WET Labs specifically for Seaglider (Fig. 4.1B). The sensor excites chlorophyll *a* fluorescence at 470 nm and measures the emission with the same broad-band detector used to measure $b_{bp}(700)$. Physical parameters, including DO, are sampled to 1000 m while optical measurements are limited to the upper 150 m. To reduce power consumption and extend mission duration Seaglider does not use a pump when collecting measurements of salinity and oxygen and these data must be used with caution or for qualitative purposes only (e.g., DO data in Figs. 4.8E-F). Methods to refine the measurements from these non-pumped sensors are currently being developed.

Optical Data Processing. All optical data presented were collected with the same ECO-BB2F instrument (SN# BB2F-010) thereby avoiding the need for inter-calibration. BB2F-010 has been used for 358 days (1314 dives) in five separate Seaglider

deployments off the Washington coast from 11 September 2002 – 23 December 2004. Typically, when a glider is recovered the optical face of the ECO-BB2F appears clean with little to no bio-fouling. This is likely due to the fact that the glider spends much of its time at depths well below the euphotic zone and because the glider cycles through a pressure range that few organisms can tolerate. Since the focus of this study was to compare patterns of optical variability, and not the absolute magnitudes of the variables, we chose not to transform the output of the ECO-BB2F into calibrated units of pigment concentration (e.g., mg m^{-3}) or $b_{\text{bp}}(\lambda)$ (e.g., m^{-1}). For our purposes we have simply subtracted an instrument-specific deep/clean water background, taken to be the lowest value observed at 150 m, from the raw instrument counts. All optical data are shown relative to this deep/clean water value (assumed to be free of phytoplankton and suspended particulate material) and are linearly related to the calibrated quantities mentioned above (Figs. 4.5-4.9). Instrument performance was consistent and stable across deployments with a <2% change in LED intensity at a given temperature (assessed using internal LED reference detectors).

Data Fusion Techniques

To qualitatively compare spatial patterns of variability a matchup procedure was developed to extract ocean color data from a single satellite image along an arbitrary Seaglider transect (e.g., Figs. 4.5-4.6). This procedure only required measurements to be co-located in space (no temporal acceptance criteria were used); however, a point of temporal coincidence is often desirable. Standard L2 ocean color data files contain georeferencing information for each observation (i.e., pixel) in a scene and Seaglider's

position is obtained via GPS at the end of each dive cycle while the vehicle is at the surface (one GPS fix is obtained immediately after surfacing and another just prior to the next dive). With this positional information near-surface optical measurements from Seaglider can be matched with co-located satellite measurements. It has been shown that 90% of the ocean color radiance is reflected from a depth shallower than the first irradiance attenuation length (z_{90} ; Gordon and McCluney, 1975). Values of the SeaWiFS-derived diffuse attenuation coefficient at 490 nm ($K(490)$) in waters seaward of the shelf-slope break suggest that z_{90} ranges from 10 – 20 m ($K(490)$ ranges from 0.05 – 0.10 m^{-1}). Using this depth range as a guide, we summarized *in-situ* optical measurements from Seaglider using a median of observations from 0 – 15 m. Satellite data were summarized as a median of all observations within 2.5 km of a Seaglider GPS fix.

Remote sensing reflectance ($R_{rs}(\lambda)$), obtained by dividing $nLw(\lambda)$ by the incoming extraterrestrial solar irradiance, is related to a weighted average of the spectral backscattering-to-absorption ratio ($b_b(\lambda)/a(\lambda)$) in the upper layer of the ocean (Zaneveld *et al.*, 2005 and references therein; $R_{rs}(\lambda)$ is closely related to the irradiance reflectance $R(\lambda)$ used in the reference and can be considered proportional for our purposes). Light absorption by phytoplankton and colored dissolved material (CDM) is minimal at 555 nm and the variability observed in $nLw(555)$ is primarily a function of $b_{bp}(555)$ (assuming that backscattering by water is constant). Stramski *et al.* (1999) showed that $R_{rs}(555)$ (and therefore $nLw(555)$) could be used as a reliable predictor of $b_{bp}(510)$ (in their study measurements of $b_b(555)$ were unavailable). Since $b_{bp}(700)$ was not a standard L2 ocean color product we chose to use $nLw(555)$ as a satellite-derived analog (Figs. 4.6, 4.7B).

To quantitatively compare surface fluorescence measurements from Seaglider with coincident (± 0.5 d) satellite-derived measurements of chl *a* it was necessary to limit the analysis to nighttime matchups only (i.e., nighttime Seaglider data matched with daytime estimates of chl *a* from SeaWiFS and/or MODIS Aqua). Non-photochemical fluorescence quenching is often observed in phytoplankton which have exposed to high irradiances for extended periods of time (e.g., Kiefer, 1973a; Falkowski and Kolber, 1995). The reduction in the fluorescence quantum yield creates a pattern of reduced fluorescence at the surface during the day, a bias that is present in almost all of the Seaglider data collected to date (e.g., Fig. 4.5). To refine our collection of point matchups a number of rigorous acceptance criteria were utilized:

- 1) Time difference between satellite/Seaglider data acquisition <0.5 d.
- 2) Used only *in-situ* Seaglider measurements collected at night.
- 3) All satellite observations within 7.5 km of a Seaglider GPS fix were cloud free (reduces cloud edge effects).
- 4) There was a minimum of 9 satellite observations within 2.5 km of a Seaglider GPS fix (accounts for poor viewing geometry).
- 5) There was a minimum of 10 *in-situ* Seaglider measurements from 0 – 15 m (ensures sufficient sampling density).

If a matchup fulfilled each of these criteria then the data were summarized as outlined above (i.e., all satellite data within 2.5 km of a Seaglider GPS fix; all *in-situ* data

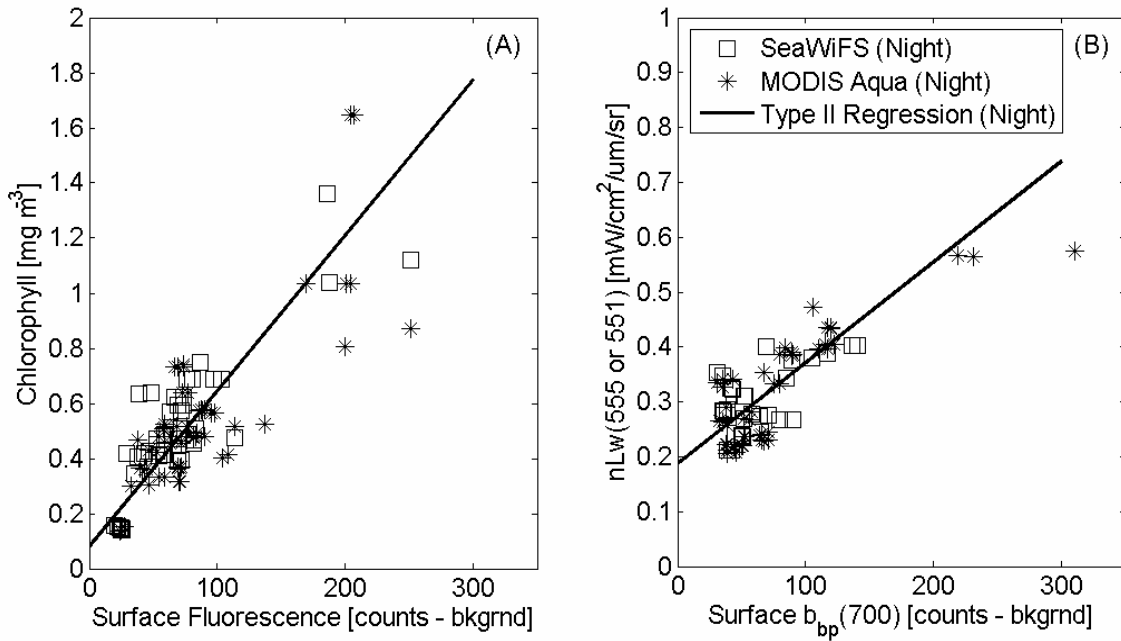


Figure 4.7 **Seaglider/satellite matchups.** Type II regressions of surface Seaglider fluorescence vs. satellite-derived chlorophyll (A) and surface Seaglider near-infrared backscatter by particles vs. satellite-derived water leaving radiance at 55X nm (B; 555/551 nm for SeaWiFS/MODIS Aqua). For consistency only nighttime matchups were used in order to avoid the bias associated with mid-day fluorescence quenching.

$$\begin{aligned}
 \text{(A)} \quad & y = 0.0057x + 0.0788; & r = 0.834 \text{ (} p < 0.001 \text{)} \\
 \text{(B)} \quad & y = 0.0018x + 0.1862; & r = 0.783 \text{ (} p < 0.001 \text{)}
 \end{aligned}$$

from 0 – 15 m). The difference between the 75th and 25th percentiles, also known as the inter-quartile range (IQR), was used as a measure of dispersion (i.e., variability) when summarizing both satellite and *in-situ* measurements. Scaling the IQR by the median (50th percentile) provided a unitless measure of relative variability, similar in interpretation to the coefficient of variation (standard deviation/mean). This measure of within-sample variability was useful to determine when data were collected in regions of strong gradients. Since the analysis could contain matchups with a time difference of up to 0.5 d we chose not to include matchups that were isolated from regions where we observed extreme horizontal and/or vertical variations. Only matchups where both satellite and *in-situ* samples had values for the IQR-to-median ratio of <0.2 were accepted. This methodology was inspired by the protocol used by the SeaWiFS Project for postlaunch validation of satellite-derived ocean color products using *in-situ* data sets (Bailey *et al.*, 2000).

The geometric mean Model II regression technique (aka reduced major axis method) was used to quantify the relationship between satellite and *in-situ* optical measurements (Fig. 4.7). This method is preferred when neither dataset is controlled or free of error. The resulting slope minimizes the absolute value of the sum of the products of the deviations between the observations and the regression line in both the X and Y directions (Ricker, 1973; Laws and Archie, 1981). Correlations between satellite and *in-situ* optical measurements were used to assess the strength and statistical significance (p-value <0.05) of a linear relationship between the observations.

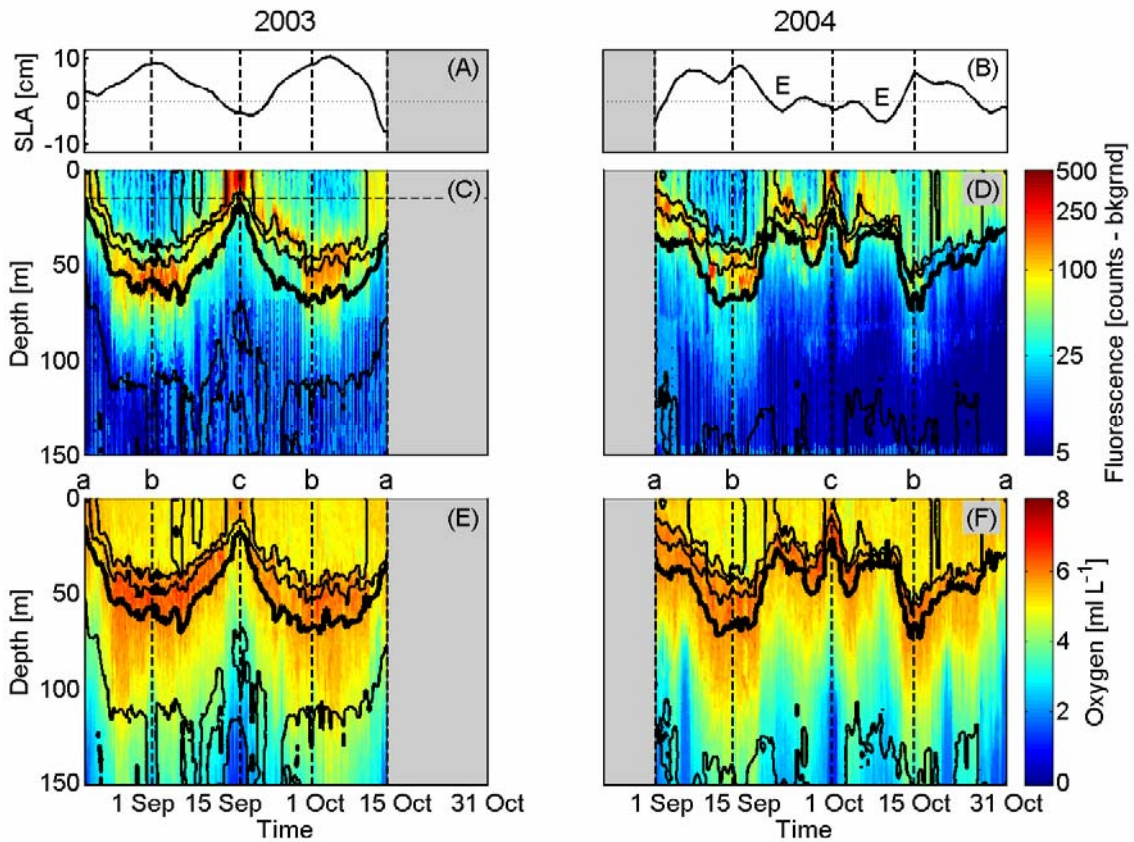


Figure 4.8 **Depth resolved fluorescence and dissolved oxygen from Seaglider.** Sea level anomaly (SLA; A-B) along with interpolated time versus depth plots of Seaglider fluorescence and dissolved oxygen from 22 August – 31 October of 2003 (C and E) and 2004 (D and F). SLA was interpolated in both space and time. On panels C-F data have been interpolated to a 0.1 day x 0.5 m grid and temperature contours are overlaid; contours are spaced at 2.5° C intervals with a bold contour at 10° C. Lower-case letters ‘a-c’ serve as spatial references as in Fig 4.2. The approximate location of the cyclonic eddy observed in September and October 2004 is denoted as ‘E’.

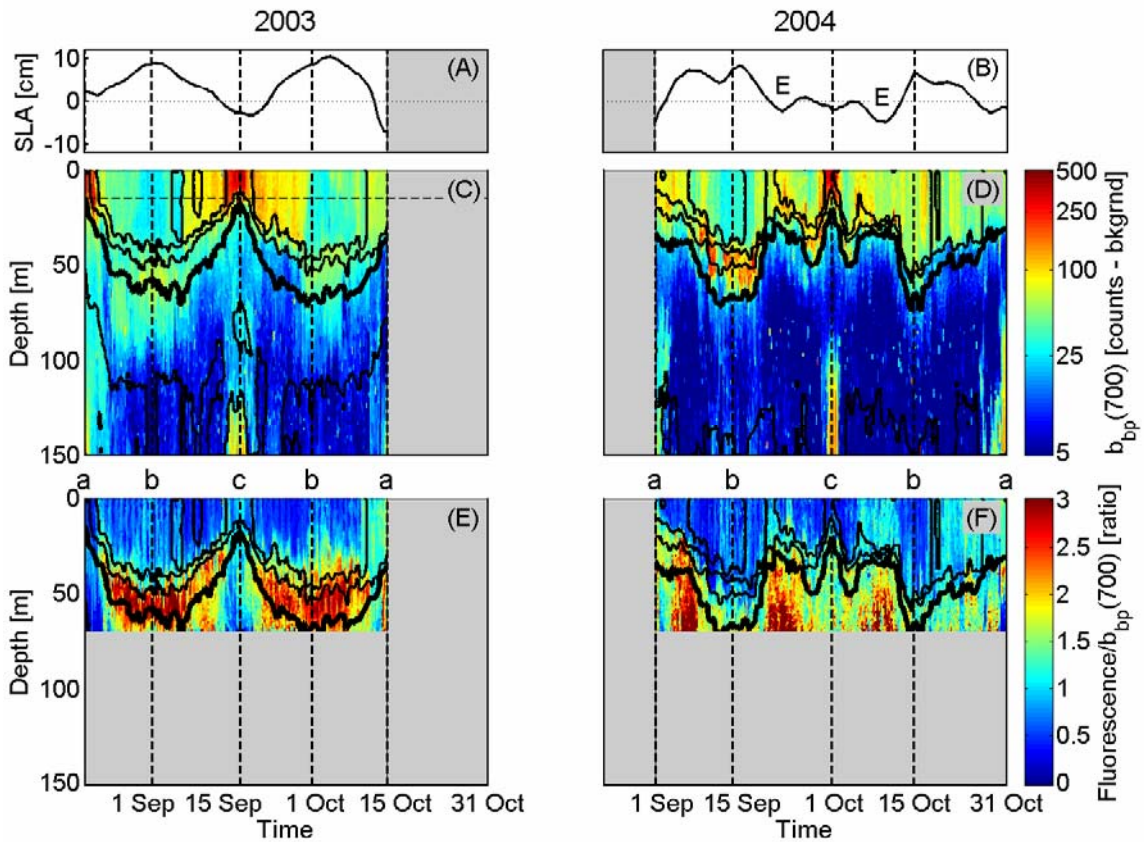


Figure 4.9 **Depth resolved near-infrared backscatter by particles and the fluorescence-to-backscatter ratio from Seaglider.** Sea level anomaly (SLA; A-B) along with interpolated time versus depth plots of Seaglider near-infrared backscatter by particles and the fluorescence-to-backscatter ratio from 22 August – 31 October of 2003 (C and E) and 2004 (D and F). SLA was interpolated in both space and time. On panels C-F data have been interpolated to a 0.1 day x 0.5 m grid and temperature contours are overlaid; contours are spaced at 2.5° C intervals with a bold contour at 10° C. Data in panels E-F are limited to the upper 70 m to avoid taking ratios in waters with low a low signal-to-noise ratio. Lower-case letters ‘a-c’ serve as spatial references as in Fig 4.2. The approximate location of the cyclonic eddy observed in September and October 2004 is denoted as ‘E’.

Regional Temperature/Nitrate/SLA Relationships.

Historical temperature and nitrate data were obtained from the World Ocean Database distributed by NOAA's National Oceanographic Data Center (<http://www.nodc.noaa.gov/OC5/indprod.html>). Data were extracted for the region between 46.5 – 48.5 N and 124 – 128 W and limited to water depths >500 m (Figs. 4.2, 4.10). Waters warmer than 10° C are often nitrate limited and the position of the 10° C isotherm is associated with the base of the deep chlorophyll maximum layer (Figs. 4.8C-D). A Model II regression was used to determine a predictive relationship between SLA and the position of the 10° C isotherm, as determined by Seaglider (Fig. 4.11).

Quasi-4-dimensional Visualization.

The interpolated (time versus depth) representations of Seaglider data shown in Figures 4.8 – 4.9 are useful to compare how parameters were distributed as a function of depth in September and October 2003 – 2004. Unfortunately, this representation of the data makes it more difficult to put Seaglider observations into a spatial context. The relationship between satellite-derived chl *a* and surface Seaglider fluorescence (Fig. 4.7) allowed us to use Matlab v. 7.0.X (The Mathworks Company) to create a quasi-4-dimensional (Seaglider data progresses in both space and time) representation of surface and sub-surface chl *a* that could be manipulated (i.e., users can adjust the zoom, pan, and tilt) and animated so that the data could be seen from different viewpoints (Fig. 4.12). This fused data product also used Smith and Sandwell (1997) bathymetric data (v. 8.2;

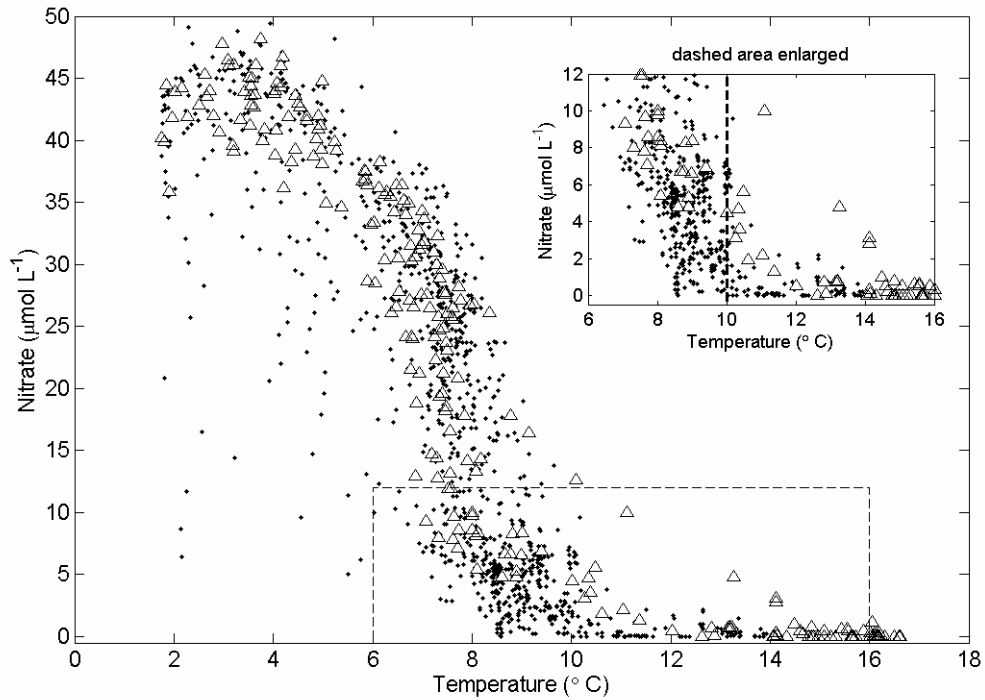


Figure 4.10 **Historical temperature versus nitrate relationship.** Regional temperature vs. nitrate relationship derived from historical data obtained from the World Ocean Database. Triangles denote observations collected from August – October. Inset suggests that waters greater than 10°C are often nitrate limited.

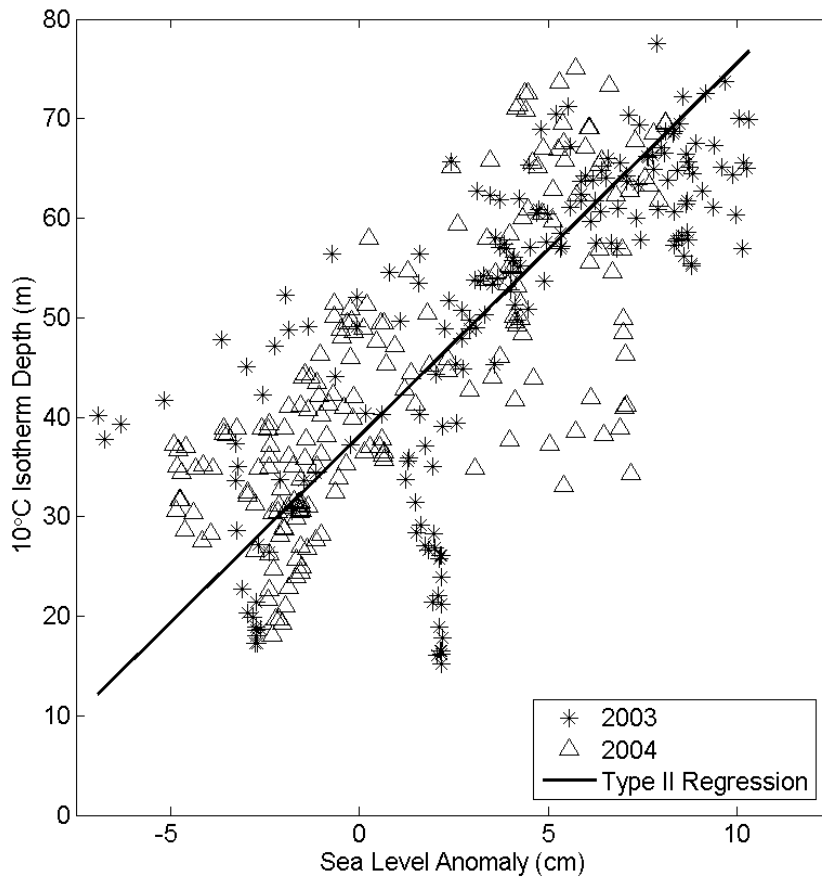


Figure 4.11 **Sea level anomaly versus 10° C isotherm depth from 22 August – 31 October of 2003 and 2004.** Type II regression of sea level anomaly vs. 10° C isotherm depth from 22 August – 31 October of 2003 and 2004. The 10° C isotherm depths were estimated from Seaglider temperature profiles. This relationship serves as a first-order approximation for the position of the nutricline (Fig. 4.10) and base of the deep chlorophyll maximum layer (Figs. 4.8C-D) in waters off the Washington coast during fall.

$$y = 3.7485x + 38.1162; \quad r = 0.755 \text{ (} p < 0.001 \text{)}$$

approx. 4 km) and topographic data (approx. 1km) from the GTOPO30 global digital elevation model. Bathymetric data were provided by NOAA's National Geophysical Data Center (<http://www.ngdc.noaa.gov/mgg/image/2minrelief.html>) and topographic data were provided by the USGS's Center for Earth Resources Observation and Science (<http://edc.usgs.gov/products/elevation/gtopo30/gtopo30.html>).

Results and Discussion

Surface Satellite Observations of the Eddy

From 4 September to 30 October 2004 Seaglider completed two consecutive V-shaped transects through a cyclonic eddy that was ~125 km in diameter (Figs. 4.3-4.4). The eddy began as a meander of the CCS which increased in size while slowly moving offshore. Once the eddy detached it remained in approximately the same location for >1 mo and appeared to intensify from 18 September to 2 October and then weaken and dissipate through 30 October (Fig. 4.3). In fall 2003 large scale meanders of the CCS could be seen in SLA, SST, and chl *a*, but a distinct eddy was not observed off the Washington coast (Figs. 4.3A, 4.4A and C). In fact, similar persistent eddies were not identified in SeaWiFS chl *a* or SLA data for the same time period from 1998 – 2003, with the possible exception of a smaller, less intense eddy in 2001 (data not shown). This is consistent with the observation that waters off the Washington coast generally have low values of eddy kinetic energy throughout the year, as compared to the rest of the CCS to the south (Strub and James, 2000).

MODIS-Aqua sea surface temperature measurements suggest that the eddy was ~1–2° C cooler at the surface compared to surrounding water masses; these results are

consistent with the cyclonic circulation and upward doming isotherms measured by Seaglider (Fig. 4.8D). Surface chlorophyll estimates from SeaWiFS were ~3–4X greater in the eddy, compared to surrounding water masses (0.6–0.8 vs. 0.2 mg m⁻³), and ~4–5X less than the maximum chlorophyll values observed at the shelf break (0.6–0.8 vs. 3.0 mg m⁻³; Figs. 4.4D, 4.5B). In 2003 offshore and shelf break chl *a* values were similar to those observed in 2004 (Figs. 4.4C-D, 4.5A-B).

It can be difficult to obtain uninterrupted sequences of ocean color images due to a regional persistence of cloud cover throughout much of the year (Sackmann *et al.*, 2004). Exceptionally clear images, similar to those chosen to represent conditions in fall of 2003 and 2004 (Fig. 4.4), are rare. Using SeaWiFS data from 1997 – 2004 we tabulated the percentage of SeaWiFS scenes, within the region bounded by the standard V-shaped Seaglider transect, where at least 1/3 of the data were unobstructed by clouds. On a monthly basis the tabulated percentages ranged from 6% in January to 30% in September, with an overall annual value of only 14%. The relative paucity of ocean color data in this region is unfortunate. However, a sustained Seaglider presence in this region has generated an almost uninterrupted dataset of *in-situ* optical measurements from August 2003 – present allowing us to continually monitor the bio-optical characteristics of these waters even when satellite observations are unavailable.

Near-surface Satellite/Seaglider Matchups

While the near-surface trends shown in Figures 4.5-4.6 are mirrored in both datasets, minor differences are evident. Even in the absence of measurement error discrepancies would be expected due to the:

- 1) Change of support between satellite and Seaglider datasets (Gotway and Young, 2002).
- 2) Temporal mis-match between datasets away from the point of coincidence (water masses could move and evolve with time; Denman and Abbott, 1988).
- 3) Possible presence of strong horizontal and/or vertical gradients (statistical summaries may not properly characterize data near the point of coincidence).

Despite these limitation, the qualitative patterns of variability observed in both the Seaglider (i.e., not-synoptic) and satellite (i.e., synoptic) datasets were consistent (Figs. 4.5-4.6). This suggests that mesoscale variability (i.e., 5-50 days, 20-200 km) is well represented in the Seaglider dataset and that meaningful comparisons between satellite and *in-situ* Seaglider data can be made at these spatial and temporal scales.

Quantitative matchups between these disparate datasets (obtained using observations from regions with minimal horizontal and vertical variability that were co-located in both time and space) yielded statistically robust relationships (Fig. 4.7). A slight (albeit statistically significant) bias was observed between Seaglider fluorescence and satellite ocean color estimates of chlorophyll *a* and work is currently underway to better understand the source of this offset. The utility of these relationships is two-fold. First, they ensure a seamless transition between *in-situ* optical measurements from Seaglider and satellite-derived products at the surface (e.g., Fig 4.10). Second, they can be used to help interpret satellite ocean color data collected in more optically complex regions (by identifying observations that deviate significantly from the expected

relationship). Currently Seaglider's standard V-shaped transect extends seaward of the shelf-slope break into 'Case I' waters (i.e., optical properties tend to co-vary with chl *a*). In more optically complex 'Case II' waters (i.e., optical properties do not co-vary with chl *a*) there are a number of factors that can bias satellite-derived ocean color measurements. For example, the overcorrection of atmospheric effects in waters where near-infrared $nL_w(\lambda)$ has been underestimated (often a problem in turbid environments with high concentrations of suspended particles) could bias satellite-derived estimates of visible $nL_w(\lambda)$ and all subsequently derived parameters (Siegel *et al.*, 2000) and increased light absorption in the blue spectral region due to variable concentrations of CDM could bias satellite-derived estimates of chl *a* when using empirical ratio-type algorithms (Siegel *et al.*, 2005).

Seaglider Sections Through the Eddy

Nutrient limitation in waters off the coast of Washington during summer leads to reduced phytoplankton growth rates and minimal chlorophyll fluorescence in the mixed layer (Fig. 4.8C-D). Within the eddy observed in 2004 the upward doming temperature and nutrient isopleths (as inferred from the regional temperature versus nitrate relationship; Fig. 10) mirror the negative SLA at the surface and elevated fluorescence was seen throughout the upper 40 m. The increased fluorescence likely reflects an increase in phytoplankton biomass due to the shallower nutricline and increased light availability (Fig. 4.8B, D). In both 2003 and 2004 fall destratification occurred in mid-October and mixed layer fluorescence increased in part due to increased biomass following injection of nutrients from below the pycnocline and in part due to the

photoadaptive response of phytoplankton to shorter day length (i.e., increased chlorophyll content per cell; Fig. 4.8C-D; Neori *et al.*, 1984; Geider *et al.*, 1998).

Measurements of $b_{bp}(\lambda)$, whether measured *in-situ* (Fig. 4.9) or derived from satellite ocean color (e.g., Roesler and Perry, 1995; Hoge and Lyon, 1996, Garver and Siegel, 1997), can be used as a proxy for in-water particle concentration (Stramski *et al.*, 2004). Recent work has also shown good relationships between $b_{bp}(\lambda)$ and particulate organic carbon (POC) concentration in various parts of the ocean (Stramski *et al.*, 1999; Loisel *et al.*, 2001; Loisel *et al.*, 2002). Interestingly, the ratio of phytoplankton carbon-to-POC has been shown to vary within a reasonably well constrained range (especially in waters dominated by organic particles) further suggesting that it might be possible to use $b_{bp}(\lambda)$ as a more specific proxy for phytoplankton carbon (Behrenfeld *et al.*, 2005 and references therein). While many of the first-order trends observed in $b_{bp}(\lambda)$ are similar to those seen in fluorescence there are numerous differences that can be seen in the fluorescence-to-backscatter ratio (fluor: $b_{bp}(\lambda)$); Figs. 4.9E-F).

If one assumes that $b_{bp}(\lambda)$ is proportional to POC and that the ratio of phytoplankton carbon-to-POC is constant then ratios of fluor: $b_{bp}(\lambda)$ should reflect changes in the chlorophyll *a*-to-phytoplankton carbon ratio as cells acclimate to different light and nutrient environments (provided that variations in the fluorescence-to-chlorophyll *a* ratio are relatively small). Near-surface values of fluor: $b_{bp}(\lambda)$ tended to reflect the effects of non-photochemical fluorescence quenching (inferred from Figs. 4.5-4.6). In the mixed layer fluor: $b_{bp}(\lambda)$ ranged from 0.5 – 1.5 with higher values observed in the eddy and after the fall destratification (Figs. 4.9E-F). A flux of nutrients into the euphotic zone at these times and locations would likely increase phytoplankton growth

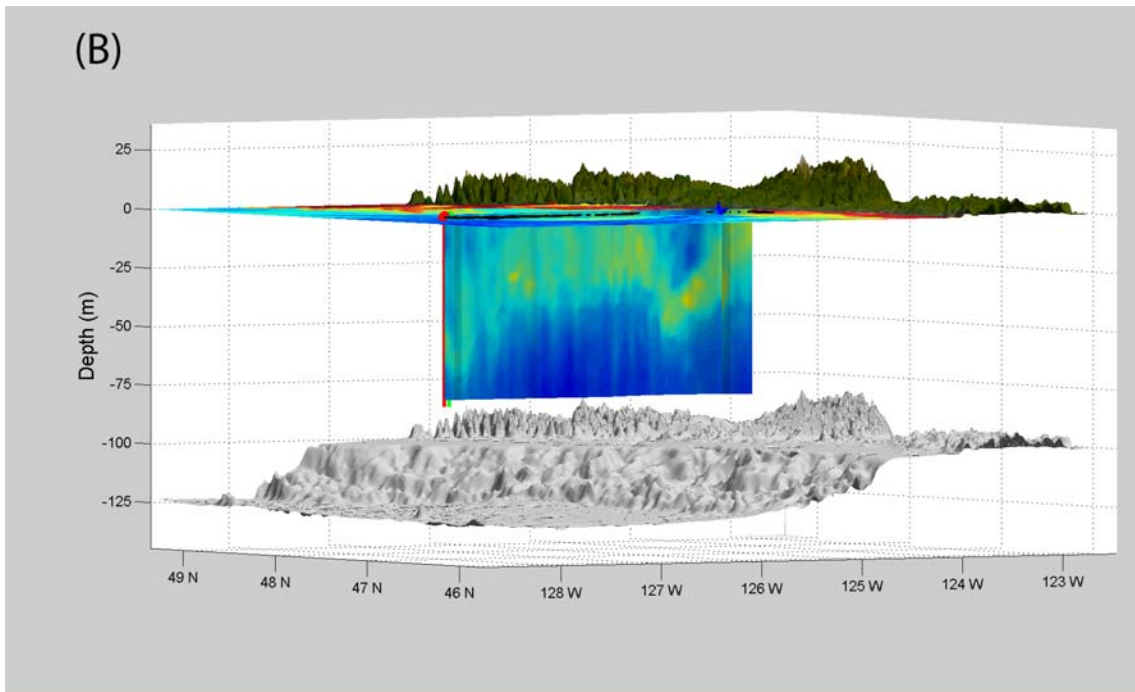
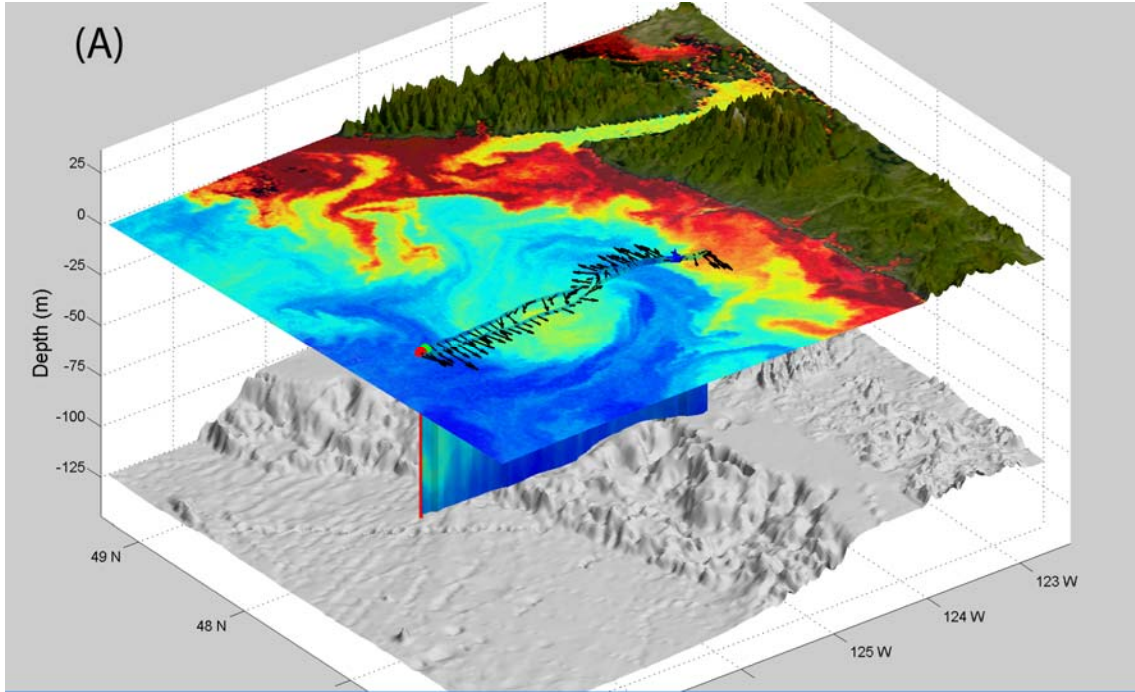
rates and is consistent with an increase in $\text{fluor:b}_{\text{bp}}(\lambda)$. As a function of depth $\text{fluor:b}_{\text{bp}}(\lambda)$ ranged from 0.5 – 3 (surface – deep), a pattern that was consistent with photoadaptive changes in the phytoplankton as they acclimated to diminished light intensity (Geider *et al.*, 1998; Behrenfeld *et al.*, 2005). These results are encouraging, especially given the numerous caveats that must be considered, and suggest that future efforts could use $\text{fluor:b}_{\text{bp}}(\lambda)$ to infer additional physiological information about the local phytoplankton population throughout the euphotic zone.

Subsurface fluorescence maxima (SFM) can be observed in many parts of the ocean although mechanisms for their formation and maintenance vary (Cullen, 1982). Off the Washington coast SFM were observed just above the nutricline (Fig. 4.10) in waters ranging from 10 – 15° C (Fig. 4.8). Using an empirical relationship between SLA and the depth of the 10° C isotherm it is possible to predict the position of SFM with reasonable accuracy (Fig. 4.11). This relationship can be used to predict the temperature, nutrient, and bio-optical characteristics of the subsurface in the absence of *in-situ* observations. The presence of elevated DO concentrations below the mixed layer suggests that the phytoplankton community, despite the sub-optimal light environment, is active and capable of net photosynthesis over the growing season (Figs. 4.8E-F). Using this unique suite of in-water measurements and the observed relationships with satellite observations at the surface we now have the means necessary to improve our understanding of the biogeochemical cycles and processes structuring the 4-dimensional distribution of phytoplankton in this dynamic environment.

Fused Satellite/Seaglider Data Products

As scientific datasets grow in size and complexity effective data representation and visualization becomes increasingly important. Tufte (2001) notes that “Modern data graphics can do much more than simply substitute for small statistical tables. At their best, graphics are instruments for reasoning about quantitative information. Often the most effective way to describe, explore, and summarize a set of numbers – even a very large set – is to look at pictures of those numbers.” With this in mind we have used the relationship between surface fluorescence from Seaglider and satellite-derived chl *a* shown in Figure 4.7 to create a new type of quasi-4-dimensional data product. Our matchup procedure successfully minimized discrepancies between the two datasets at the surface and allowed us to fuse observations from these disparate remote sensing platforms. Using this new visual representation of the data one can more easily see how offshore oceanic waters (i.e., low chl *a* at the surface) tended to circulate around the eddy and how the vertical structure of phytoplankton within these offshore waters differed from the phytoplankton structure within the eddy itself (Fig. 4.12). This product has been used successfully in GK-12 and public outreach activities and appears to be a particularly effective way of communicating information to a general audience.

Figure 4.12 **Fused Seaglider/SeaWiFS data product.** Fused Seaglider/SeaWiFS data product showing spatial variability of surface and subsurface chlorophyll concentrations within the cyclonic eddy observed in September and October 2004. SeaWiFS image is same as in Fig. 4.4D. Vertical structure of chlorophyll within the eddy is derived from Seaglider chlorophyll *a* fluorescence; fluorescence measurements have been converted into units of chlorophyll (mg m^{-3}), scaled logarithmically, and shaded using the color bar in Fig. 4.4D. Bathymetric data were scaled by 0.01 and offset by 100 m. Vectors in A indicate depth-averaged current velocities derived from the difference between the estimated dead-reckoned position and the GPS position of the glider obtained after each dive. Maximum velocities correspond to $\sim 20 \text{ cm s}^{-1}$.



Summary and Conclusions

Our goal was to describe how measurements from Seaglider and ocean color satellites are being combined to systematically monitor the bio-optical status of waters off the Washington coast. By combining these two disparate datasets, a new quasi-4-dimensional data product was created (Fig. 4.12) that clearly resolved the offshore phytoplankton distribution in and around a cyclonic eddy that was observed in September and October 2004. From an ecological standpoint, monitoring the biological response to large, persistent, cyclonic eddies will be difficult if analyses are limited to data from a single remote sensing platform. There are a diversity of autonomous and Lagrangian platforms and sensors (ALPS) now available for operational deployment that can provide highly-resolved measurements in the vertical (z) dimension. The overall influence of mesoscale eddies on regionally-integrated phytoplankton production off the Washington coast is a question that can be effectively addressed by combining state of the art ALPS technology with satellite-derived ocean products. Continued development of new sensors (e.g., low-profile beam attenuation meters and spectral radiometers) will ensure an even more complete characterization the inherent and apparent optical properties of the euphotic zone (Daly *et al.*, 2004) and allow us to move beyond first-order estimates of phytoplankton standing stock and our current reliance on ‘climatological means’ for parameterization of the bio-optical status of the subsurface.

Methods developed here can help the oceanographic community integrate a variety of large remotely sensed datasets as we move into an era of real-time, regional ocean observing systems (ORION Executive Steering Committee 2005; Dickey *et al.*, 2006). Currently, Seaglider measurements can help improve the interpretation of satellite

ocean color data by resolving optical variability in the vertical dimension and by providing much needed ground truth and observations under persistently cloudy conditions. These measurements are needed to further reduce uncertainties associated with converting measurements of ocean color into useful biogeochemical proxies (e.g., chl *a*, carbon, etc.) and to create a more complete understanding of the distribution of optically-active materials in the ocean.

Acknowledgements

This work is supported by the NSF Seaglider Project (OCE 9911037) and the National Science Foundation Graduate Research Fellowship Program.

Chapter 5

USING SEAGLIDER TO QUANTIFY VARIABILITY IN SURFACE MID-DAY FLUORESCENCE QUENCHING

Seaglider, a long-range autonomous glider, was deployed routinely in waters off the coast of Washington, USA, from April 2002 – December 2005. Measurements of chlorophyll fluorescence (proxy for chlorophyll *a* concentration) and optical backscatter (proxy for particle concentration) were collected on both the continental shelf and along a standard V-shaped transect that extended 200 km from the continental shelf into deep oceanic waters. The effects of mid-day fluorescence quenching (i.e., the reduction in the fluorescence quantum yield often observed during the daytime) could be detected throughout the dataset, at all times of the year, with daytime fluorescence values being quenched by >80% during summer. Using a high resolution dataset with measurements collected in April 2002 over the continental shelf an algorithm that used ratios of fluorescence to optical backscatter from within the mixed layer was developed to adjust daytime estimates of surface biomass from Seaglider. The ability to ‘correct’ an individual fluorescence profile for the effects of mid-day quenching (as opposed to simply discarding the biased data) allowed us to maintain the spatial and temporal integrity of the dataset. We estimate the maximum error in these ‘corrected’ fluorescence estimates to be <10%. From August 2003 – December 2005 a statistical method was used to quantify spatial and temporal patterns in mid-day fluorescence quenching. Quenching was observed throughout the region of interest and at all times of the year. The degree of quenching was positively correlated with incoming solar insolation and the

observed pattern was remarkably similar to what was observed in the eastern equatorial Pacific suggesting some degree of universality for the underlying relationship.

Introduction

The ease with which *in vivo* fluorescence can be measured in the ocean has led, in part, to its routine use as a proxy for *in situ* pigment concentrations (e.g., chlorophyll *a*) and phytoplankton distributions since the mid 1960's (Lorenzen, 1966). Unfortunately, the lack of a universal relationship between *in vivo* fluorescence and chlorophyll *a* has been a source of ongoing frustration for researchers. When *in vivo* fluorescence measurements are normalized by corresponding estimates of extracted chlorophyll *a*, the resulting fluorescence:chlorophyll *a* ratio has been shown to vary by as much as 10X over relatively short spatial and temporal distances (Loftus and Seliger, 1975; Alpine *et al.*, 1979). This variability has a wide range of underlying causes and has been related to changes in phytoplankton size (Alpine and Cloern, 1985), species assemblage (Strickland, 1968; Slovacek and Hannan, 1977), pigment composition (Neori *et al.*, 1984), intra-cellular organization of the chloroplasts (in larger cells), light history, nutrient stress (Kiefer, 1973a, b; Loftus and Seliger, 1975; Slovacek and Hannan, 1977), as well as a host of internal photosynthetic and physiological processes (Kiefer and Reynolds, 1992, Falkowski and Kolber, 1995). In natural populations it is often difficult to separate the effects that these factors have on overall fluorescence output since many different processes can act simultaneously.

In both laboratory studies, and in the field, researchers have observed a daily rhythm of *in vivo* fluorescence that is not correlated with diel changes in chlorophyll *a*.

During periods of high irradiance, like those associated with mid-day, fluorescence tends to be lower than it is at night (Kiefer, 1973a; Loftus and Seliger, 1975; Falkowski and Kolber, 1995; Dandonneau and Neveux, 1997). This decrease in the fluorescence quantum yield (i.e., the ratio of photons emitted as fluorescence to those absorbed) is often ascribed to a process known as non-photochemical fluorescence quenching (Falkowski, 1992; Falkowski and Kolber, 1995; Krause and Jahns, 2004).

The two major components of non-photochemical quenching are ‘photoinhibitory quenching’ and ‘energy-dependent quenching’. Photoinhibitory quenching is thought to arise from damage to the PSII reaction center protein, D1, which leads to enhanced thermal dissipation of absorbed excitation energy within the reaction center (Takahashi *et al.*, 1971; Ohad *et al.*, 1990; Falkowski *et al.*, 1994; Krause and Jahns, 2004). The effects of photoinhibition increase non-linearly as a function of photon-dose and recovery is relative slow (O-hours) as it requires the synthesis of new D1 protein by the organism (Kyle *et al.*, 1984) and because additional D1 protein damage can occur under both low and high irradiance conditions (Falkowski, 1992). Unlike photoinhibitory quenching, which reflects actual damage to the photosynthetic machinery within a phytoplankton cell, energy-dependent quenching is associated with short-term variations (O-minutes) in the functional absorption cross-section of PSII and enhanced thermal dissipation in the antennae (Falkowski and Kolber, 1995; Krause and Jahns, 2004). In many types of algae this process is correlated with light-mediated, and reversible, changes in various oxygenated carotenoids known as xanthophylls (Demmig-Adams and Adams, 1992). Regardless of the underlying cause (i.e., photoinhibitory and/or energy-dependent quenching), the net result is often a systematic decrease in *in vivo* fluorescence per unit

chlorophyll *a* observed during periods of increased irradiance. For this reason we refer to the observed pattern, more generally, as mid-day fluorescence quenching.

The use of new autonomous and Lagrangian platforms (e.g., glider, drifters, etc.) has revolutionized sampling of the ocean. The incorporation of *in vivo* fluorometers into many of these systems has reinforced the need for a thorough understanding of this measurement and its associated variability and biases. Seaglider, a long range autonomous glider, has been deployed routinely in waters off the Washington coast since April 2002. This effort has generated a unique dataset that has allowed us to quantify patterns of variability in mid-day fluorescence quenching across a range temporal scales, from days to years. Our goals in this project were two-fold: (i) use data from Seaglider's first Washington coast deployment, in April 2002, to develop a method to assess and 'correct' *in vivo* fluorescence measurements for the bias due to mid-day fluorescence quenching; (ii) use surface fluorescence measurements collected from August 2003 – December 2005 (a nearly continuous data record) to determine if the patterns of mid-day fluorescence quenching observed in April 2002 were consistent throughout the time series.

Data and Methods

Description of Seaglider Deployments

Seaglider is an autonomous underwater glider that samples the ocean in a sawtooth pattern and has a depth rating of 1000 m (Eriksen *et al.*, 2001). To date, two types of deployments have been conducted off the Washington coast. The first was a 'higher resolution-shorter duration' mission that was completed in April 2002 (Fig. 5.1).

Seaglider was launched at the mouth of the Strait of Juan de Fuca and was programmed to make its way towards the southwest, across the continental shelf and slope off Washington. Once Seaglider moved beyond the strong tidal currents near the entrance to the Strait of Juan de Fuca it took 6 days to cross the continental shelf (approx. 75 km) and made approximately 150 dives to an average depth of 125 m (approx. 25 dives/day with 0.5 km spacing between dives; Figs. 5.2-5.6).

Since August 2003 Seaglider has been conducting 'lower resolution-longer duration' missions along a V-shaped transect (approx. 450 km) that extends off the Washington coast (Fig. 5.1, 5.7-5.11). To complete one V-shaped transect takes Seaglider an average of 30 days where it makes approximately 90 dives to a depth of 1000 m (approx. 3 dives/day with 5 km spacing between dives). Typically, this type of Seaglider deployment lasts between 5 – 6 months. During each mission Seaglider measures a suite of parameters that includes conductivity (Sea-Bird Electronics SBE 4), temperature (Sea-Bird Electronics SBE 3), pressure (Paine Corporation 211-75-710-05 1500PSIA), dissolved oxygen (DO; Sea-Bird Electronics 43F Clark-type oxygen electrode), chlorophyll *a* fluorescence (proxy for phytoplankton concentration), two wavelengths of optical backscatter by particles ($b_{bp}(470)$ and $b_{bp}(700)$; proxies for particle concentration), and GPS position. Measurements of $b_{bp}(\lambda)$ and fluorescence are obtained from a single miniaturized instrument, the ECO-BB2F, which was developed by WET Labs specifically for Seaglider. Seaglider usually ascends more slowly than it descends and 'up-casts' are more highly resolved near the surface. For this reason we chose to limit our statistical analyses to data from up-cast profiles only.

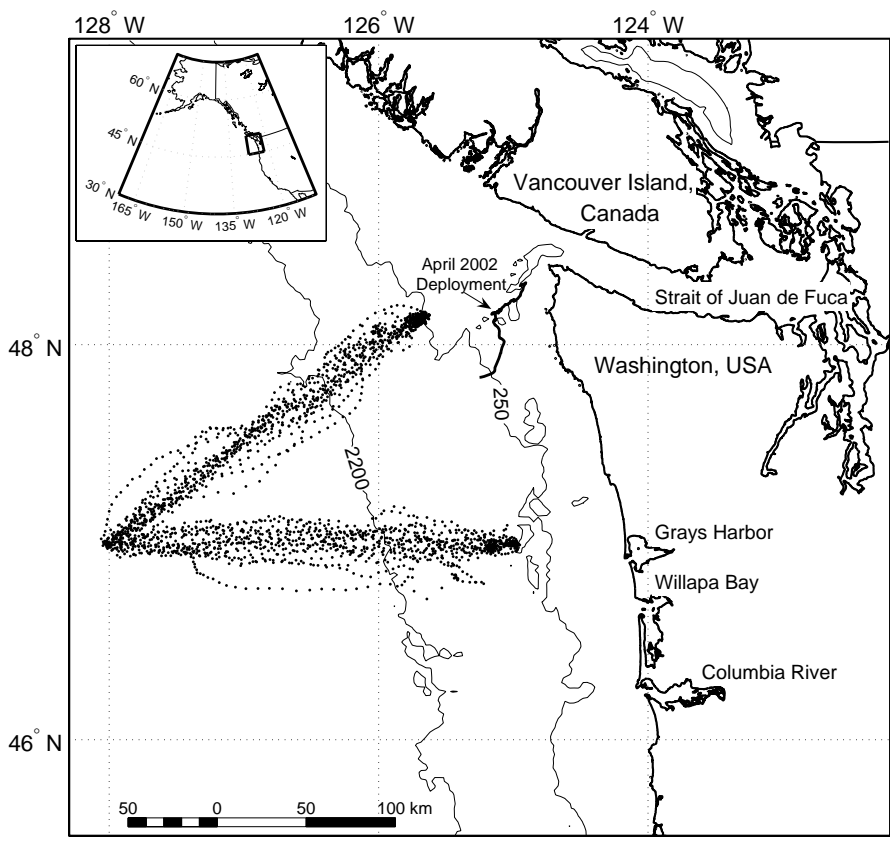
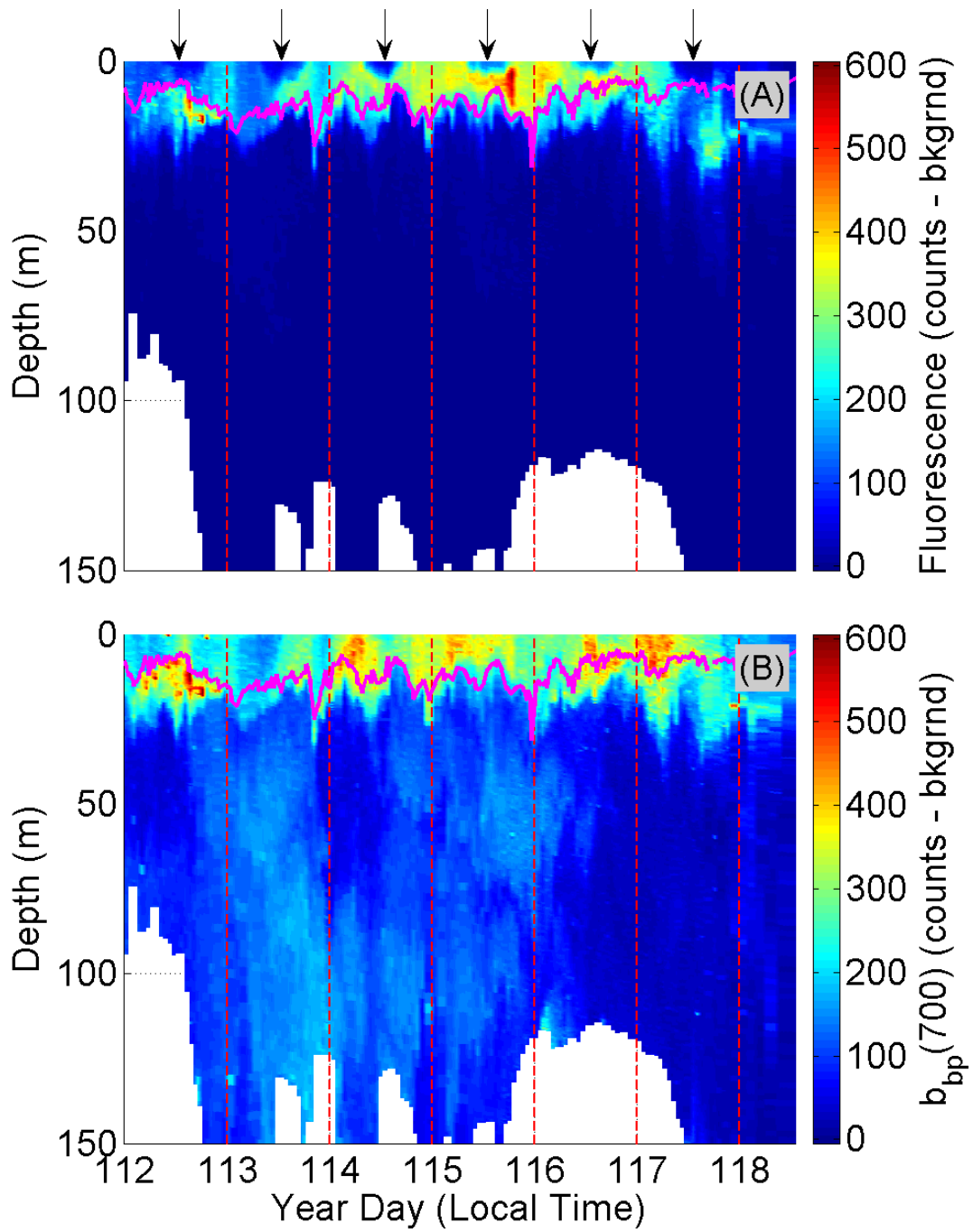


Figure 5.1 **Map of Washington coast.** Map of Washington coast. Heavy solid line illustrates the portion of the April 2002 Seaglider deployment analyzed in the text. Dots denote locations of Seaglider GPS fixes from August 2003 – December 2005.

Optical Data Processing

The WET Labs ECO-BB2F excites chlorophyll *a* fluorescence at 470 nm and measures the emission with the same broad-band detector used to measure $b_{bp}(700)$. When a glider is recovered the optical face of the ECO-BB2F appears clean with little to no bio-fouling. This is likely due to the fact that the glider spends much of its time at depths well below the euphotic zone and because the glider cycles through a pressure range that few organisms can tolerate. Many of our statistical analyses were performed using relative measures fluorescence and $b_{bp}(700)$ (e.g., Figs. 5.8-5.11), thereby eliminating the need to transform the output of the ECO-BB2F into calibrated units of pigment concentration (e.g., mg m^{-3}) or $b_{bp}(\lambda)$ (e.g., m^{-1}). For our purposes we simply subtracted an instrument-specific deep/clean water background, taken to be the lowest value observed at 150 m, from the raw instrument counts. From August 2003 – December 2005 three different ECO-BB2F sensors were used during the various Seaglider deployments. For these sensors the manufacturer's scale factors (used to transform fluorescence counts above the deep/clean water background into calibrated units of pigment concentration) differed by $< 3\%$. In situations where relative fluorescence measurements were not used the similarity in instrument response ensured that raw instrument counts from these units could be compared directly once the clean/deep water background had been subtracted (Fig. 5.7).

Figure 5.2 **Seaglider fluorescence and backscatter by particles.** Seaglider fluorescence (A) and backscatter by particles ($b_{bp}(700)$); B) from April 2002. Pink line denotes depth of the mixed layer. Arrows point to regions of reduced surface fluorescence resulting from mid-day quenching. Dotted lines are positioned at midnight for temporal reference.

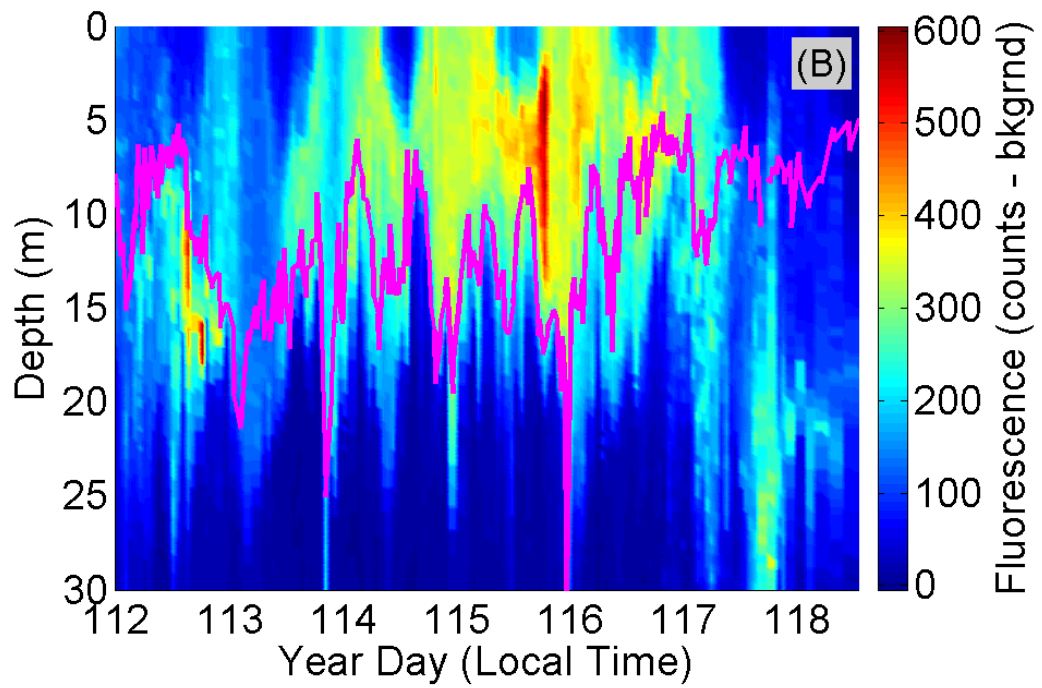
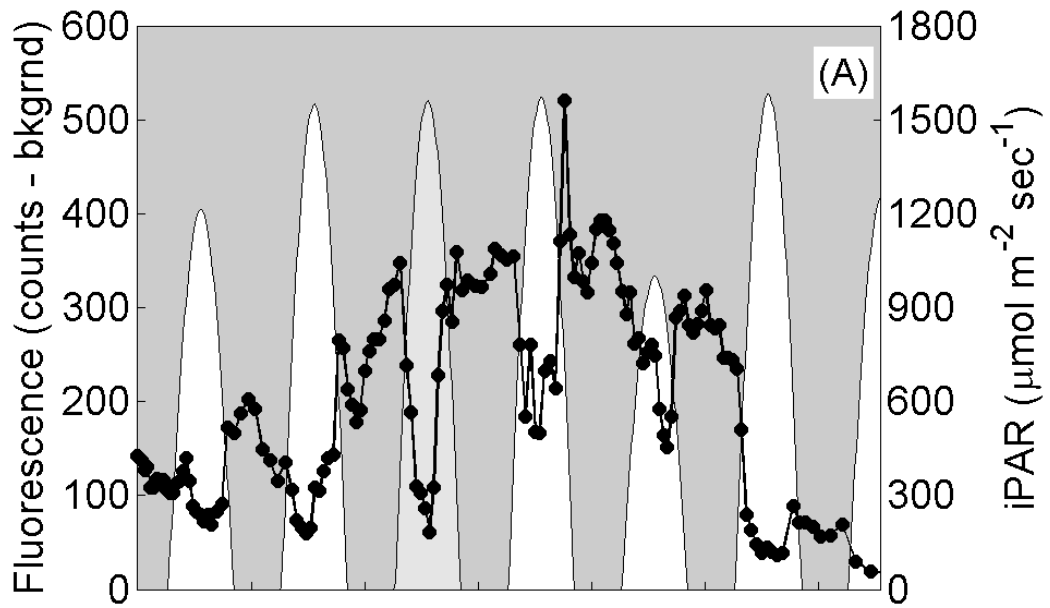


Instantaneous Surface PAR from SeaWiFS

Estimates of daily photosynthetically active radiation (i.e., 24-hour averaged; daily-PAR) were obtained using radiometric measurements from the Sea-viewing Wide Field-of-View Sensor (SeaWiFS). The SeaWiFS project defines daily-PAR at the sea surface as the quantum energy flux from the Sun in the spectral range from 400 – 700 nm expressed in mol/m²/day. Level 3 Binned data files with 9 km² spatial resolution and a 1-day temporal bin width were obtained from NASA's OceanColor WEB (<http://oceancolor.gsfc.nasa.gov>). Detailed algorithm descriptions and processing methodologies can be found on NASA's OceanColor WEB website.

Each Level 3 Binned data file was mapped using an isotropic Transverse Mercator projection with an average pixel size of 1.1 km². A time series of daily-PAR was created by calculating the median daily-PAR value observed within 50 km of Seaglider's position. A smooth sinusoidal curve (from sunrise to sunset) was used to estimate time-resolved, instantaneous PAR (iPAR; expressed in μmol/m²/sec) from the 24-hour averaged quantities provided (Kirk, 1994). The integral of iPAR, from sunrise to sunset, is numerically equivalent to the daily-PAR estimates recorded by SeaWiFS. Local times for sunrise and sunset were calculated using functions from the 'AIR_SEA' toolbox developed for Matlab (http://woodshole.er.usgs.gov/operations/sea-mat/air_sea.html/index.html).

Figure 5.3 **Near-surface fluorescence and satellite-derived estimates of iPAR.** Median near-surface fluorescence (0 – 5 m; A), satellite-derived iPAR (A), and depth resolved (B) fluorescence from April 2002. Pink line denotes depth of the mixed layer. A satellite-derived estimate of daily-PAR was not available for year day 114 and an average value, derived from year days 113 and 115, was used to calculate iPAR.



Quantifying Mid-day Fluorescence Quenching

Manual Method. To remove the effects of mid-day quenching from daytime estimates of fluorescence at the surface during Seaglider's 'higher resolution-shorter duration' mission in April 2002 a correction strategy needed to be developed. Ratios of fluorescence-to-near infrared backscatter ($F:b_{bp}(700)$) were observed to be relatively constant throughout the mixed layer over small spatial/temporal windows during nighttime. However, mid-day fluorescence quenching led to large decreases in $F:b_{bp}(700)$ near the surface during daytime (Fig. 5.4). With this in mind the following strategy was devised (Fig. 5.5):

- 1) The mixed layer depth (MLD) was objectively defined as the depth where density increased by 0.125 kg m^{-3} relative to the surface (Monterey and Levitus, 1997).
- 2) Individual daytime profiles of $F:b_{bp}(700)$ were evaluated to determine if $F:b_{bp}(700)$ was uniform in the mixed layer below the surface region affected by mid-day fluorescence quenching.
- 3) When values of $F:b_{bp}(700)$ were constant throughout most of the mixed layer values from deeper within the mixed layer were extrapolated to the surface where they were multiplied by $b_{bp}(700)$ to derive estimates of 'unquenched' fluorescence.

Each cast was processed independently and assigned a numerical ranking from 1 – 3 that was used for quality control purposes. A value of 1 was used to identify profiles where the correction methodology was applied successfully and without complications.

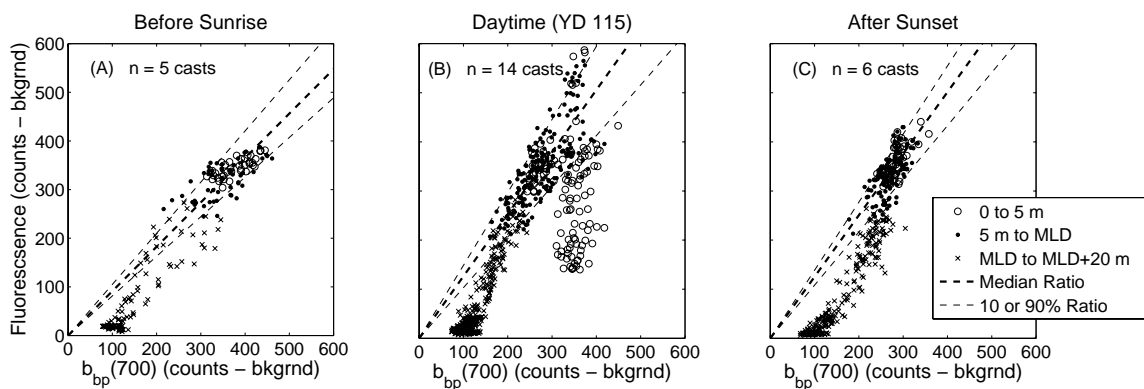


Figure 5.4 **Scatterplots of fluorescence versus backscatter by particles.** Scatterplots of fluorescence (F) versus backscatter by particles ($b_{bp}(700)$) from year day 115. Estimates of $F:b_{bp}(700)$ before sunrise (A) and after sunset (C) were derived using all observations shallower than the mixed layer depth (MLD). Estimates of $F:b_{bp}(700)$ between sunrise and sunset (i.e., daytime; B) were calculated using only observations >5 m and $<MLD$.

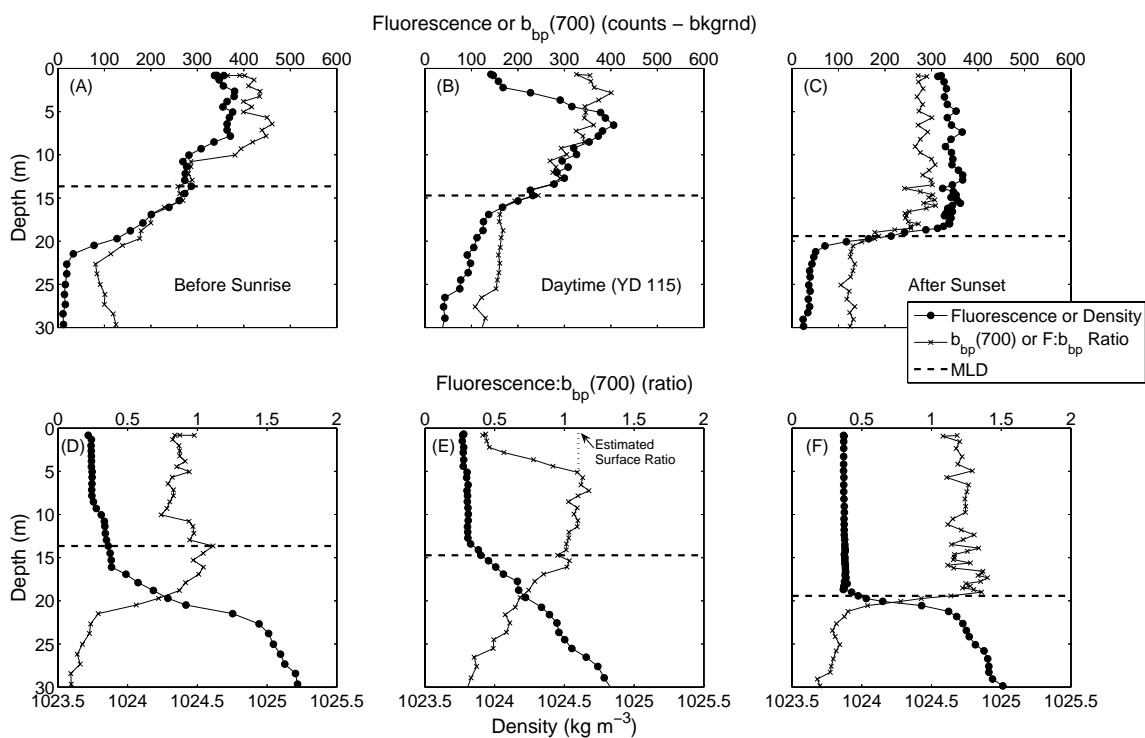


Figure 5.5 Correcting for the bias due to mid-day fluorescence quenching. Selected profiles of fluorescence (F), backscatter by particles ($b_{bp}(700)$), $F:b_{bp}(700)$, and density from year day 115. Mid-day fluorescence quenching resulted in a dramatic decrease in fluorescence near the surface during the day that was not associated with a similar decrease in $b_{bp}(700)$ (B). An estimate of $F:b_{bp}(700)$ from near the base of the mixed layer was extrapolated to the surface (E) and multiplied by the observed $b_{bp}(700)$ to estimate unquenched fluorescence at the surface during the daytime.

A value of 2 was used to identify profiles where mid-day fluorescence quenching penetrated to a depth below the MLD but a region of uniform $F:b_{bp}(700)$ could still be identified below the estimated MLD. In these cases a value of $F:b_{bp}(700)$ from just below the MLD was extrapolated to the surface and the results are still thought to be reliable. A value of 3 was used to identify profiles where a region of uniform $F:b_{bp}(700)$ could not be identified and no correction could be performed.

To compare spatial patterns of variability between corrected Seaglider fluorescence and SeaWiFS-derived estimates chlorophyll *a* a matchup procedure was developed to extract ocean color data from a single satellite image along an arbitrary Seaglider transect. Standard Level 2 ocean color data files contain georeferencing information for each observation (i.e., pixel) in a scene and Seaglider's position is obtained via GPS at the end of each dive cycle while the vehicle is at the surface (one GPS fix is obtained immediately after surfacing and another just prior to the next dive). With this positional information near-surface optical measurements from Seaglider were matched with co-located satellite measurements and satellite data were summarized as a median of all observations within 2.5 km of a Seaglider GPS fix (Fig. 5.6).

Statistical Method. From August 2003 – December 2005 Seaglider made over 2500 dives off the Washington coast and additional missions have continued to the present. Manually characterizing mid-day fluorescence quenching as outlined above is very time consuming with a dataset this size. Therefore, a statistical method to quickly and routinely characterize patterns in mid-day fluorescence quenching was developed.

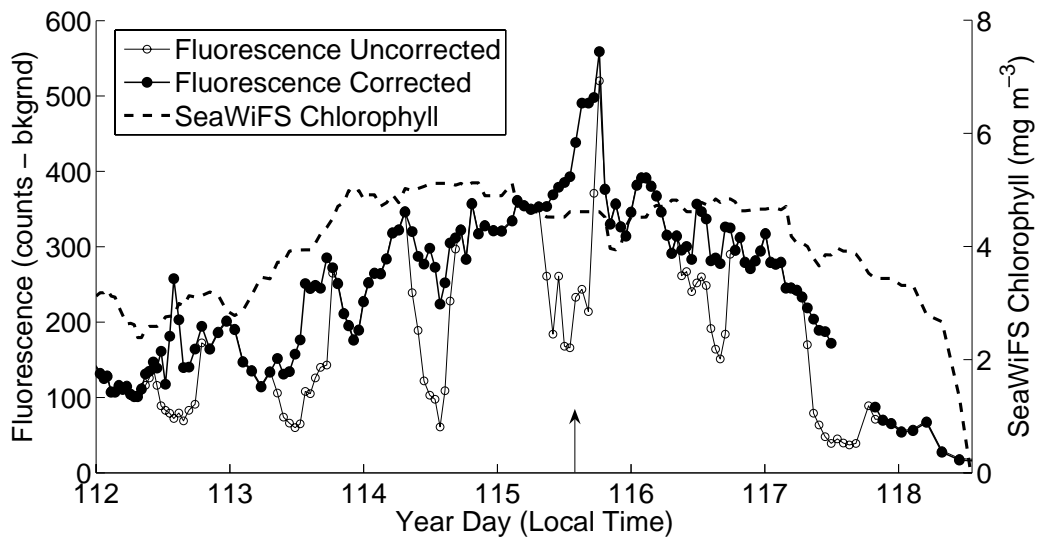


Figure 5.6 **Near-surface fluorescence from Seaglider compared with satellite-derived estimates of chlorophyll *a*.** Comparison between median near-surface (0 – 5 m) fluorescence from Seaglider and satellite-derived estimates of chlorophyll *a* from SeaWiFS (data extracted from a single scene). Arrow denotes when the SeaWiFS image was acquired. The ability to correct individual fluorescence profiles improved our estimates chlorophyll *a* at the surface and allowed us to maintain the spatial and temporal resolution of the dataset. A few profiles from year day 117 could not be corrected (quality control rank = 3) because a region of uniform $F:b_{bp}(700)$ could not be identified.

First, median fluorescence values from 0 – 5 m were calculated for each profile (Fig. 5.7). By comparing daytime fluorescence measurements (presumably suffering from mid-day fluorescence quenching) with interpolated values derived from adjacent nighttime fluorescence measurements (assumed to be free of the effects of mid-day fluorescence quenching) a ‘daytime fluorescence-to-nighttime fluorescence ratio’ ($F_D:F_N$) was calculated. For presentation purposes we have chosen to plot $1-F_D:F_N$ which is analogous to $(F_N-F_D)/F_N$ (e.g., Figs. 5.8-5.11). This metric is sensor independent allowing for comparisons between data from different Seaglider deployments. For each daytime fluorescence measurement (i.e., F_D) the estimated unquenched value (i.e., F_N) was derived using simple linear interpolation between the two closest (in time) nighttime fluorescence measurements. Nighttime was defined as any time before sunrise or after sunset. Initial efforts to model observed values of $1-F_D:F_N$ using a simple 2-parameter differential equation model which used iPAR as input are presented in Appendix B.

The two methods outlined above for assessing mid-day fluorescence quenching (termed ‘Manual’ and ‘Statistical’) were compared by performing both methods using approximately 10% of the daytime fluorescence profiles collected from August 2003 – December 2005 ($n = 145$), chosen at random. There were 24 instances where the ‘Manual’ method could not be applied as $F:b_{bp}(700)$ did not appear uniform in the mixed layer (i.e., quality control rank = 3). This resulted in a final sample size of $n = 121$ profiles with which to compare the performance of the two methods. The geometric mean Model II regression technique (aka reduced major axis method) was used to quantify the relationship between results from each method. This method is preferred when neither dataset is controlled or free of error. The resulting slope minimizes

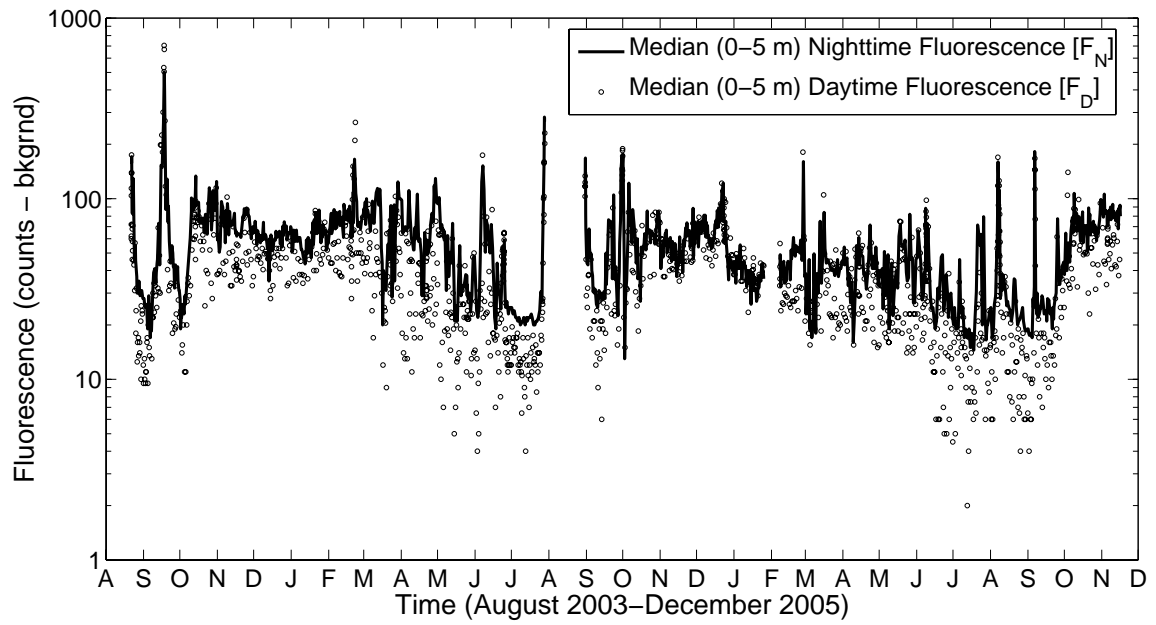


Figure 5.7 **Near-surface fluorescence from August 2003 – December 2005.** Near-surface (0 – 5 m) fluorescence from Seaglider from August 2003 – December 2005. Heavy solid line runs through nighttime fluorescence (F_N) values only.

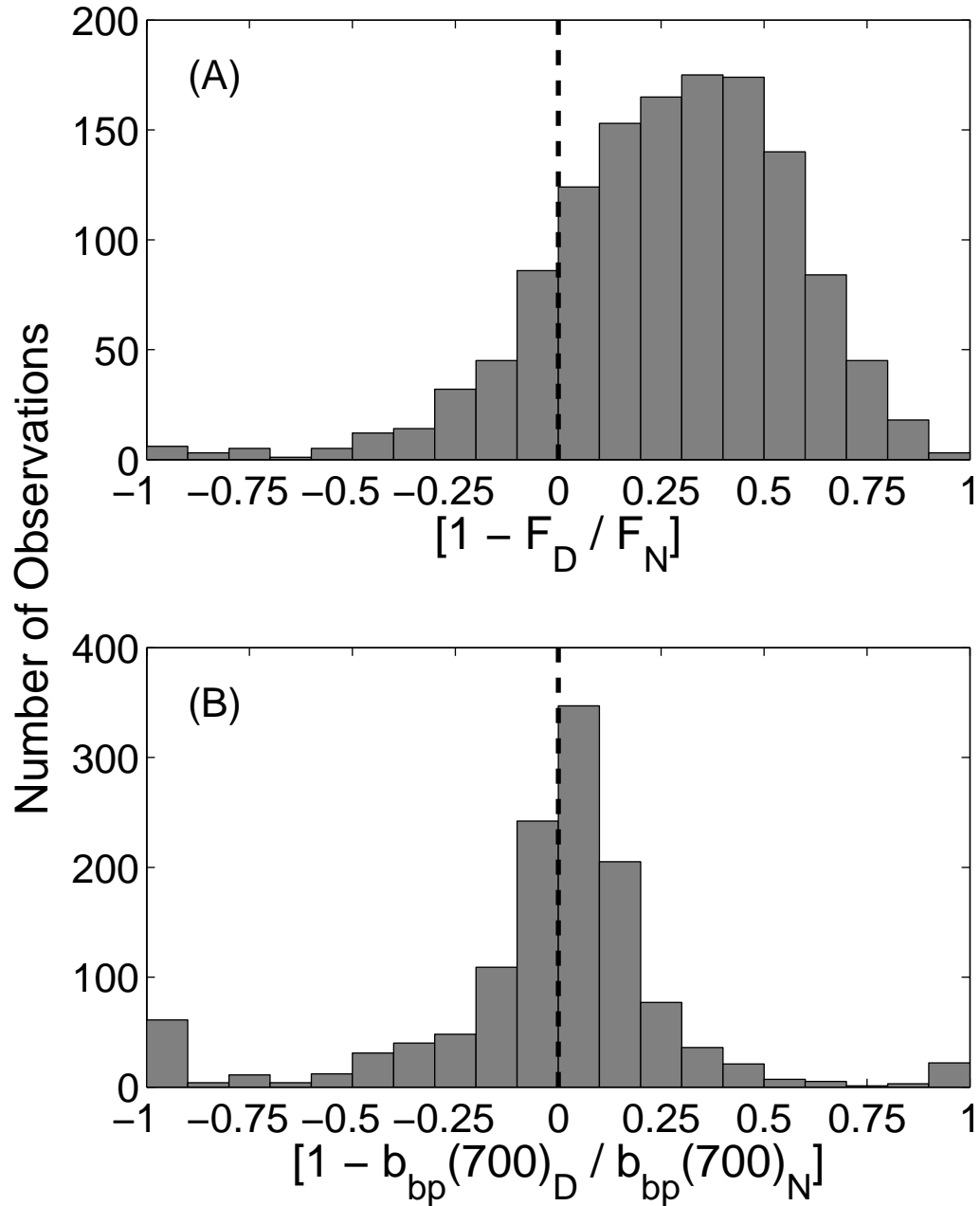


Figure 5.8 **Histograms of $1-F_D:F_N$ and $1-b_{bp}(700)_D/b_{bp}(700)_N$ from Seaglider.** Histograms of $1-F_D:F_N$ (A) and $1-b_{bp}(700)_D/b_{bp}(700)_N$ (B) from Seaglider showing the tendency for daytime fluorescence measurements to be reduced relative to expected nighttime values (due to mid-day fluorescence quenching). A similar pattern was not observed in measurements daytime measurements of $b_{bp}(700)$.

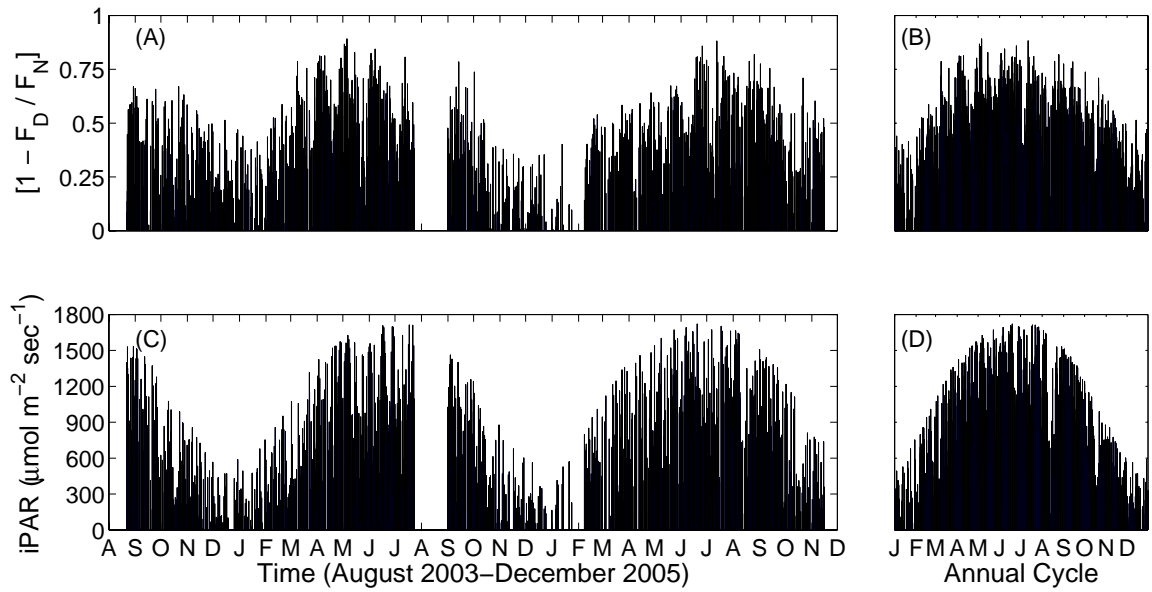


Figure 5.9 **Estimates of $1-F_D:F_N$ and $iPAR$.** Seaglider-derived estimates of $1-F_D:F_N$ (A-B) and $iPAR$ (C-D) from August 2003 – December 2005.

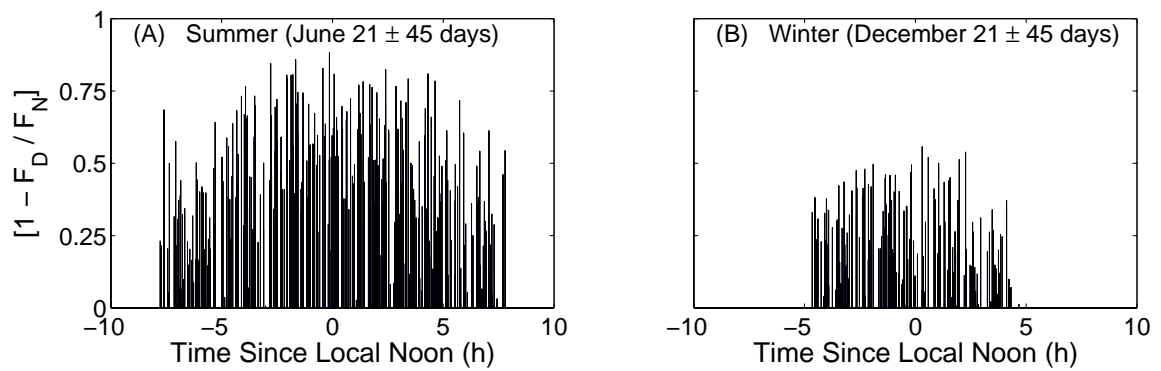
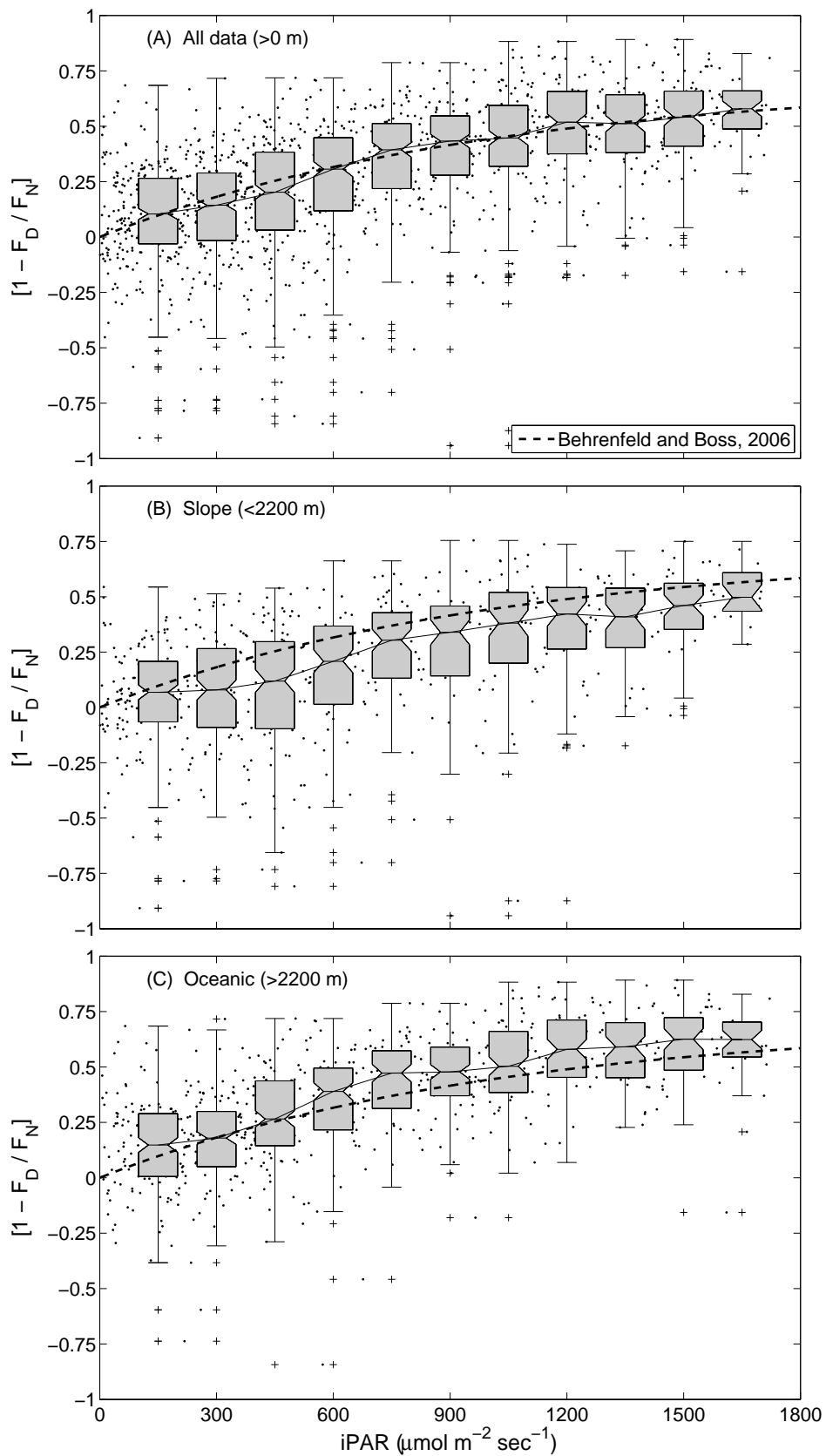


Figure 5.10 **Summer and winter values of $1 - F_D / F_N$.** Seaglider-derived estimates of $1 - F_D / F_N$ as a function of time since local noon for summer (June 21 ± 45 days; A) and winter (December 21 ± 45; B).

Figure 5.11 **Scatterplots of $1-F_D:F_N$ versus iPAR.** Scatterplots of Seaglider-derived estimates of $1-F_D:F_N$ versus satellite-derived estimates of iPAR for complete dataset (A) as well as ‘Slope’ (B) and ‘Oceanic’ (C) subregions. Box plots were calculated from the data using using half-overlapping $300 \mu\text{mol m}^{-2} \text{sec}^{-1}$ bins. Regression from Behrenfeld and Boss (2006) is included for reference.

$$y = 1 - (0.3 + 0.7\exp^{-0.001*iPAR})$$



the absolute value of the sum of the products of the deviations between the observations and the regression line in both the X and Y directions (Ricker, 1973; Laws and Archie, 1981). The correlation between results from each method was used to assess the strength and statistical significance (p-value <0.05) of a linear relationship between the datasets (Fig. 5.12).

Results and Discussion

Manifestation of Quenching in Seaglider Fluorescence Measurements (April 2002)

From 22 – 28 April 2002 (YD 112 – 118) Seaglider collected *in situ* measurements of fluorescence and $b_{bp}(700)$ as it crossed the continental shelf off Washington (Fig. 5.1). Throughout this region mixed layer fluorescence varied by a factor of five. Despite the large gradients, clear and dramatic depressions in fluorescence could be seen during the day near the surface (Figs. 5.2-5.3). In fact, daytime fluorescence measurements collected on YD 114 were reduced by >80% compared to nighttime values (Fig. 5.3A). While gross patterns in $b_{bp}(700)$ were similar to those seen in fluorescence (i.e., increased signal at depths <25 m), fine-scale structure was markedly different between the two datasets and no coincident decreases in $b_{bp}(700)$ were observed during the day (Fig. 5.2). Since a fraction of the $b_{bp}(700)$ signal would have been due to phytoplankton (Stramski and Kiefer, 1991; Vaillancourt *et al.*, 2004) this suggested that fluorescence patterns near the surface were likely biased by mid-day fluorescence quenching and not actually reflecting changes in chlorophyll *a* or phytoplankton biomass. In all cases the quenched fluorescence signal was restricted to the upper 10 m.

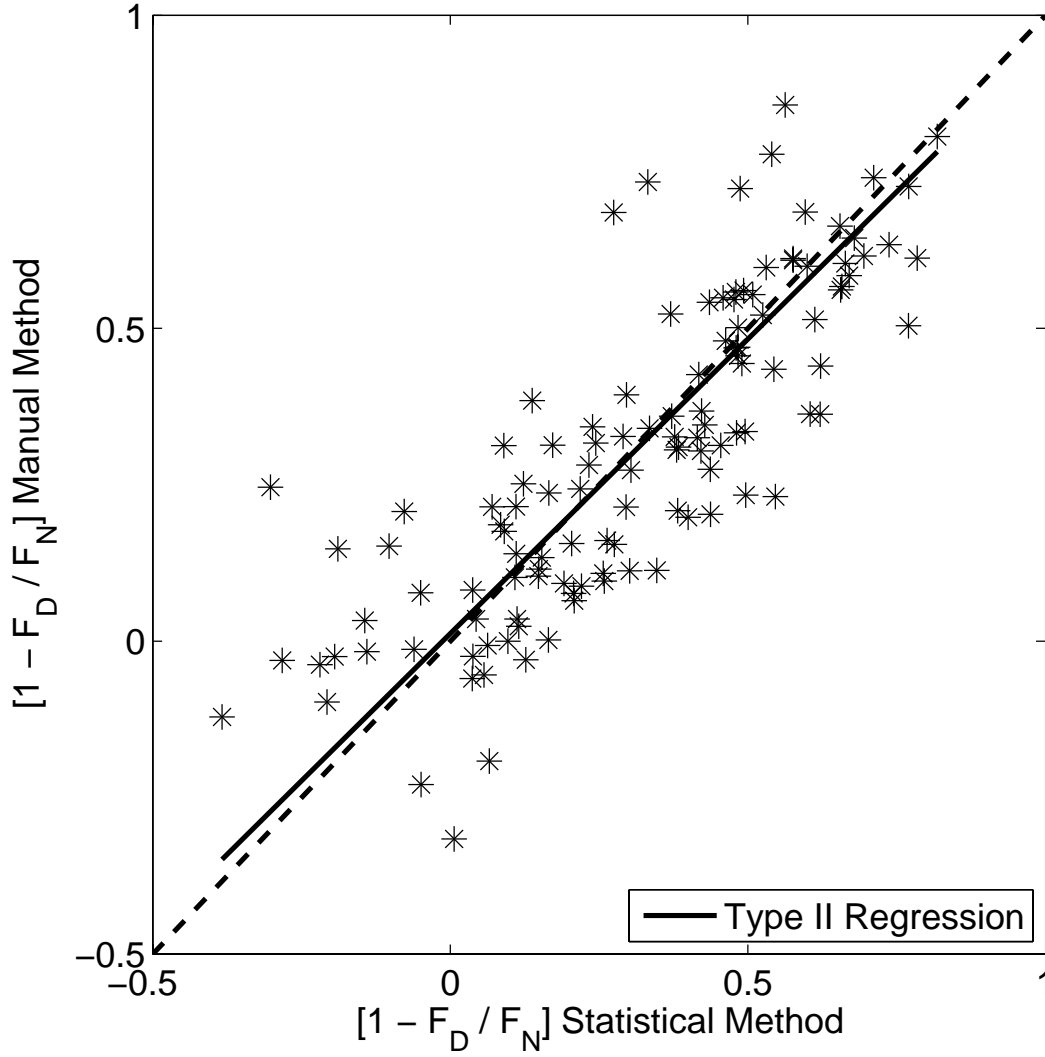


Figure 5.12 **Comparison of methods for assessing mid-day fluorescence quenching.** Type II regression of $1-F_D:F_N$ calculated using both ‘Manual’ and ‘Statistical’ methods for 121 daytime fluorescence profiles collected from August 2003 – December 2005. The resulting slope and offset did not differ significantly from 1 and 0, respectively, and the median absolute deviation between results from the two methods was approximately 0.10.

$$y = 0.94117x + 0.011881; \quad r = 0.815 \text{ (} p < 0.001 \text{)}$$

However, there was a tendency for the quenched fluorescence signal to be limited to shallower depths in regions where a stronger fluorescence signal could be seen near the base of mixed layer; the likely result of increased attenuation and absorption of the downwelling irradiance by phytoplankton throughout the mixed layer in these areas (Fig. 5.3).

Unlike fluorescence, where the signal disappeared at depths >25 m, elevated $b_{bp}(700)$ could be detected throughout much of the water column (up to 200 counts above background) below the pycnocline. These regions of increased $b_{bp}(700)$, without any associated fluorescence, could have been due to sediment resuspension (e.g., due to strong tidal currents near the bottom and/or enhanced upcanyon flows and topographically mediated upwelling associated with the Juan de Fuca canyon system) which may have distributed fine, non-biogenic particles from the bottom into overlying waters (Freeland and Denman, 1982; Allen, 1996; Foreman and Thomson, 1997; Cummins *et al.*, 2000; Fig. 5.2). The restriction of this resuspended material to depths below the pycnocline is important to note as it means that these particles would not have interfered with the F: $b_{bp}(700)$ ratios that were observed in the mixed layer.

'Correcting' Fluorescence Profiles for the Effects of Quenching

Over small spatial and temporal distances the F: $b_{bp}(700)$ ratio was remarkably constant ($\pm 10\%$) throughout the mixed layer despite >2X variations in both fluorescence and $b_{bp}(700)$ (Figs. 5.4-5.5). This is not to say that the $b_{bp}(700)$ signal was due entirely to phytoplankton, only that changes in the overall particle concentration (for which $b_{bp}(700)$ is a proxy) were associated with proportional changes in chlorophyll *a* (for which

fluorescence is a proxy). Below the mixed layer the $F:b_{bp}(700)$ ratio decreased rapidly, suggestive of a change in particle type to more non-biogenic material (Figs. 5.4, 5.5D-F). Before sunrise and after sunset the $F:b_{bp}(700)$ ratio in waters from 0 – 5 m was consistent with what was observed throughout the mixed layer (Figs. 5.4A,C). However, during the daytime a clear depression in the near surface $F:b_{bp}(700)$ ratio could be seen. This unique optical signature (Figs. 5.4B, 5.5E) helped to identify portions of individual fluorescence profiles that were affected by mid-day quenching. For each profile a more appropriate estimate of $F:b_{bp}(700)$ at the surface was obtained by extrapolating from the values of $F:b_{bp}(700)$ found deeper in the mixed layer (Fig. 5.5). The product of the estimated $F:b_{bp}(700)$ ratio and the observed $b_{bp}(700)$ yielded near-surface fluorescence estimates that were unaffected by the bias due to mid-day quenching (Fig. 5.6). Despite the subjective nature of this correction scheme (in terms of the exact value of $F:b_{bp}(700)$ ratio that was chosen for use at the surface) we are confident that the ‘corrected’ fluorescence values are quantitatively much closer to what would have been observed in the absence of mid-day fluorescence quenching. We estimate the maximum error in these new fluorescence estimates to be <10% (given the variability in $F:b_{bp}(700)$ that was observed in the mixed layer in the absence of mid-day quenching).

Even within a surface layer that was completely homogeneous with respect to density variability in fluorescence and/or $b_{bp}(700)$ could still develop. A well-mixed surface layer does not necessarily imply active mixing at the time the measurements are collected. Differential growth and grazing, settling, and motility of the phytoplankton in a non-circulating mixed layer could lead to real changes in phytoplankton biomass that would result in non-uniform profiles of fluorescence and/or $b_{bp}(700)$. A lack of

circulation in the mixed layer might also allow the phytoplankton enough time to photoadapt to a particular light environment, thereby changing both the quantity and type of pigments they contain. The ECO-BB2F excites chlorophyll *a* fluorescence at 470 nm and its ability to stimulate fluorescence is particularly sensitive to changes in accessory pigments which absorb light in this part of the electromagnetic spectrum. Photoadaptive changes alone could result in non-uniform fluorescence profiles, even if phytoplankton biomass remained constant (Neori *et al.*, 1984).

Vertical structure in fluorescence and/or $b_{bp}(700)$ could also develop in an actively mixing surface layer. Stommel (1949) was the first to show how ‘retention zones’ could develop as a result of quasi-organized circulation patterns in the mixed layer (e.g., Langmuir turbulence). Under ideal circumstances convective-type motions in the mixed layer, with timescales $O(30 \text{ min})$, could crudely ‘sort’ particles and planktonic organisms based upon their different settling velocities. Buoyant particles tend to accumulate in the convergent downwelling regions of the circulation, whereas sinking particles accumulate in upwelling limbs of the circulation. Neutrally buoyant particles would be predicted to be distributed uniformly (Smayda, 1970; Denman and Gargett, 1983). This mechanism might possibly lead to small scale patchiness in both the horizontal and vertical dimensions within the mixed layer and lead to changes in both fluorescence and/or $b_{bp}(700)$. Unfortunately, various factors such as plankton behavior and motility, predator-prey interactions, density-dependent aggregation of particles, rapid changes in wind speed and direction, and the degree of stratification (even when it is very weak) can all complicate this idealized pattern (Ledbetter, 1979; Evans and Taylor, 1980; Buranathanitt *et al.*, 1982; Bees *et al.*, 1998; Pershing *et al.*, 2001).

The natural variability in fluorescence and $b_{bp}(700)$, even in the ‘mixed layer’, made it difficult to characterize the effects of mid-day quenching within individual fluorescence profiles. For example, Fig. 5.5B shows a fluorescence profile with low values near the surface and a subsurface maximum near 7 m. Using only this fluorescence profile it would have been difficult to determine if this pattern reflected a true decrease in near-surface phytoplankton biomass or was the result of mid-day fluorescence quenching (both would have been plausible in the absence of other measurements). By focusing on the patterns of the $F:b_{bp}(700)$ ratio in the mixed layer (which tended to be less variable as a function of depth) it was easier to make the necessary distinction between the two processes. The high spatial and temporal resolution that was achieved by Seaglider as it collected profiles across the continental shelf, and the simultaneous measurement of both fluorescence and $b_{bp}(700)$, were crucial to our ability to properly characterize the effects of mid-day fluorescence quenching in this region.

A comparison between the corrected fluorescence measurements from Seaglider and satellite-derived estimates of chlorophyll *a* from SeaWiFS revealed similar patterns. While it may be true that the simple removal of the biased measurements from the dataset would have yielded the same general pattern of phytoplankton biomass across the continental shelf, it would have also hindered our ability to resolve some of the higher-frequency variations (<12 h) that may be important in certain applications. By correcting the near-surface fluorescence measurements for the effects of mid-day quenching we were able to preserve the high spatial and temporal resolution of the dataset (Fig. 5.6).

Seasonal and Inter-annual Patterns of Fluorescence Quenching (August 2003 – December 2005)

With this longer time series we hoped to determine whether the patterns we observed over the continental shelf in April 2002 were consistent throughout all of the Seaglider missions off the Washington coast. Seaglider typically begins its ‘lower resolution-longer duration’ missions seaward of the shelf-slope break (250 m; Fig. 5.1). Seaglider then moves offshore into more oligotrophic waters ($<1 \text{ mg chl } a \text{ m}^{-3}$; Sackmann *et al.*, 2004). Despite our success in characterizing mid-day fluorescence quenching using the ratio of $F:b_{bp}(700)$ in the mixed layer over the continental shelf (termed ‘Manual’ method), the time required to evaluate each profile and the reduced signal:noise ratio in both fluorescence and $b_{bp}(700)$ made this method difficult to apply to this larger dataset. By comparing daytime fluorescence measurements (F_D) with estimates of what the nighttime fluorescence might have been at a the same location (F_N) we were able to use values of $1-F_D:F_N$ to indicate the degree of mid-day quenching (termed ‘Statistical’ method). A comparison between the ‘Manual’ and ‘Statistical’ methods was performed using a subset of the available daytime fluorescence profiles and both methods provided quantitatively similar results (Fig. 5.12).

Consistent with our observations from the continental shelf in April 2002, much of the variability in near-surface fluorescence (0 – 5 m) in these offshore waters was related to a diel rhythm in fluorescence that was not seen in $b_{bp}(700)$ (Figs. 5.7-5.8). We observed values of $1-F_D:F_N > 0$ (suggesting some level of mid-day quenching) in 84% of the daytime fluorescence profiles that were collected from August 2003 – December 2005. Many of the observed values of $1-F_D:F_N < 0$ were collected over the continental

slope where stronger spatial gradients may have lead to large errors in the estimates of $1-F_D:F_N$. Considering just values of $1-F_D:F_N > 0$ we observed marked variability across a range of timescales, from days to years, which was positively correlated with changes in iPAR (Figs. 5.9-5.10). Maximum winter values of $1-F_D:F_N$ were usually <0.5 , however, maximum summer values were >0.8 (similar to what was observed on the continental shelf in April 2002; Figs. 5.3, 5.10). Clearly mid-day quenching must be taken into account at all times of year in these waters in order to properly interpret fluorescence measurements collected near the sea surface.

Interestingly, when values of $1-F_D:F_N$ were plotted as a function of iPAR the resulting pattern was remarkably similar to that observed by Behrenfeld and Boss (2006) in the eastern equatorial Pacific in late 2003 (Fig. 5.11A). This suggests that, at least to first-order, the relationship between incoming solar insolation and the degree of mid-day fluorescence quenching might be parameterized by a relatively simple exponential function that would be applicable to wide-range of oceanographic environments. However, additional measurements from other areas and times of year will be needed to ultimately determine the universality of the prescribed relationship.

While the overall pattern observed in Seaglider-derived estimates of $1-F_D:F_N$ was similar to what was observed by Behrenfeld and Boss (2006) there were consistent differences observed within spatial subsets of the dataset. Two spatial subregions, ‘Slope’ and ‘Oceanic’, were defined using the 2200 m isobath to separate the region of interest (Sackmann *et al.*, 2004). Values of $1-F_D:F_N$ in ‘Slope’ waters were consistently lower than values observed in ‘Oceanic’ waters for any given value of iPAR. This suggested that the effects of mid-day quenching were proportionally more pronounced in

‘Oceanic’ waters; likely the result of higher subsurface irradiances and/or increased nutrient stress for phytoplankton in this more oligotrophic environment (Fig. 5.11B-C). Nutrient stress promotes an increase in effective absorption cross-section of PSII, thus nutrient-limited cells will tend to become photoinhibited at lower photon fluence rates than cells growing in nutrient-rich regimes (Kolber *et al.*, 1988; Falkowski, 1992).

Summary and Conclusions

Our analyses and observations suggest that it is possible to statistically characterize mid-day fluorescence quenching using a relatively small suite of optical measurements (i.e., fluorescence, b_{bp} , and PAR). As the collection of these measurements, especially from autonomous platforms such as Seaglider, becomes more routine it may be possible to dramatically improve fluorescence based estimates of near-surface chlorophyll *a* collected during the daytime. In summary, we have: (i) developed a method to assess and ‘correct’ *in vivo* fluorescence measurements for the bias due to mid-day fluorescence quenching using ratios of $F:b_{bp}(700)$ obtained from deeper within the mixed layer; (ii) confirmed that mid-day fluorescence quenching can be detected throughout the region of interest and at all times of the year; (iii) determined that the relationship between mid-day fluorescence quenching and incoming solar insolation off the Washington coast was remarkably similar to what was observed in the eastern equatorial Pacific suggesting some degree of universality for the observed relationship.

The prevalence of mid-day fluorescence quenching in waters off the Washington coast is striking. This pattern of variability can make it difficult to interpret individual fluorescence profiles, especially if they taken out of context. A subsurface fluorescence

maximum is a common feature in many parts of the ocean. Unfortunately, without a thorough understanding of mid-day fluorescence quenching it could be difficult to determine whether this subsurface structure represents real changes in the quantity of pigment or whether it is due to quenching.

Our ability to ‘correct’ an individual fluorescence profile for the effects of mid-day quenching (as opposed to simply discarding the biased data) allowed us to maintain the spatial and temporal integrity of the dataset and improved our interpretation of fluorescence measurements collected near the surface during the daytime. Using nighttime or corrected daytime estimates of chlorophyll *a* from Seaglider, in combination with pigment estimates from ocean color satellites, it is possible to create an almost 4-dimensional representation of the phytoplankton distribution using only remotely sensed observations (Sackmann and Perry, unpub.). However, in situations when only daytime fluorescence measurements are available correcting for the bias due to mid-day fluorescence quenching is required if these measurements are to have any relevance in larger spatial or temporal contexts.

Mid-day fluorescence quenching is likely to be most pronounced near the surface; however its effects can potentially influence fluorescence measurements throughout the mixed layer. The time it takes phytoplankton cells to recover from the effects imposed by high light intensities varies; factors such as length of exposure, intensity of the ambient light, and nutrient status will influence the recovery kinetics. Experimental data collected at the Darling Marine Center in the summers of 2005 and 2006 suggest that even for cells that were collected during the day and stored in total darkness for 20 min, a marked decrease in fluorescence could still be observed (Drzewianowski and Perry,

unpub.). Even though the analyses presented here focused only on near-surface patterns in mid-day fluorescence there is evidence to suggest that circulation within the mixed layer is fast enough to distribute near-surface phytoplankton populations throughout the mixed layer before full recovery from mid-day quenching can be achieved (Denman and Gargett, 1983; Sackmann and Perry, unpub.). Work is currently underway to determine under what circumstances fluorescence quenching can be detected throughout the mixed layer and when recovery is fast enough to constrain the phenomena to the near-surface.

Acknowledgements

This work is supported by the NSF Seaglider Project (OCE 9911037) and the National Science Foundation Graduate Research Fellowship Program.

Chapter 6

SUMMARY AND CONCLUSIONS

Currently no single remote sensing platform is capable of providing synoptic oceanographic measurements in all 4 dimensions (i.e., x, y, depth, time). Therefore, to truly understand how various oceanographic processes affect phytoplankton distributions in the ocean observations from a variety of disparate platforms must be combined. Satellite ocean color provides one level of insight into ecosystem-level changes by resolving variability in the horizontal (x and y) and temporal dimensions (to the extent allowed by cloud cover). However, more work needs to be done before we can accurately interpret ocean color data in more optically complex regions and fully realize its potential for monitoring global and regional changes with respect to phytoplankton in the ocean. Seaglider is capable of making highly resolved observations of fluorescence and optical backscatter in the vertical (z) dimension over long distances and/or time spans and is unique in its ability to revisit features of interest once they have been detected. Optical measurements from Seaglider represent an efficient way of providing the ground truth and observations under persistently cloudy conditions that are needed to reduce uncertainties associated with converting measurements of ocean color into useful biogeochemical proxies. By combining these two disparate datasets (i.e., ocean color satellite data with in-water optical data from Seaglider) we now have the unprecedented ability to create 4-dimensional views of phytoplankton in the ocean.

Satellite ocean color data was used to characterize variability in near-surface chlorophyll *a* across a range of spatial and temporal scales ranging from 1 – 500 km and

from days – years in waters off the Washington coast (Chapters 2 – 3). Data from the Sea-viewing Wide Field-of-view Sensor (SeaWiFS) showed large negative chlorophyll anomalies in 1998 (due to the lingering affects of the intense 1997 El Niño) and positive anomalies in 2002 (due to a region-wide invasion of Subarctic water). Such analyses would have been difficult, if not impossible, to perform without satellite data (Chapter 2). Similarly, using ocean color measurements to define unique spectral characteristics of water masses off the Washington coast allowed waters from the Juan de Fuca Eddy to be tracked and monitored as they moved southward along the coast. The sustained high biomass in these waters have been correlated with the presence of *Pseudo-nitzschia* spp. and using satellite data to track the trajectories of such patches maybe useful to initiate intensified conditional sampling for domoic acid in the region (Chapter 3). While these examples clearly confirm that satellite-derived products are powerful tools, changes in total water column biomass remain difficult to assess due to the inherent limitation of ocean color measurements to the near-surface. The utility of satellite data is greatly increased when combined with *in-situ* observations.

In Chapter 4 surface satellite imagery was merged with subsurface Seaglider observations to produce a quasi-4-dimensional representation of phytoplankton distributions in September and October 2004 which coincided with the occurrence of a persistent offshore eddy. The California Current System has a well documented network of eddies, meanders, and jets, although relatively little effort has been focused on documenting the prevalence or ecological significance of these features off the Washington coast. This particular eddy was located in deep water off the coast and remained in approximately the same location for more than a month. By combining

satellite and Seaglider data, it was possible to assess the vertical distribution of phytoplankton biomass associated with the eddy and compare it with surrounding water masses and conditions from the previous year.

Despite qualitative agreement between Seaglider and satellite-derived estimates of surface phytoplankton biomass, mid-day quenching of Seaglider fluorescence near the surface makes quantitative comparisons difficult. Data from Seaglider's first 28-day deployment on the Washington shelf and slope in April 2002 indicated that fluorescence could be quenched up to 80% at the surface (at mid-day) and that quenching could penetrate to depths of 10 m. Typically one must relate nighttime fluorescence measurements to daytime satellite measurements in order to avoid the bias due to mid-day fluorescence quenching. It is necessary to understand the magnitude and variability in mid-day fluorescence quenching to be able to use fluorescence as an independent validation for phytoplankton biomass at the surface. A detailed statistical characterization of mid-day fluorescence quenching in April 2002 and from August 2003 – December 2005 was presented in Chapter 5.

With this research I have tried characterize some of the processes that shape the 4-D phytoplankton distributions observed off the Washington coast. Methods developed here can help the oceanographic community integrate large remotely sensed datasets obtained from disparate platforms. This ability is necessary to monitor change in an evolving ocean as we move forward into an era with real-time, regional ocean observing capabilities.

REFERENCES

- Adams, N.G., Lesoing, M., Trainer, V.L., 2000. Environmental conditions associated with domoic acid in razor clams on the Washington coast. *Journal of Shellfish Research* 19(2), 1007-1015.
- Allen, S.E., 1996. Topographically generated, subinertial flows within a finite length canyon. *Journal of Physical Oceanography* 26, 1608-1632.
- Alpine, A.E., Cloern, J.E., 1985. Differences in *in vivo* fluorescence yield between three phytoplankton size classes. *Journal of Plankton Research* 7(3), 381-190.
- Alpine, A.E., Cloern, J.E., Cole, B.E., 1979. Variations in the relationship between *in vivo* fluorescence and chlorophyll *a* in the San Francisco Bay Estuary. *Trans. Am. Geophys. Union* 60, 851.
- Anderson, C.G., 1964. The seasonal and geographic distribution of primary productivity off the Washington and Oregon coasts. *Limnology and Oceanography* 9(3), 284-302.
- Bailey, S.W., McClain, C.R., Werdell, P.J., Schieber, B.D., 2000. Normalized water-leaving radiance and chlorophyll *a* match-up analyses. In: McClain, C.R., Barnes, R.A., Eplee, Jr., R.E., Franz, B.A., Hsu, N.C., Patt, F.S., Pietras, C.M., Robinson, W.D., Schieber, B.D., Schmidt, G.M., Wang, M., Bailey, S.W., Werdell, P.J., SeaWiFS Postlaunch Calibration and Validation Analyses, Part 2. NASA Tech. Memo. 2000-206892, Vol. 10, Hooker, S.B., Firestone, E.R. (Eds), NASA Goddard Space Flight Center, Greenbelt, Maryland, pp. 45-52.

- Bees, M.A., Mezić, I., McGlade, J., 1998. Planktonic interactions and chaotic advection in Langmuir circulation. *Mathematics and Computers in Simulation* 44, 527-544.
- Behrenfeld, M.J., Boss, E., Siegel, D.A., Shea, D.M., 2005. Carbon-based ocean productivity and phytoplankton physiology from space. *Global Biogeochemical Cycles* 19, GB1006.
- Bottom, D.L., Lichatowich, J.A., Frissell, C.A., 1998. Variability of Pacific Northwest marine ecosystems and relation to salmon production. In: McMurray, G.R., Bailey, R.J. (Eds.), Change in Pacific Northwest Coastal Ecosystems. Proceedings of the Pacific Northwest Coastal Ecosystems Regional Study Workshop, August 13-14, 1996, Troutdale, Oregon. NOAA Coastal Ocean Program Decision Analysis Series No. 11. NOAA Coastal Ocean Office, Silver Spring, Maryland, pp. 181-152.
- Boyd, P., Harrison, P.J., 1999. Phytoplankton dynamics in the NE subarctic Pacific. *Deep Sea Research II* 46, 2405-2432.
- Brink, K.H., Jones, B.H., van Leer, J.C., Mooers, C.N., Stuart, D.W., Stevenson, M.R., Dugdale, R.C., Heburn, G.W., 1981. Physical and biological structure and variability in an upwelling center off Peru near 15S during March, 1977. In: Richards, F.A. (Ed.), Coastal Upwelling. American Geophysical Union, pp. 473-495.
- Buranathanitt, T., Cockrell, D.J., John, P.H., 1982. Some effects of Langmuir circulation on the quality of water resource systems. *Ecological Modelling* 15, 49-74.
- Campbell, J.W., 1995. The lognormal distribution as a model for bio-optical variability in the sea. *Journal of Geophysical Research* 100, 13237-13254.

- Cullen, J.J., 1982. The deep chlorophyll maximum: Comparing vertical profiles of chlorophyll *a*. *Canadian Journal of Fisheries and Aquatic Sciences* 39, 791-803.
- Cummins, P.F., Masson, D., Foreman, M.G.G., 2000. Stratification and mean flow effects on diurnal tidal currents off Vancouver Island. *Journal of Physical Oceanography* 30, 15-30.
- Daly, K.L., Byrne, R.H., Dickson, A.G., Gallagher, S.M., Perry, M.J., Tivey, M.K., 2004. Chemical and biological sensors for time-series research: Current status and new directions. *Marine Technology Society Journal* 38(2), 121-143.
- Dandonneau, Y., Neveux, J., 1997. Diel variations of *in vivo* fluorescence in the eastern equatorial Pacific: an unvarying pattern. *Deep Sea Research II* 44(9-10), 1869-1880.
- Demmig-Adams, B., Adams, W.W., 1992. Photoprotection and other responses of plants to high light stress. *Annual Review of Plant Physiology and Plant Molecular Biology* 43, 599-626.
- Denman, K.L., Gargett, A.E., 1983. Time and space scales of vertical mixing and advection of phytoplankton in the upper ocean. *Limnology and Oceanography* 28(5), 801-815.
- Denman, K.L., Abbott, M.R., 1988. Time evolution of surface chlorophyll patterns from cross-spectrum analysis of satellite color images. *Journal of Geophysical Research* 93, 6789-6798.
- Denman, K.L., Abbott, M.R., 1994. Time scales of pattern evolution from cross-spectrum analysis of advanced very high resolution radiometer and coastal zone color scanner imagery. *Journal of Geophysical Research* 99, 7433-7442.

- Denman, K.L., Mackas, D.L., Freeland, H.J., 1981. Persistent upwelling and mesoscale zones of high productivity off the west coast of Vancouver Island, Canada. In: Richards, F.A. (Ed.), Coastal Upwelling. American Geophysical Union, pp. 514-521.
- Dickey, T., Lewis, M., Chang, G., 2006. Optical oceanography: Recent advances and future directions using global remote sensing and in situ observations. *Review of Geophysics* 44, RG1001.
- Ekman, V.W., 1905. On the influence of the earth's rotation on ocean currents. *Arch. Math. Astron. Phys.* 2, 1-52.
- Emery, W.J., Tomas, A.C., Collins, M.J., Crawford, W.R., Mackas, D.L., 1986. An objective method for computing advective surface velocities from sequential infrared satellite images. *Journal of Geophysical Research* 91, 12865-12878.
- Eriksen, C.C., Osse, T.J., Light, R.D., Wen, T., Lehman, T.W., Sabin, P.L., Ballard, J.W., Chiodi, A.M., 2001. A long-range autonomous underwater vehicle for oceanographic research. *IEEE Journal of Oceanic Engineering* 26(4), 424-436.
- Evans, G.T., Taylor, F.J.R., 1980. Phytoplankton accumulation in Langmuir cells. *Limnology and Oceanography* 25(5), 840-845.
- Falkowski, P.G., Kolber, Z., 1995. Variations in chlorophyll fluorescence yields in phytoplankton in the world oceans. *Australian Journal of Plant Physiology* 22, 341-355.
- Falkowski, P.G., 1992. Molecular ecology of phytoplankton photosynthesis. In: Falkowski, P.G., Woodhead, A.D. (Eds.), Primary Productivity and Biogeochemical Cycles in the Sea, Plenum Press, New York, pp. 47-67.

- Falkowski, P.G., Kolber, Z., 1995. Variations in chlorophyll fluorescence yields in phytoplankton in the world oceans. *Australian Journal of Plant Physiology* 22, 341-355.
- Falkowski, P.G., Greene, R., Kolber, Z., 1994. Light utilization and photoinhibition of photosynthesis in marine phytoplankton. In: Baker, N.R., Bowes, J. (Eds.), Photoinhibition of photosynthesis: from molecular mechanisms to the field, Bios Scientific, Oxford, pp. 407-432.
- Fang, W., Hsieh, W.W., 1993. Summer sea surface temperature variability off Vancouver Island from satellite data. *Journal of Geophysical Research* 98, 14391-14400.
- Fisher, J.P., Pearch, W.G., 1988. Growth of juvenile coho salmon (*Oncorhynchus kisutch*) in the ocean off Oregon and Washington, USA, in years of differing coastal upwelling. *Canadian Journal of Fisheries and Aquatic Sciences* 45, 1036-1044.
- Foreman, M.G.G., Thomson, R.E., 1997. Three-dimensional model simulations of tides and buoyancy currents along the west coast of Vancouver Island. *Journal of Physical Oceanography* 27, 1300-1325.
- Freeland, H.J., Gatién, G., Huyer, A., Smith, R.L., 2003. Cold halocline in the northern California Current: An invasion of subarctic water. *Geophysical Research Letters* 30, doi:10.1029/2002GL016663.
- Freeland, H.J., Denman, K.L., 1982. A topographically controlled upwelling centre off southern Vancouver Island. *Journal of Marine Research* 40(4), 1069-1093.

- Fritz, L., Quilliam, M.A., Wright, J.L.C., Beale, A.M., Work, T.M., 1992. An outbreak of domoic acid poisoning attributed to the pennate diatom *Pseudo-nitzschia australis*. *Journal of Phycology* 28, 604-607.
- Garver, S.A., Siegel, D.A., 1997. Inherent optical property inversion of ocean color spectra and its biogeochemical interpretation: 1. Time series from the Sargasso Sea. *Journal of Geophysical Research* 102, 18607-18625.
- Geider, R.J., MacIntyre, H.L., Kana, T.M., 1998. A dynamic regulatory model of phytoplanktonic acclimation to light, nutrients, and temperature. *Limnology and Oceanography* 43(4), 679-694.
- Gordon, H.R., McCluney, W.R., 1975. Estimation of the depth of sunlight penetration in the sea for remote sensing. *Applied Optics* 14(2), 413-416.
- Gordon, H.R., Brown, O.B., Evans, R.H., Brown, J.W., Smith, R.C., Baker, K.S., Clark, D.K., 1988. A semianalytic radiance model of ocean color. *Journal of Geophysical Research* 93, 10909-10924.
- Gotway, C.A., Young, L.J., 2002. Combining incompatible spatial data. *Journal of the American Statistical Association* 97, 632-648.
- Gruen, A., 1985. Adaptive Least Squares Correlation: A powerful image matching technique. *South African Journal of Photogrammetry, Remote Sensing and Cartography* 14(3), 175-187.
- Hickey, B.M., 1979. The California current system – Hypotheses and facts. *Progress in Oceanography* 8, 191-279.

- Hickey, B.M., 1989. Patterns and processes of circulation over the Washington continental shelf and slope. In: Landry, M.R., Hickey, B.M. (Eds.), Coastal Oceanography of Washington and Oregon. Elsevier, Amsterdam, pp. 41-115.
- Hickey, B.M., Banas, N.S., 2003. Oceanography of the U.S. Pacific Northwest Coastal Ocean and Estuaries with Application to Coastal Ecology. *Estuaries* 26, 1010-1031.
- Hickey, B.M., Geier, S., Kachel, N., MacFadyen, A., 2005. A bi-directional river plume: The Columbia in summer. *Continental Shelf Research* 25, 1631-1656.
- Hickey, B.M., Thomson, R.E., Yih, H., LeBlond, P.H., 1991. Velocity and temperature fluctuations in a buoyancy-driven current off Vancouver Island. *Journal of Geophysical Research* 96, 10507-10538.
- Hickey, B.M., Thomson, R.E., Yih, H., LeBlond, P.H., 1991. Velocity and temperature fluctuation in a buoyancy-driven current off Vancouver Island. *Journal of Geophysical Research* 96, 10507-10538.
- Hoge, F.E., Lyon, P.E., 1996. Satellite retrieval of inherent optical properties by linear matrix inversion of oceanic radiance models: An analysis of model and radiance measurement errors. *Journal of Geophysical Research* 101, 16631-16648.
- Horner, R.A., Garrison, D.L., Plumley, F.G., 1997. Harmful algal bloom and red tide problems on the US west coast. *Limnology and Oceanography* 42, 1076-1088.
- Horner, R.A., Hickey, B.M., Postel, J.R., 2000. Harmful algal blooms and physical oceanography off Washington State, USA. *South African Journal of Marine Science* 22, 299-308.

- Huyer, A., Sobey, E.J.C., Smith, R.L., 1979. The spring transition in currents over the continental shelf. *Journal of Geophysical Research* 84, 6995-7011.
- Huyer, A.E., Smith, R.L., 1985. The signature of El Nino off Oregon, 1982-1983. *Journal of Geophysical Research* 90, 7133-7142.
- Ikeda, M., Emery, W.J., Mysak, L.A., 1984. Seasonal variability in meanders of the California Current System off Vancouver Island. *Journal of Geophysical Research* 89, 3487-3505.
- Ikeda, M., Emery, W.J., 1984. A continental shelf upwelling event off Vancouver Island as revealed by satellite infrared imagery. *Journal of Marine Research* 42, 303-317.
- Ikeda, M., Mysak, L.A., Emery, W.J., 1984. Observation and modeling of satellite-sensed meanders and eddies off Vancouver Island. *Journal of Physical Oceanography* 14, 3-21.
- Kahru, M., Mitchell, B.G., 2000. Influence of the 1997-98 El Niño on the surface chlorophyll in the California Current. *Geophysical Research Letters* 27, 2937-2940.
- Kiefer, D.A., 1973a. Fluorescence properties of natural phytoplankton populations. *Marine Biology* 22, 263-269.
- Kiefer, D.A., 1973b. Chlorophyll *a* fluorescence in marine centric diatoms: Responses of chloroplasts to light and nutrient stress. *Marine Biology* 23, 39-46.

- Kiefer, D.A., Reynolds, R.A., 1992. Advances in understanding phytoplankton fluorescence and photosynthesis. In: Falkowski, P.G., Woodhead, A.D. (Eds.), Primary Productivity and Biogeochemical Cycles in the Sea, Plenum Press, New York, pp. 155-174.
- Kirk, J.T.O., 1994. Light and Photosynthesis in Aquatic Ecosystems, Cambridge University Press, New York.
- Kolber, Z., Zehr, J., Falkowski, P.G., 1988. Effects of growth irradiance and nitrogen limitation on photosynthetic energy conversion in photosystem II. *Plant Physiology* 88, 923-929.
- Krause, G.H., Jahns, P., 2004. Non-photochemical energy dissipation determined by chlorophyll fluorescence quenching: characterization and function. In: Papageorgiou, G.C. and Govindjee (Eds.), Chlorophyll a fluorescence: a signature of photosynthesis. Springer, Dordrecht, pp. 463-495.
- Krauss, W., 1993. Ekman drift in homogeneous water. *Journal of Geophysical Research* 98, 20187-20209.
- Kyle, D.J., Ohad, I., Arntzen, C.J., 1984. Membrane protein damage and repair: Selective loss of quinine protein function in chloroplast membranes. *Proceedings of the National Academy of Sciences* 81(13), 4070-4074.
- Landry, M.R., Postel, J.R., Peterson, W.K., Newman, J., 1989. Broad-scale distributional patterns of hydrographic variables on the Washington/Oregon shelf. In: Landry, M.R., Hickey, B.M. (Eds.), Coastal Oceanography of Washington and Oregon. Elsevier, Amsterdam, pp. 1-40.

- Laws, E.A., Archie, J.W., 1981. Appropriate use of regression analysis in marine biology. *Marine Biology* 65, 13-16.
- Ledbetter, M., 1979. Langmuir circulations and plankton patchiness. *Ecological Modelling* 7, 289-310.
- Loftus, M.E., Seliger, H.H., 1975. Some limitations of the *in vivo* fluorescence technique. *Chesapeake Science* 16, 79-92.
- Loisel, H., Bosc, E., Stramski, D., Oubelkheir, K., Deschamps, P.-Y., 2001. Seasonal variability of the backscattering coefficient in the Mediterranean Sea based on Satellite SeaWiFS imagery. *Geophysical Research Letters* 28(22), 4203-4206.
- Loisel, H., Nicolas, J.-M., Deschamps, P.-Y., Frouin, R., 2002. Seasonal and inter-annual variability of particulate organic matter in the global ocean. *Geophysical Research Letters* 29(24), 2196-2199.
- Lorenzen, C., 1966. A method for the continuous measurement of *in vivo* chlorophyll concentration. *Deep Sea Research* 13, 223-227.
- Lynn, R.J., Schwing, F.B., Hayward, T.L., 1995. The effect of the 1991-93 ENSO on the California Current System. *California Cooperative Oceanic Fisheries Investigation Reports* 36, 19-39.
- MacFadyen, A., Hickey, B.M., Foreman, M.G.G., 2005. Transport of surface waters from the Juan de Fuca eddy region to the Washington coast. *Continental Shelf Research* 25, 2008-2021.
- Mackas, D.L., Yelland, D.R., 1999. Horizontal flux of nutrients and phytoplankton across and along the British Columbia continental margin. *Deep Sea Research II* 46, 2941-2967.

- Mackas, D.L., Sefton, H.A., 1982. Plankton species assemblages of southern Vancouver Island: Geographic pattern and temporal variability. *Journal of Marine Research* 40(4), 1173-1200.
- Mackas, D.L., Yelland, D.R., 1999. Horizontal flux of nutrients and phytoplankton across and along the British Columbia continental margin. *Deep-Sea Research II* 46, 2941-2967.
- Marchetti, A., Trainer, V.L., Harrison, P.J., 2004. Environmental conditions and phytoplankton dynamics associated with *Pseudo-nitzschia* abundance and domoic acid in the Juan de Fuca eddy. *Marine Ecology Progress Series* 281, 1-12.
- McFarlane, G.A., Ware, D.M., Thomson, R.E., Mackas, D.L., Robinson, C.L.K., 1997. Physical, biological and fisheries oceanography of a large ecosystem (west coast of Vancouver Island) and implications for management. *Oceanologica Acta* 20, 191-200.
- McGillicuddy, D.J., Signell, R.P., Stock, C.A., Keafer, B.A., Keller, M.D., Hetland, R.D., Anderson, D.M., 2003. A mechanism for offshore initiation of harmful algal blooms in the coastal Gulf of Maine. *Journal of Plankton Research* 25(9), 1131-1138.
- McGowan, J.A., Cayan, D.R., Dorman, L.M., 1998. Climate-ocean variability and ecosystem response in the Northeast Pacific. *Science* 28, 210-217.
- Naval Research Laboratory, 2001. NAAPS study of April 2001 (20010406-19) Asian dust event. http://www.nrlmry.navy.mil/aerosol/Case_studies/20010413_epac/.
Last updated: April 19, 2001.

- Neori, A., Holm-Hansen, O., Mitchell, B.G., Kiefer, D.A., 1984. Photoadaptation in Marine Phytoplankton. *Plant Physiology* 76, 518-524.
- NOAA/NESDIS CoastWatch, 2003. El Niño Watch Advisories (1998-2002).
<http://coastwatch.pfel.noaa.gov/elnino.html>. Last accessed: July 23, 2003.
- Ohad, I., Adir, N., Koike, H., Kyle, D.J., Inoue, Y., 1990. Mechanism of photoinhibition *in vivo*. *Journal of Biological Chemistry* 265, 1972-1979.
- ORION Executive Steering Committee, 2005, Ocean Observatories Initiative Science Plan. Washington, DC, 102 pp.
- Pearcy, W.G., 1992. Ocean Ecology of North Pacific Salmonids. University of Washington Press, Seattle.
- Perry, M.J., Bolger, J.P., English, D.C., 1989. Primary production in Washington coastal waters. In: Landry, M.R., Hickey, B.M. (Eds.), Coastal Oceanography of Washington and Oregon. Elsevier, Amsterdam, pp. 117-138.
- Pershing, A.J., Wiebe, P.H., Manning, J.P., Copley, N.J., 2001. Evidence for vertical circulation cells in the well-mixed area of Georges Bank and their biological implications. *Deep Sea Research II* 48, pp. 283-310.
- Ricker, W.E., 1973. Linear regressions in fishery research. *Journal of the Fisheries Research Board of Canada* 30, 409-434.
- Rienecker, M.M., Mooers, C.N.K., 1986. The 1982-83 El Niño signal off northern California. *Journal of Geophysical Research* 91, 6597-6608.
- Roegner, C.G., Hickey, B.M., Newton, J.A., Shanks, A.L., Armstrong, D.A., 2002. Wind-induced plume and bloom intrusions into Willapa Bay, Washington. *Limnology and Oceanography* 47(4) 1033-1042.

- Roesler, C.S., Perry, M.J., 1995. In situ phytoplankton absorption, fluorescence emission, and particulate backscattering spectra determined from reflectance. *Journal of Geophysical Research* 100, 13279-13294.
- Rudnick, D.L., Perry, M.J. (Eds), 2003, ALPS: Autonomous and Lagrangian Platforms and Sensors. Workshop Report, 64 pp.
- Rudnick, D.L., Davis, R.E., Eriksen, C.C., Fratantoni, D.M., Perry, M.J., 2004. Underwater gliders for ocean research. *Marine Technology Society Journal* 38(1), 48-59.
- Sackmann, B.S., Mack, L., Logsdon, M., Perry, M.J., 2004. Seasonal and inter-annual variability of SeaWiFS-derived chlorophyll *a* concentrations in waters off the Washington and Vancouver Island coasts, 1998-2002. *Deep Sea Research II* 51, 945-965.
- Sackmann, B.S., Perry, M.J., 2006. Ocean color observations of a surface water transport event: Implications for *Pseudo-nitzschia* on the Washington coast. *Harmful Algae* 5, 608-619.
- Sathyendranath, S., Bukata, R.P., Arnone, M.D., Dowell, M.D., Davis, C.O., Babin, M., Berthon, J.F., Kopelevich, O.V., Campbell, J.W., 2000. Colour of case 2 waters. In: S. Sathyendranath (Ed.), Remote sensing of ocean colour in coastal, and other optically-complex, waters. Reports of the International Ocean-Colour Coordinating Group, No. 3, IOCCG, Dartmouth, Canada, pp. 23-46.
- Scholun, C.A., Gulland, F., Douchette, G.J., Benson, S. and 22 others, 2000. Mortality of sea lions along the central California coast linked to a toxic diatom bloom. *Nature* 403, 80-84.

- Siegel, D.A., Wang, M., Maritorena, S., Robinson, W., 2000. Atmospheric correction of satellite ocean color imagery: the black pixel assumption. *Applied Optics* 39(21), 3582-3591.
- Siegel, D.A., Maritorena, S., Nelson, N.B., Behrenfeld, M.J., C.R. McClain, 2005. Colored dissolved organic matter and its influence on the satellite-based characterization of the ocean biosphere. *Geophysical Research Letters* 32, L20605.
- Siegel, D.A., Wang, M., Maritorena, S., Robinson, W., 2000. Atmospheric correction of satellite ocean color imager: the black pixel assumption. *Applied Optics* 39(21), 3582-3591.
- Slawomir, B.W., Stramski, D., 2004. Modeling the optical properties of mineral particles suspended in seawater and their influence on ocean reflectance and chlorophyll estimation from remote sensing algorithms. *Applied Optics* 43(17), 3489-3503.
- Slovacek, R.E., Hannan, P.J., 1977. In vivo fluorescence determinations of phytoplankton chlorophyll *a*. *Limnology and Oceanography* 22(5), 919-925.
- Smayda, T.J., 1970. The suspension and sinking of phytoplankton in the sea. *Oceanography and Marine Biology Annual Review* 8, 353-413.
- Smith, R.L., 1995. The physical process of coastal ocean upwelling systems. In: Summerhays, C.P., Emis, K.C., Angel, M.V., Smith, R.L., Zeitzschel, B. (Eds.), Upwelling in the Oceans: Modern Processes and Ancient Records. Wiley and Sons, New York, pp. 40-64.
- Smith, W.H.F., Sandwell, D.T., 1997. Global sea floor topography from satellite altimetry and ship depth soundings. *Science* 26, 1956-1962.

- Smith, W.O., Heburn, G.W., Barber, R.T., O'Brien, J.J., 1983. Regulation of phytoplankton communities by physical processes in upwelling ecosystems. *Journal of Marine Research* 41(3), 539-556.
- Stommel, H., 1949. Trajectories of small bodies sinking slowly through convection cells. *Journal of Marine Research* 8, 25-29.
- Stramski, D., Kiefer, D.A., 1991. Light scattering by microorganisms in the open ocean. *Progress in Oceanography* 28, 343-383.
- Stramski, D., Boss, E., Bogucki, D., Voss, K.J., 2004. The role of seawater constituents in light backscattering in the ocean. *Progress in Oceanography* 61, 27-56.
- Stramski, D., Reynolds, R.A., Kahru, M., Mitchell, G., 1999. Estimation of particulate organic carbon in the ocean from satellite remote sensing. *Science* 285, 239-242.
- Strickland, J.D.H., 1968. Continuous measurement of *in vivo* chlorophyll; a precautionary note. *Deep Sea Research* 15, 225-227.
- Strub, P.T., James, C., 2000. Altimeter-derived variability of surface velocities in the California Current System: 2. Seasonal circulation and eddy statistics. *Deep Sea Research II* 47, 831-870.
- Strub, P.T., James, C., Thomas, A.C., Abbot, M.R., 1990. Seasonal and nonseasonal variability of satellite-derived surface pigment concentration in the California Current. *Journal of Geophysical Research* 95, 11501-11530.
- Strub, P.T., Kosro, P.M., Huyer, A., 1991. The nature of cold filaments in the California current system. *Journal of Geophysical Research* 96, 14743-14768.

- Stumpf, R.P., Arnone, R.A., Gould, R.W., Martinolich, P.M., Ransibrahmanakul, V.,
2003. A partially coupled ocean-atmosphere model for retrieval of water-leaving
radiance from SeaWiFS in coastal waters. In: S.B. Hooker, Firestone, E.R.
(Eds.), Algorithm Updates for the fourth SeaWiFS data reprocessing. NASA
Tech. Memo. 2003-206892, Vol. 22, Chapter 9. NASA Goddard Space Flight
Center, Greenbelt, Maryland, pp. 51-59.
- Takahashi, M., Shimura, S., Yamaguchi, Y., Fujita, Y., 1971. Photo-inhibition of
phytoplankton photosynthesis as a function of exposure time. *Journal of
Oceanography* 27, 43-50.
- Thomas, A., Strub, P.T., 2001. Cross-shelf phytoplankton pigment variability in the
California Current. *Continental Shelf Research* 21, 1157-1190.
- Thomas, A., Strub, P.T., Brickley, P., 2003. Anomalous satellite-measured chlorophyll
concentrations in the northern California Current in 2001-2002. *Geophysical
Research Letters* 30, doi:10.1029/2003GL017409.
- Trainer, V.L., Adams, N.G., Bill, B.D., Stehr, C.M., Wekell, J.C., Moeller, P., Busman,
M., Woodruff, D., 2000. Domoic acid production near California coastal
upwelling zones, June 1998. *Limnology and Oceanography* 47, 1438-1446.
- Trainer, V.L., Hickey, B.M., Horner, R.A., 2002. Biological and physical dynamics of
domoic acid production off the Washington coast. *Limnology and Oceanography*
47(5), 1438-1446.
- Trainer, V.L., Suddleson, M., 2005. Monitoring approaches for early warning of domoic
acid events in Washington State. *Oceanography* 18(3), 228-237.

- Tufte, E.R., 2001. The Visual Display of Quantitative Information, Graphics Press, Cheshire, Connecticut.
- Tully, J.P., 1942. Surface non-tidal currents in the approaches to Juan de Fuca strait. *Journal of the Fisheries Research Board of Canada* 5(4), 398-409.
- Twardowski, M., Boss, E., Macdonald, J.B., Pegau, W.S., Barnard, A.H., Zaneveld, J.R., 2001. A model for estimating bulk refractive index from the optical backscattering ratio and the implications for understanding particle composition in case I and case II waters. *Journal of Geophysical Research* 106, 14129-14142.
- Vaillancourt, R.D., Brown, C.W., Guillard, R.R.L., Balch, W.M., 2004. Light backscattering properties of marine phytoplankton: relationships to cell size, chemical composition and taxonomy. *Journal of Plankton Research* 26(2), 191-212.
- Venkatesh, S., Crawford, W.R., 1993. Spread of oil from the *Tenyo Maru*, off the southwest coast of Vancouver Island. *Natural Hazards* 8, 75-91.
- Walsh, J.J., 1991. Importance of continental margins in the marine biogeochemical cycling of carbon and nitrogen. *Nature* 350, 53-55.
- Wekell, J.C., Trainer, V.L., Ayres, D., Simons, D., 2002. A study of spatial variability of domoic acid in razor clams: recommendations for resource management on the Washington coast. *Harmful Algae* 1, 35-43.

- Welty, L.J., Stein, M.L., Lesht, B.M., Vanderploeg, H.A., Johengen, T.H., 2004. A quantitative correction for non-photochemical quenching in the calibration of chlorophyll fluorescence to chlorophyll *a* concentration, applied to Lake Michigan. *The University of Chicago Center for Integrating Statistical and Environmental Science Technical Reports* 17, 1-26.
- Wheeler, P.A., Huyer, J., and Fleischbein, J., 2003. Cold halocline, increased nutrients and higher productivity off Oregon in 2002. *Geophysical Research Letters* 30 (15), doi:10.1029/2003GL017395.
- Zaneveld, J.R., Barnard, A.H., Boss, E.B., 2005. Theoretical derivation of the depth average of remotely sensed optical parameters. *Optics Express* 13(2), pp. 9052-9061.
- Zar, J.H., 1999. *Biostatistical Analysis (4th Edition)*. Prentice Hall, Upper Saddle River, New Jersey.

APPENDICES

Appendix A. Maps of monthly and six-month median (50th percentile) chlorophyll *a* concentrations with corresponding estimates of data density

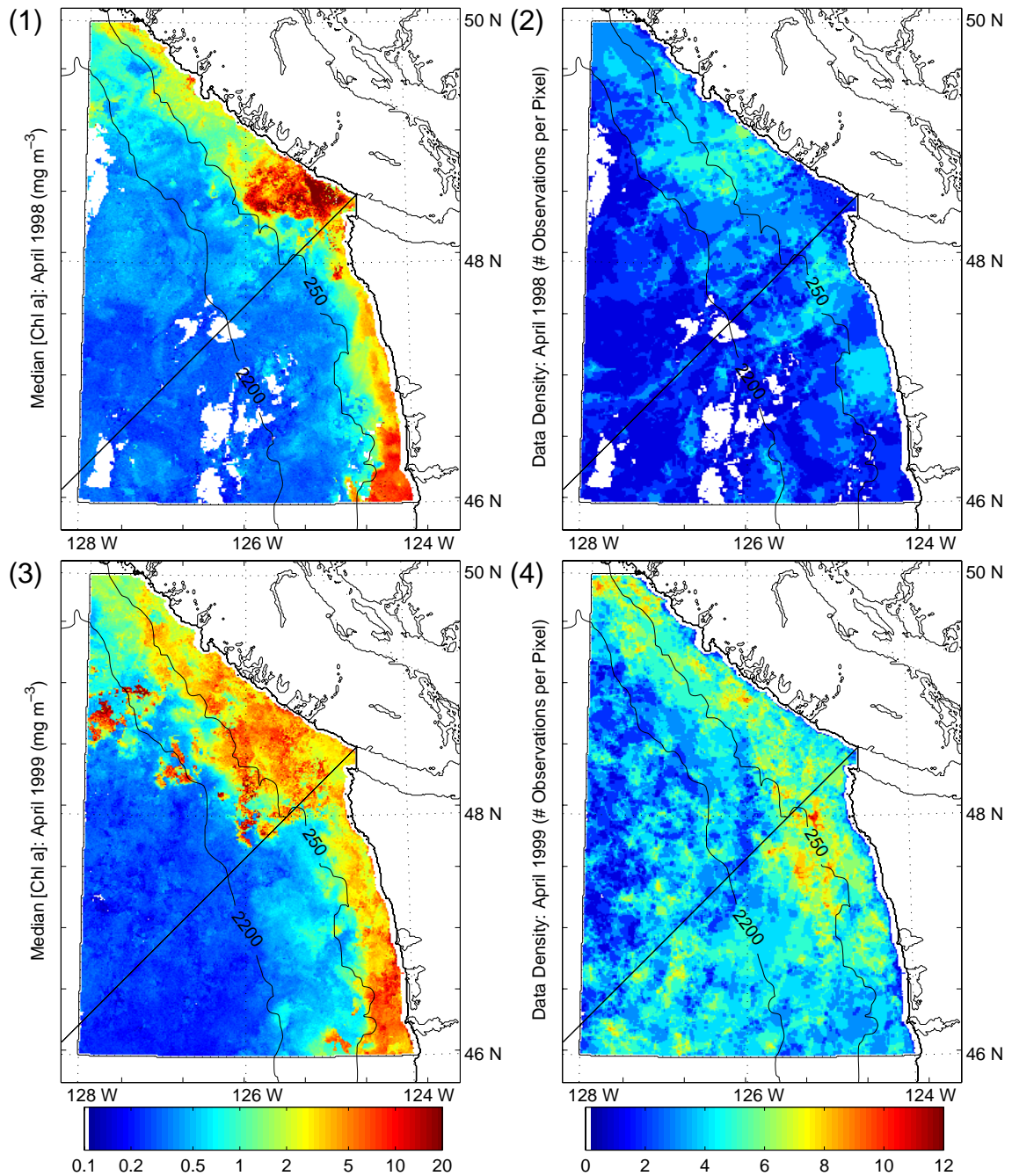


Figure A.1 Maps of monthly and six-month median (50th percentile) chlorophyll *a* concentrations for April – September of 1998 – 2002 (panels 1-70, odd) with corresponding estimates of data density (panels 1-70, even).

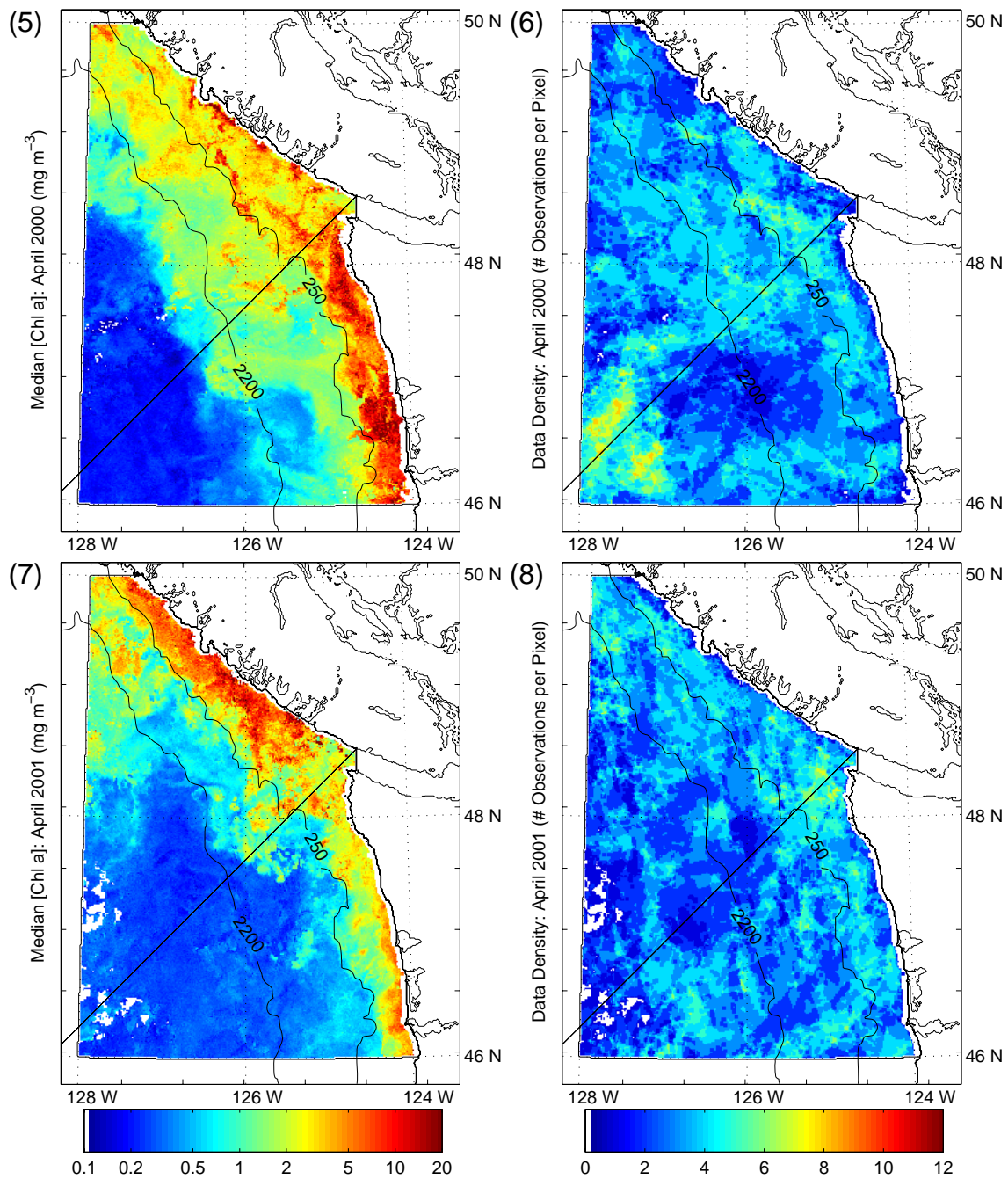


Figure A.1 cont.

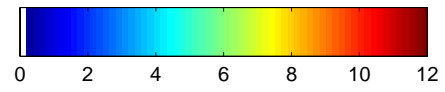
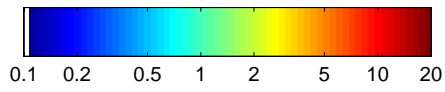
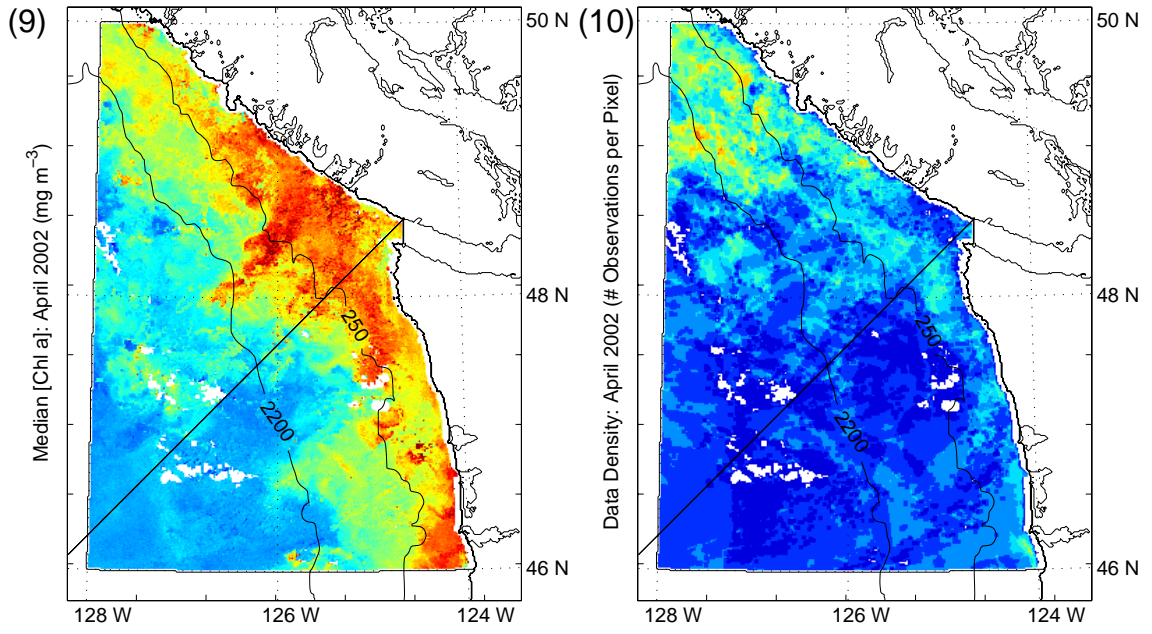


Figure A.1 cont.

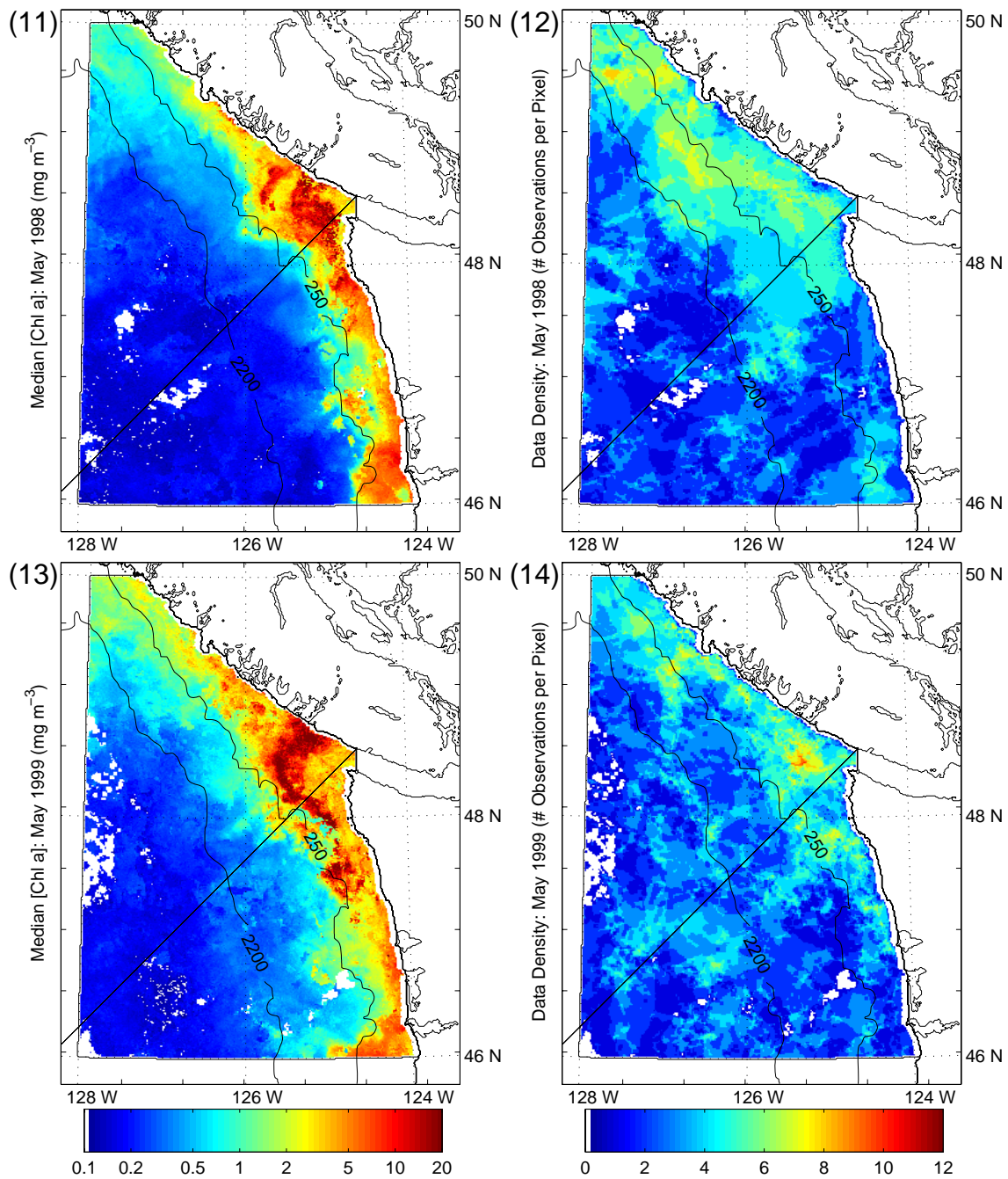


Figure A.1 cont.

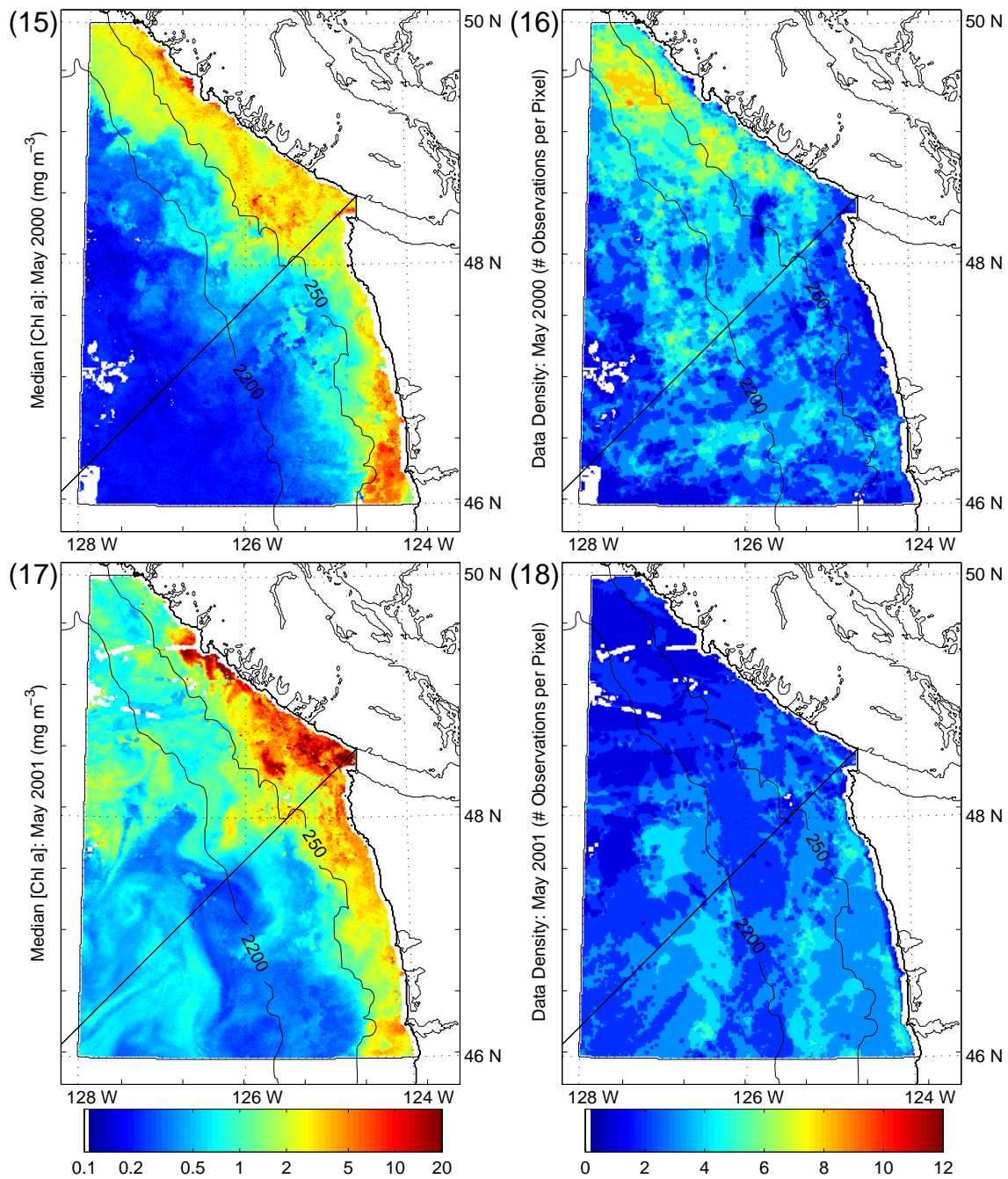


Figure A.1 cont.

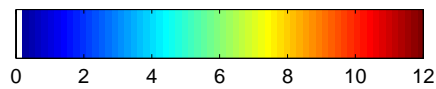
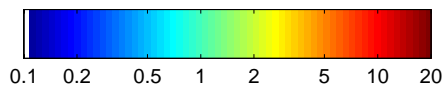
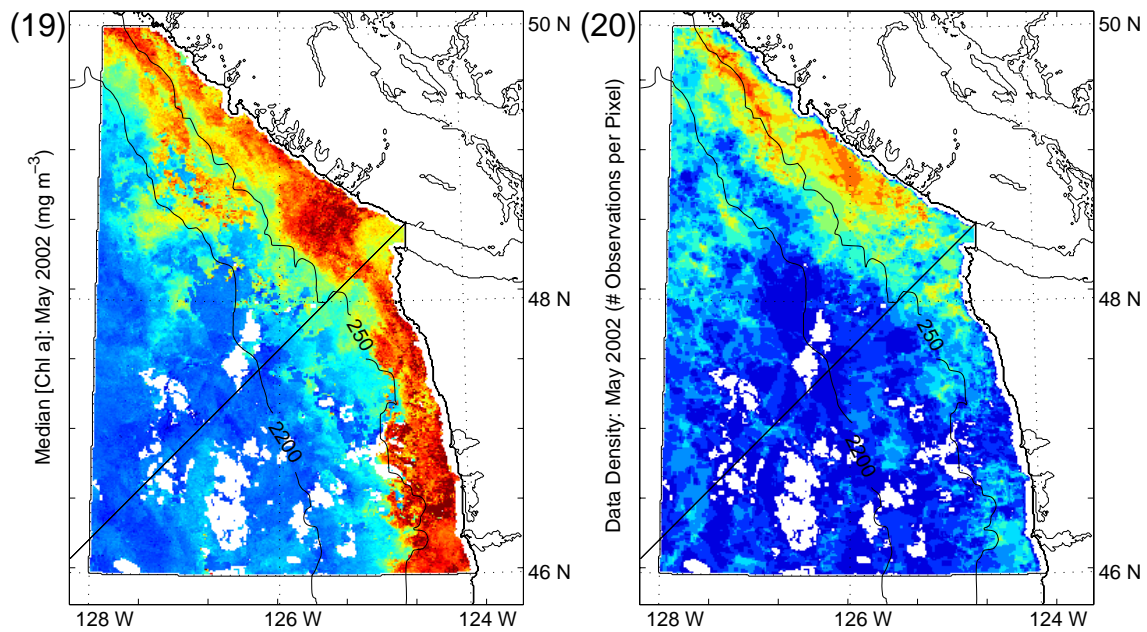


Figure A.1 cont.

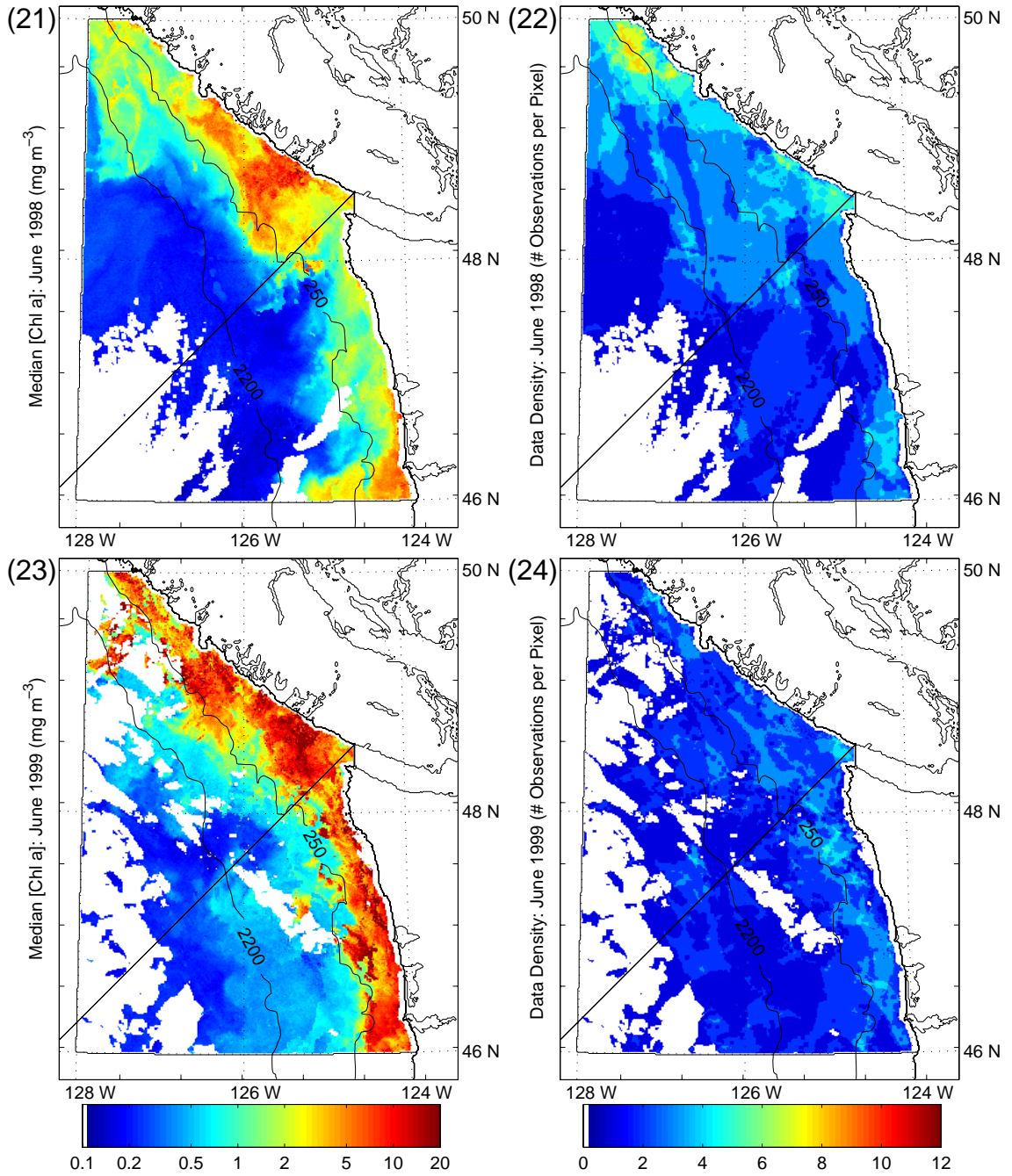


Figure A.1 cont.

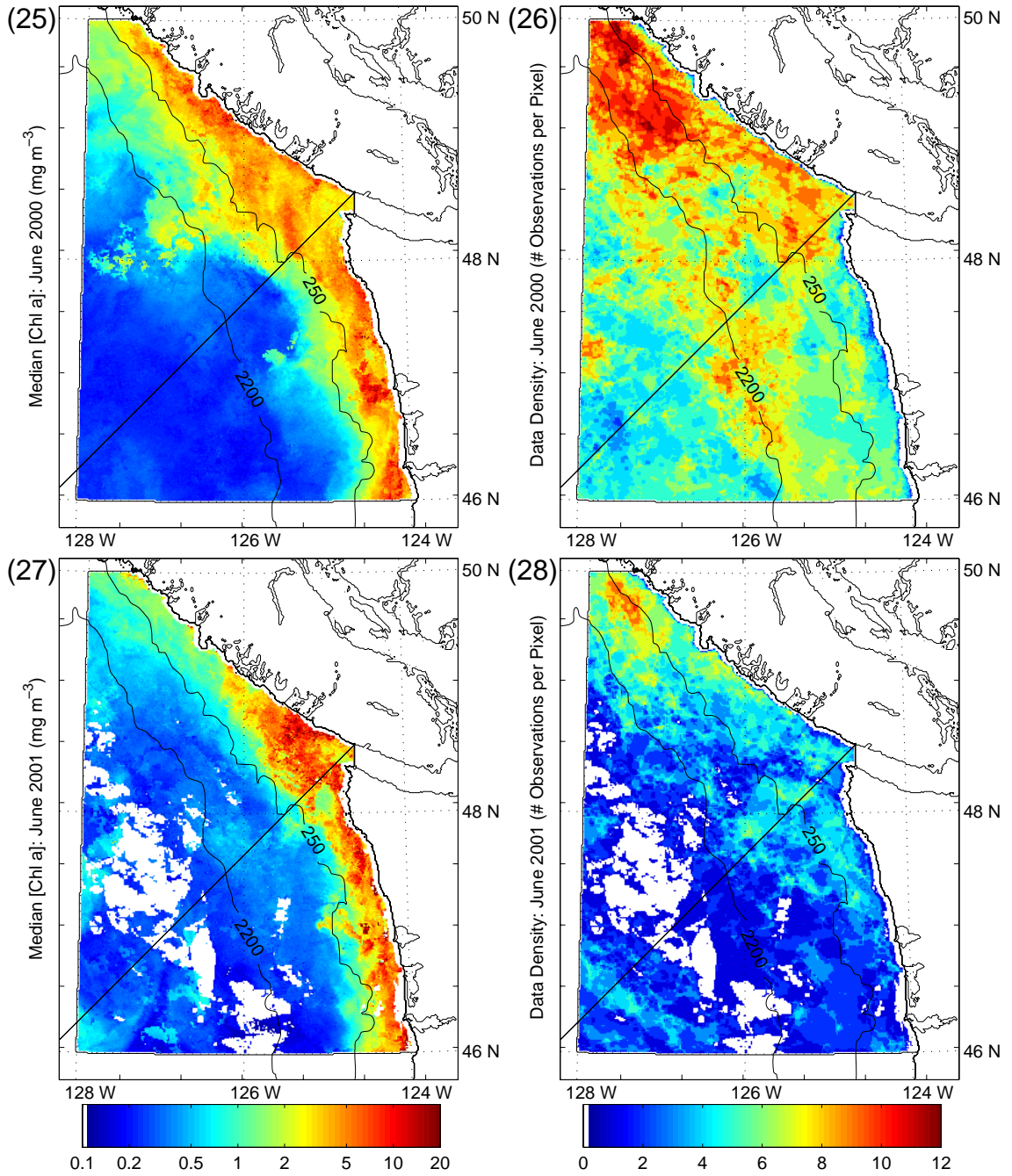


Figure A.1 cont.

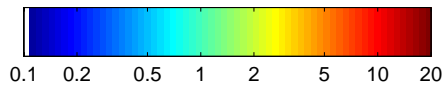
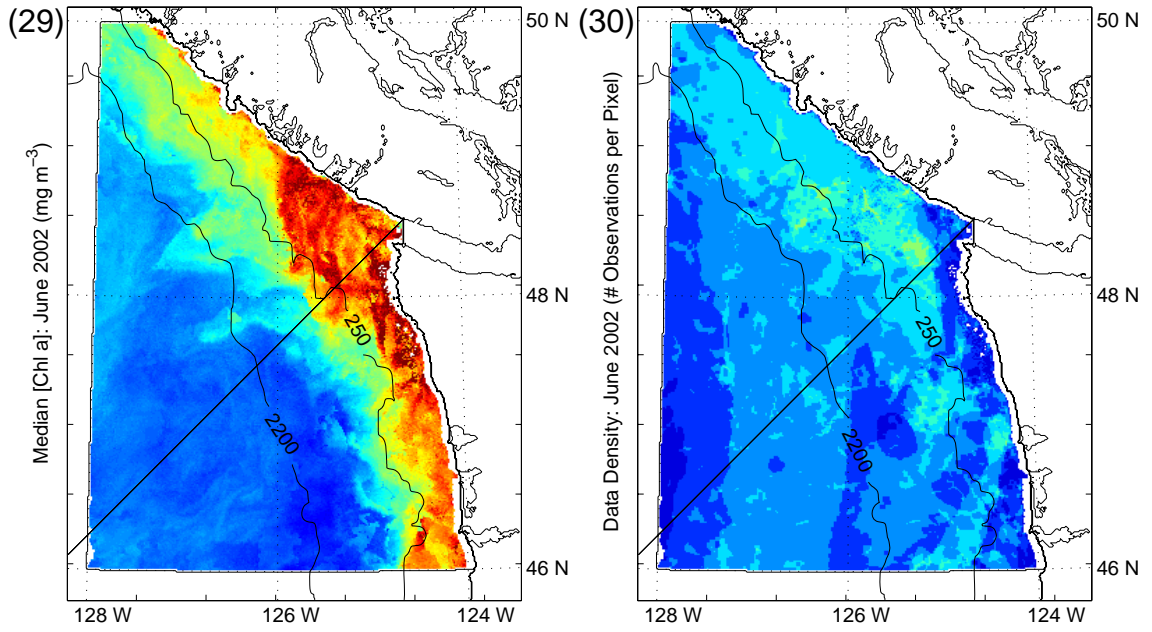


Figure A.1 cont.

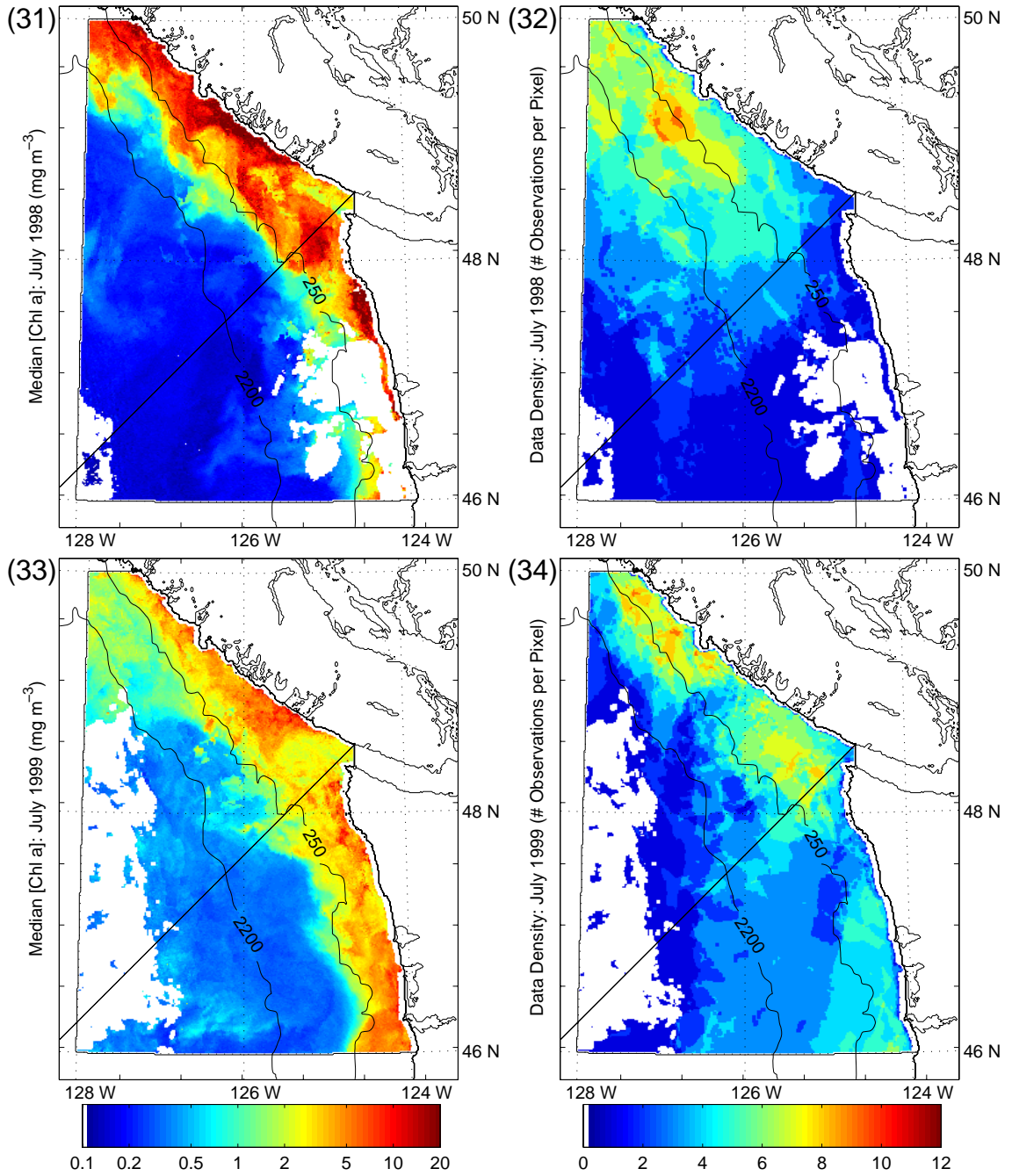


Figure A.1 cont.

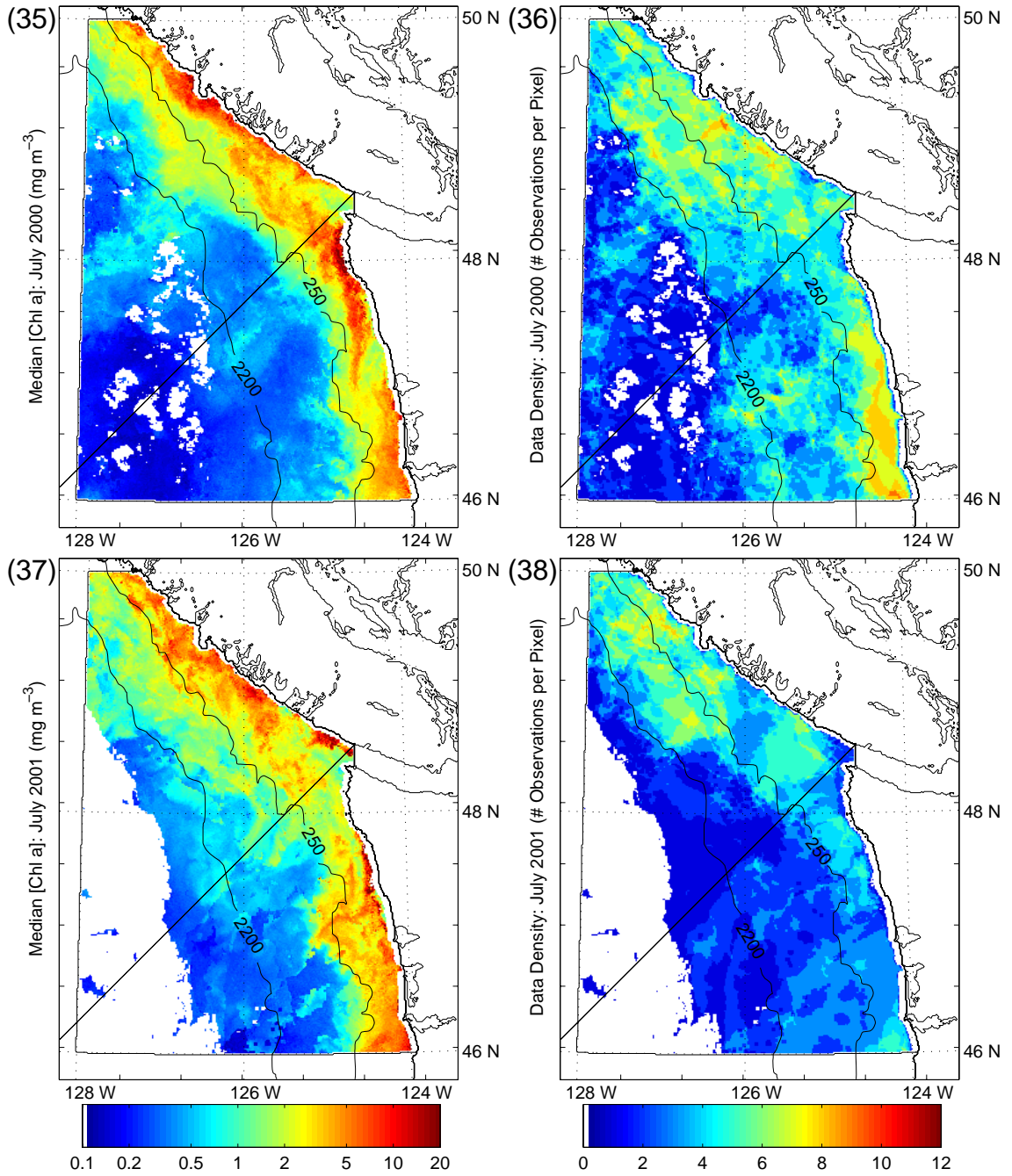


Figure A.1 cont.

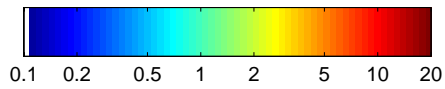
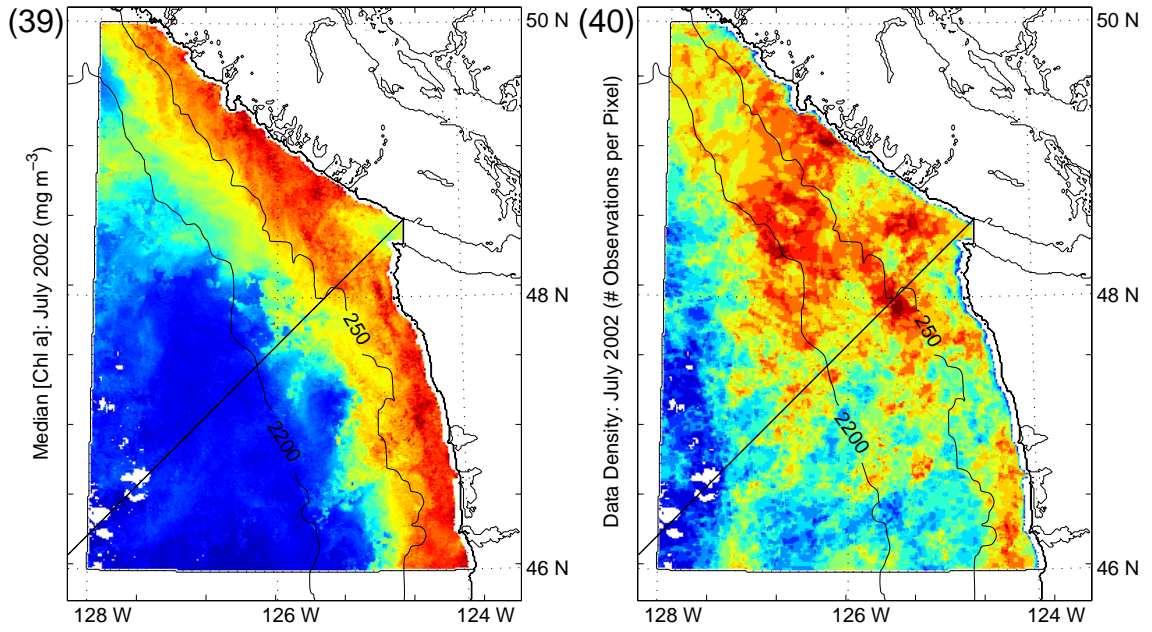


Figure A.1 cont.

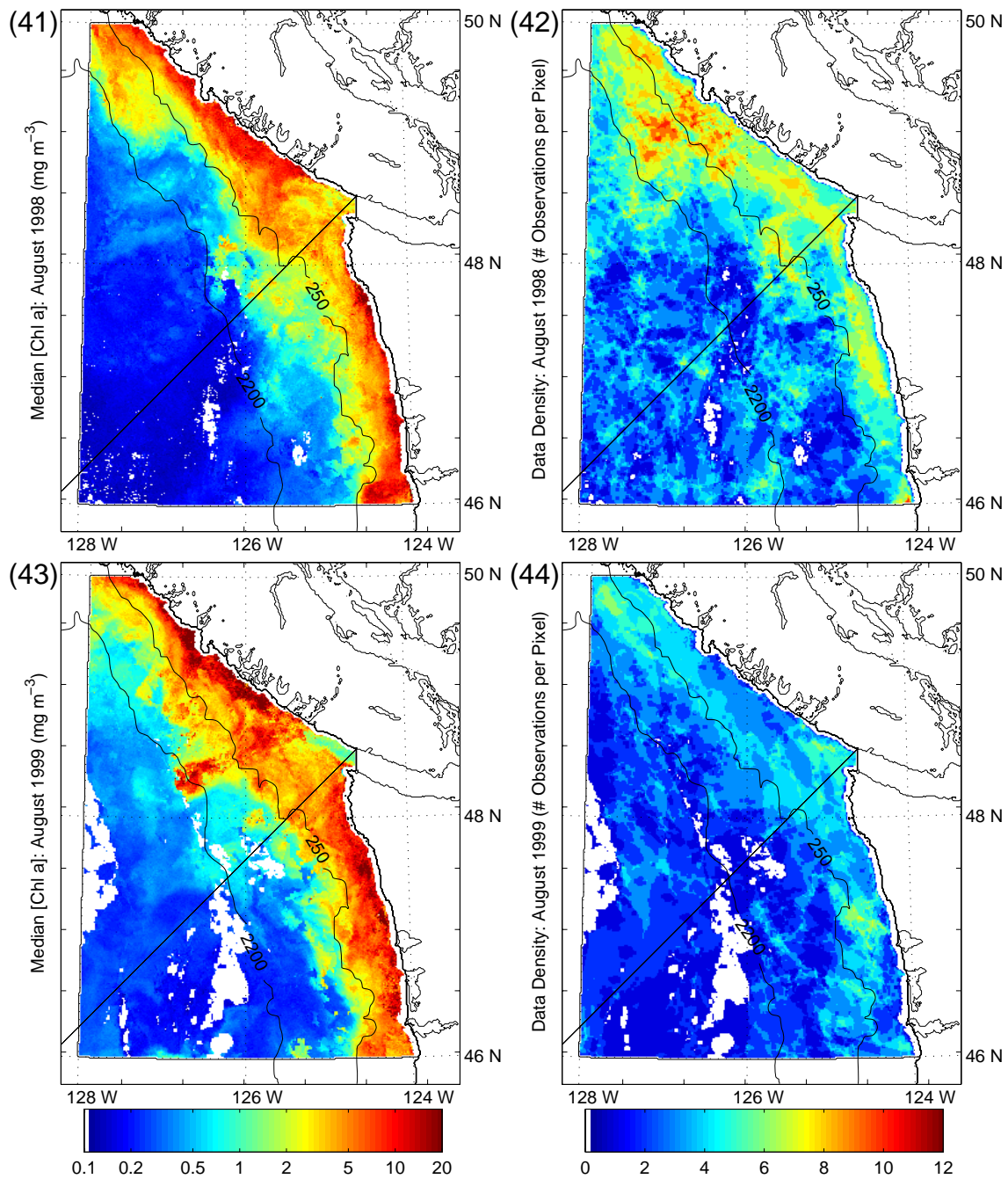


Figure A.1 cont.

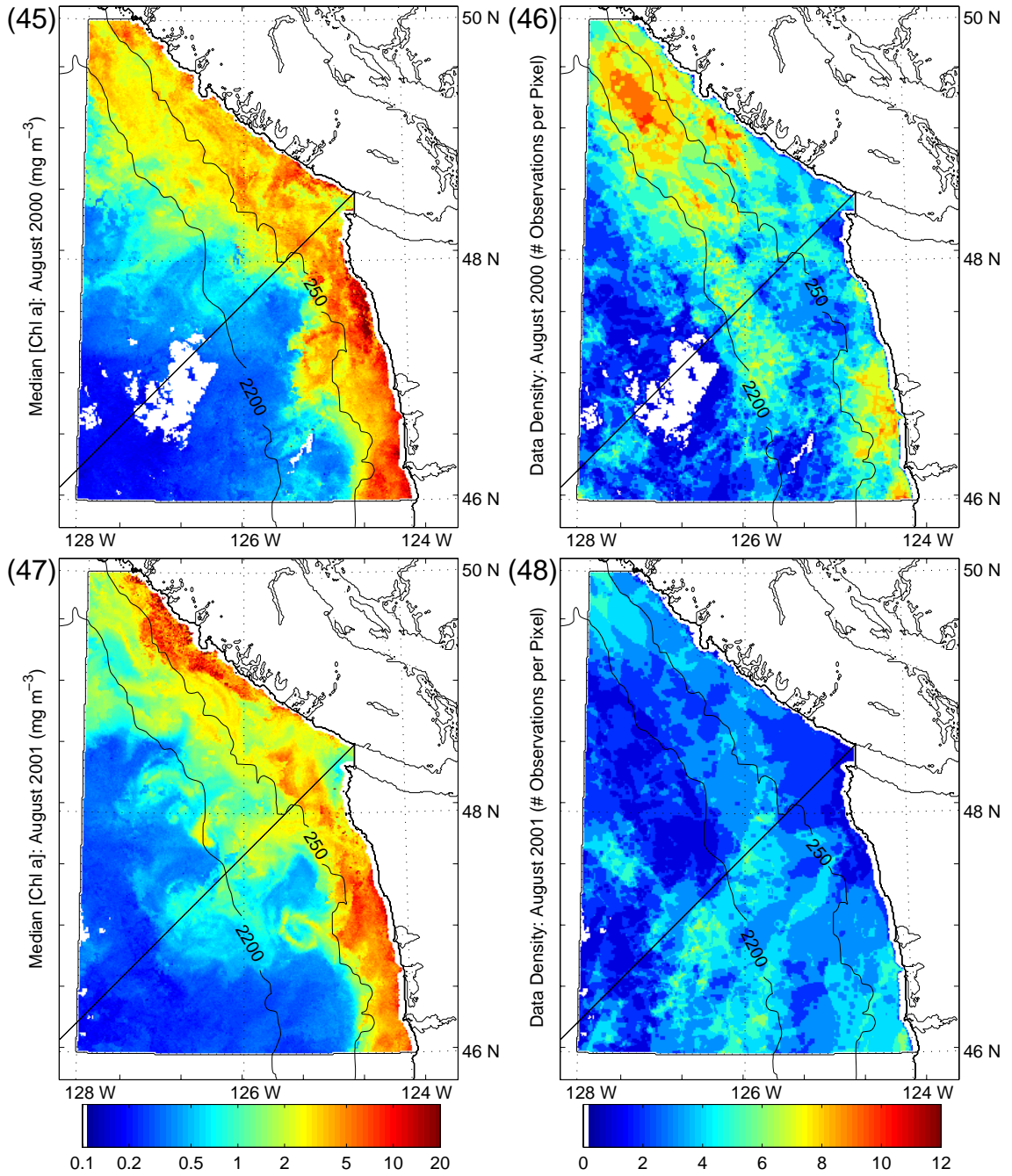


Figure A.1 cont.

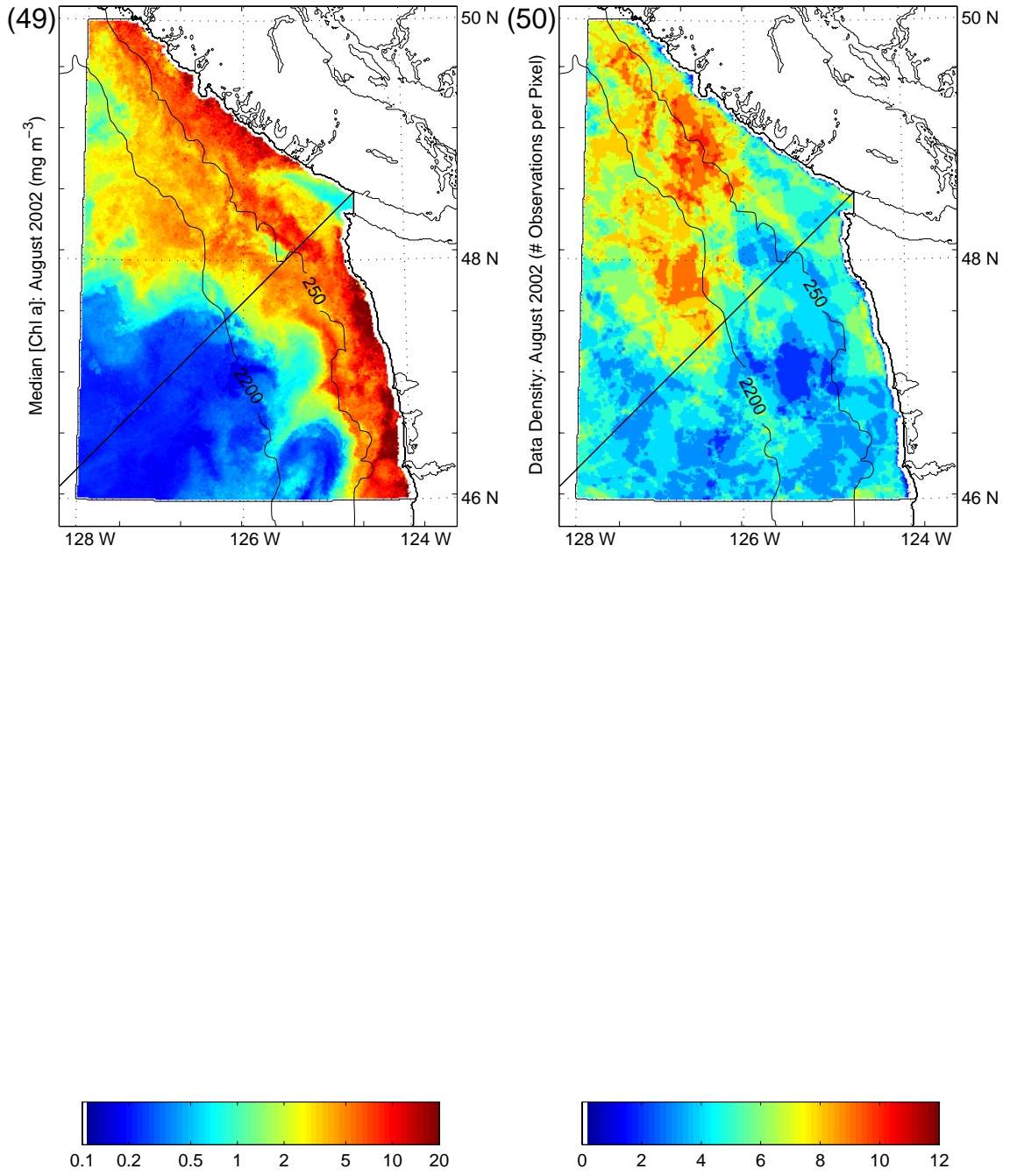


Figure A.1 cont.

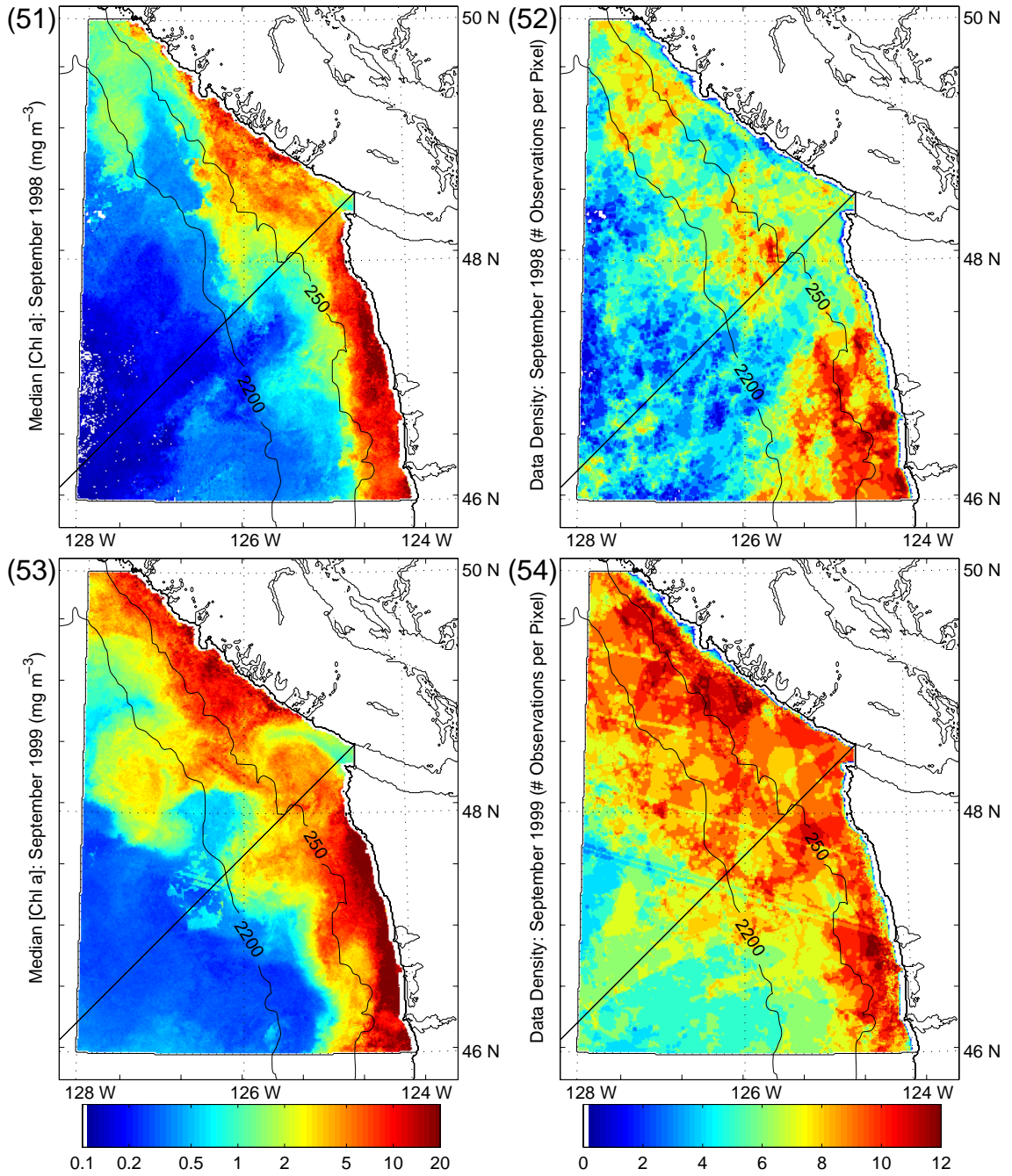


Figure A.1 cont.

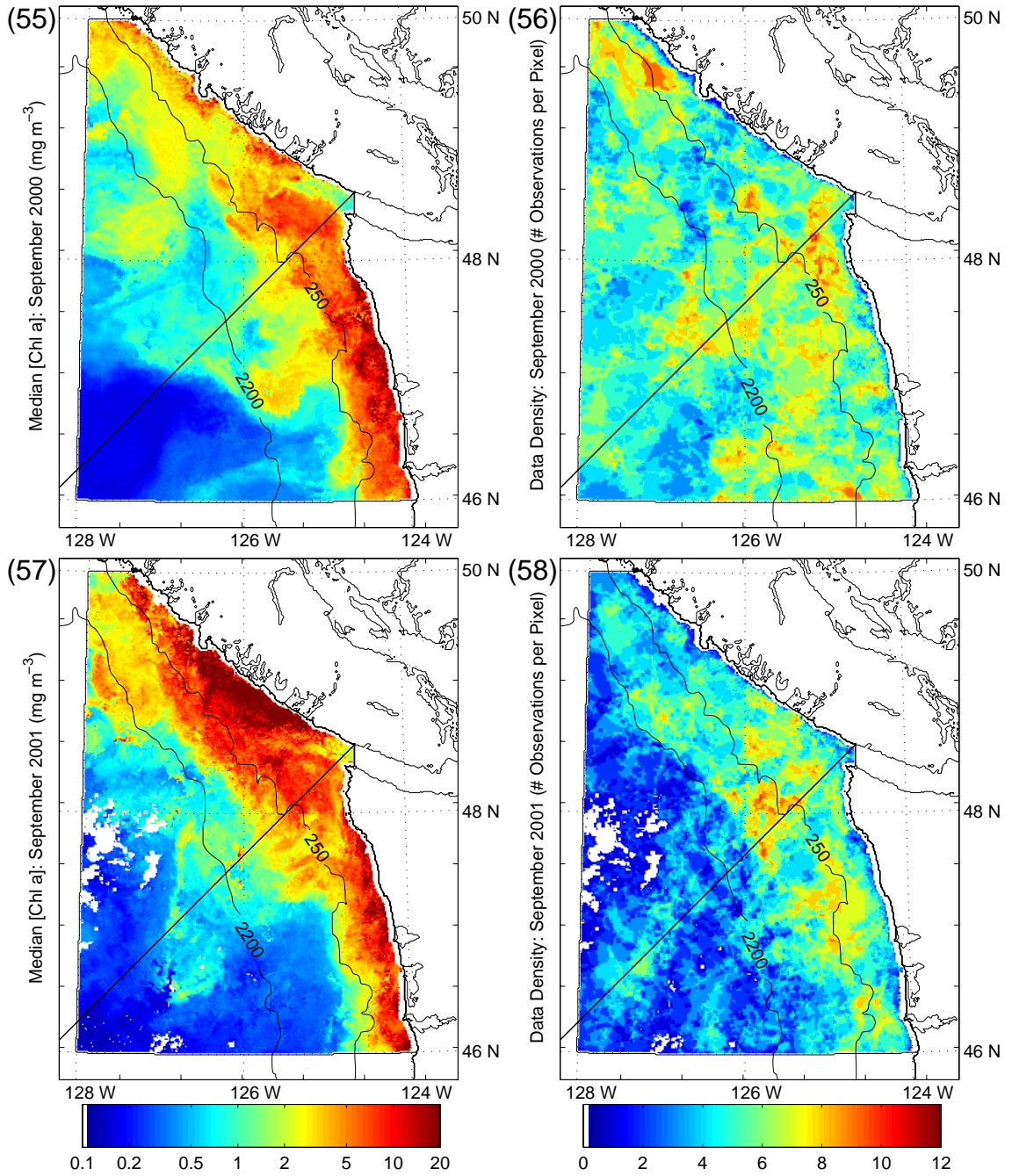


Figure A.1 cont.

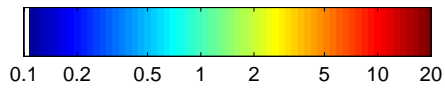
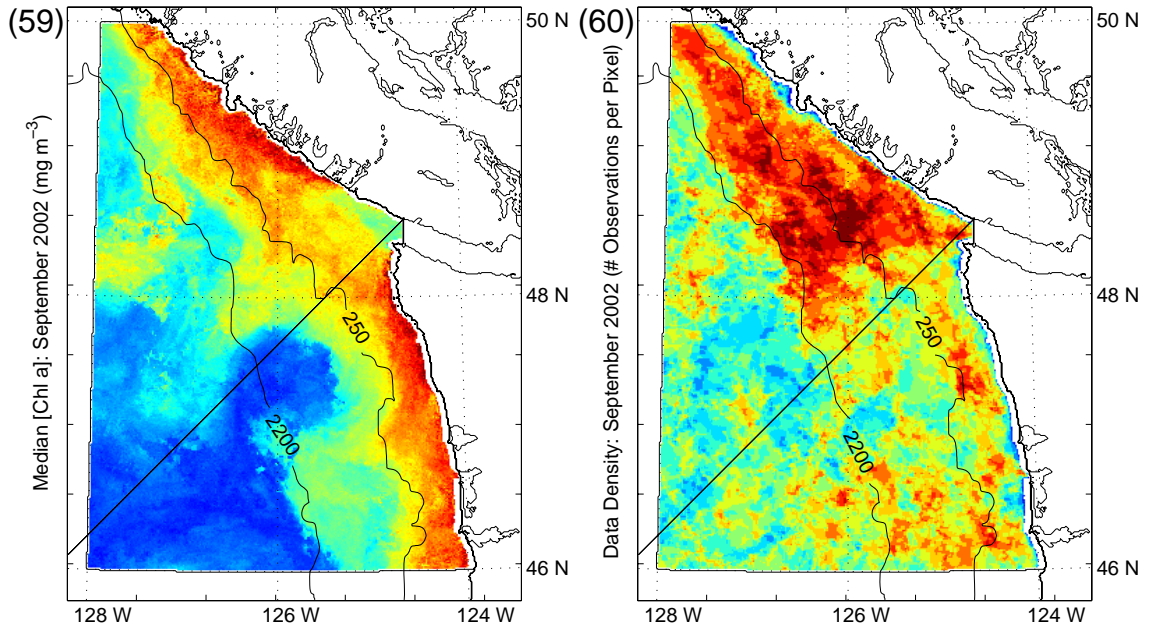


Figure A.1 cont.

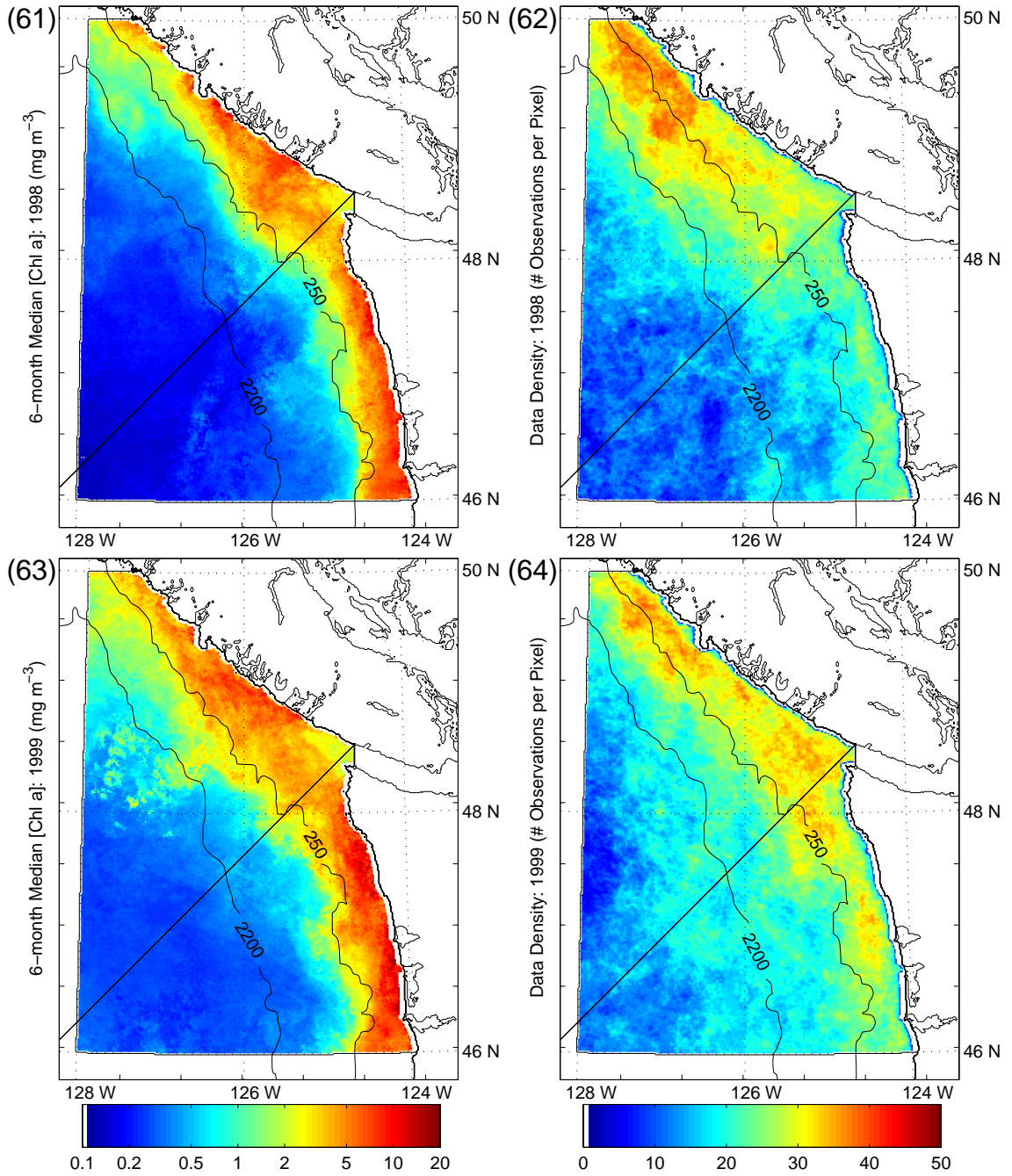


Figure A.1 cont.

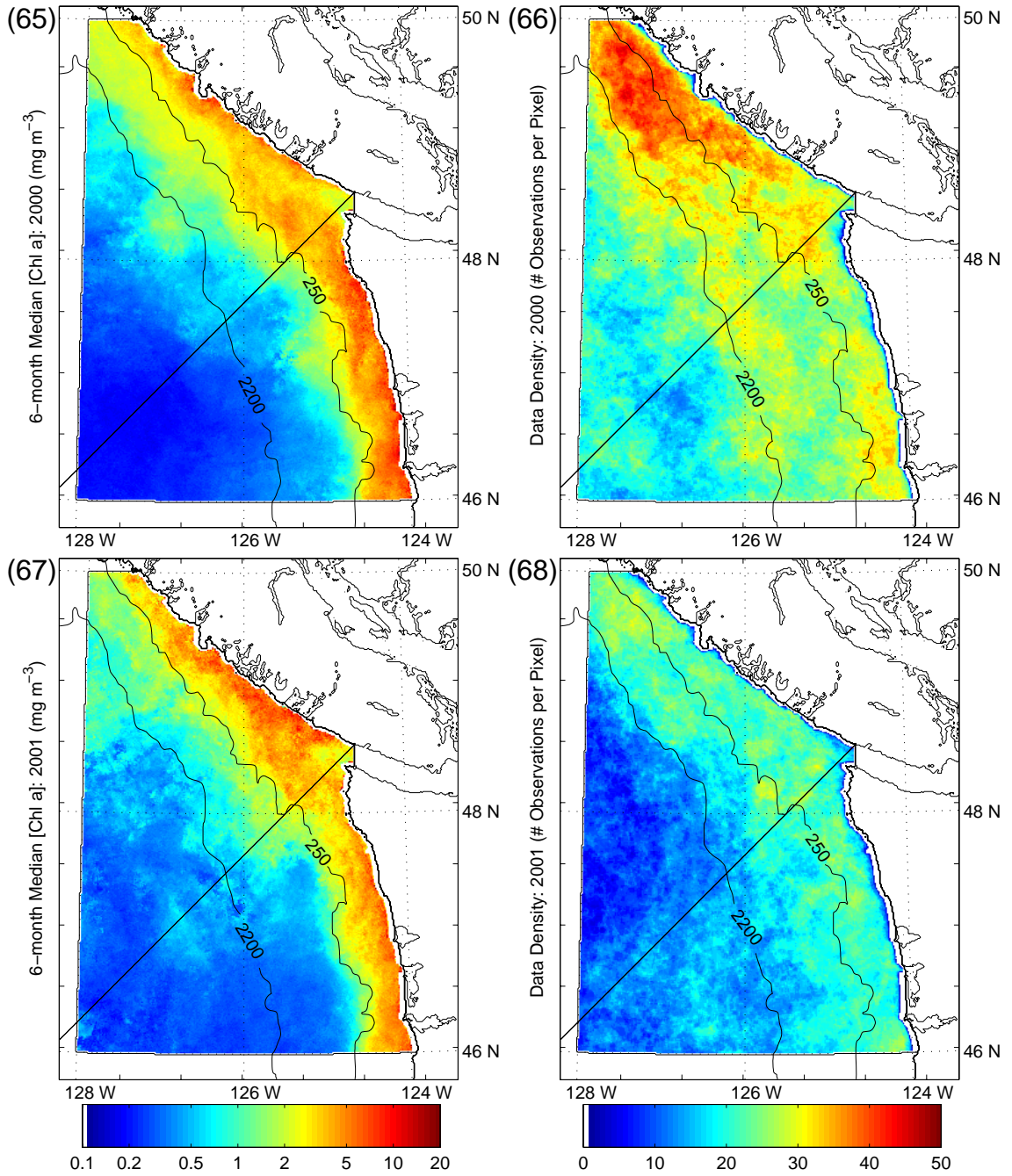


Figure A.1 cont.

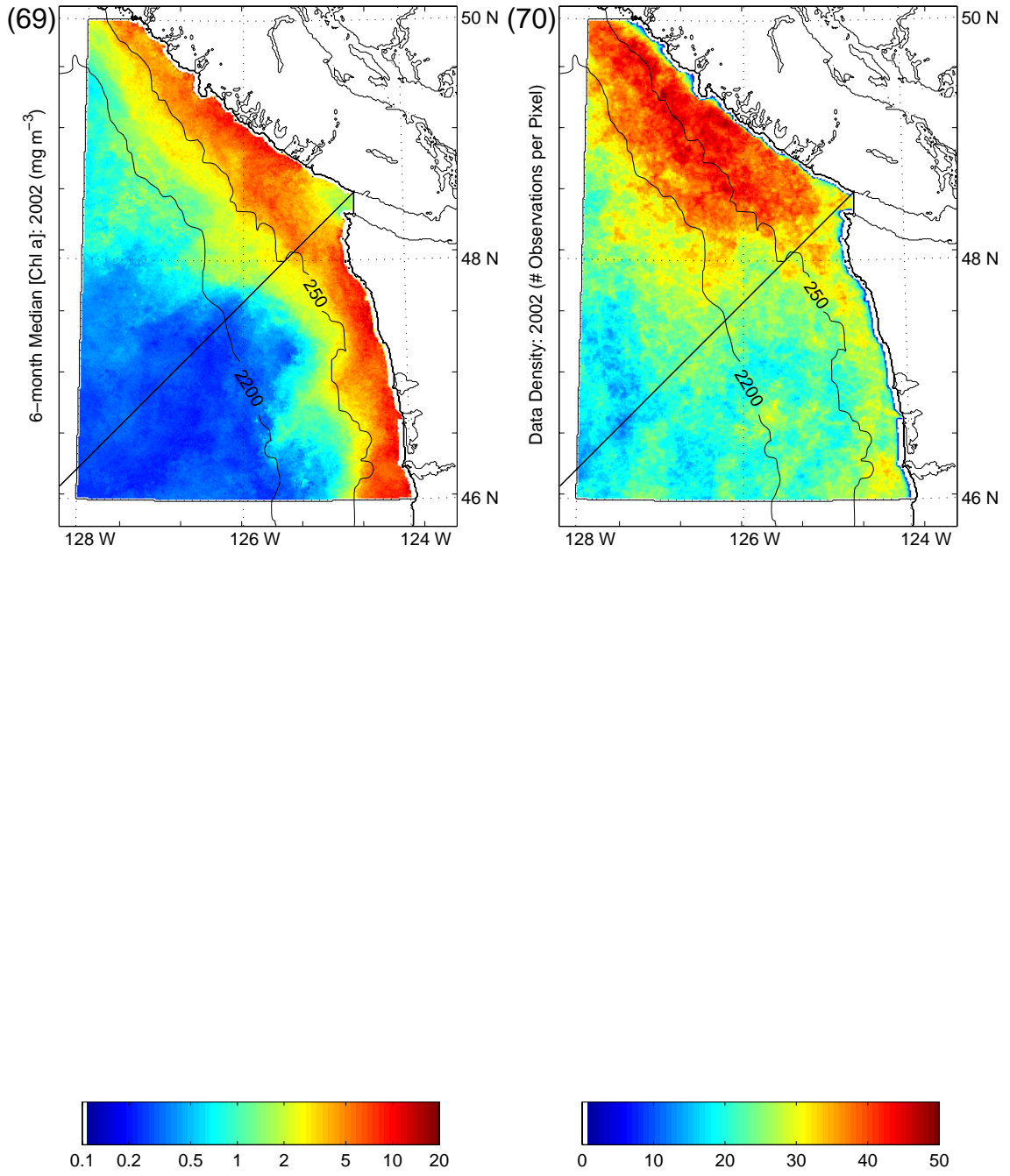


Figure A.1 cont.

Appendix B. Statistical Model of Fluorescence Quenching

To quantify spatio-temporal patterns in mid-day fluorescence quenching a differential equation model, consistent with a basic physical understanding of quenching, was used. The model is patterned after one developed and applied to fluorescence data collected in Lake Michigan (Welty *et al.*, 2004). In the model (Equation B.1) the observed (i.e., quenched) fluorescence is a function of both position (\mathbf{x}) and time (t) and denoted as $f(\mathbf{x}, t)$. Unquenched fluorescence is simply a function of position and denoted as $f^0(\mathbf{x})$. Solar radiation at the sea surface is given iPAR and denoted as $s(\mathbf{x}, t)$. The rate of fluorescence decrease is represented by $\alpha > 0$, and the rate of recovery by $\beta > 0$.

$$\frac{df(\mathbf{x}, t)}{dt} = -\alpha f(\mathbf{x}, t)s(\mathbf{x}, t) + \beta[f^0(\mathbf{x}) - f(\mathbf{x}, t)]. \quad \text{Equation B.1}$$

The model implies that the rate of quenching will be proportional to solar radiation. Fluorescence will decrease quickly just after the onset of solar radiation when $f(\mathbf{x}, t) \approx f^0(\mathbf{x})$ and then slowly approach a local minima around mid-day as $f(\mathbf{x}, t) \rightarrow 0$. As solar radiation decreases in the afternoon fluorescence values recover quickly at first and then more slowly as $f(\mathbf{x}, t) \rightarrow f^0(\mathbf{x})$. Full recovery is often observed near sunset, however other factors such as nutrient limitation and photoinhibition due to increased light intensities throughout the day (e.g., during summer) can delay full recovery until much later (Falkowski, 1992).

Solving Equation B.1 and dividing by $f^0(\mathbf{x})$ yields our final quenching model (Equation B.2) which can be related to $F_D:F_N$ as calculated above.

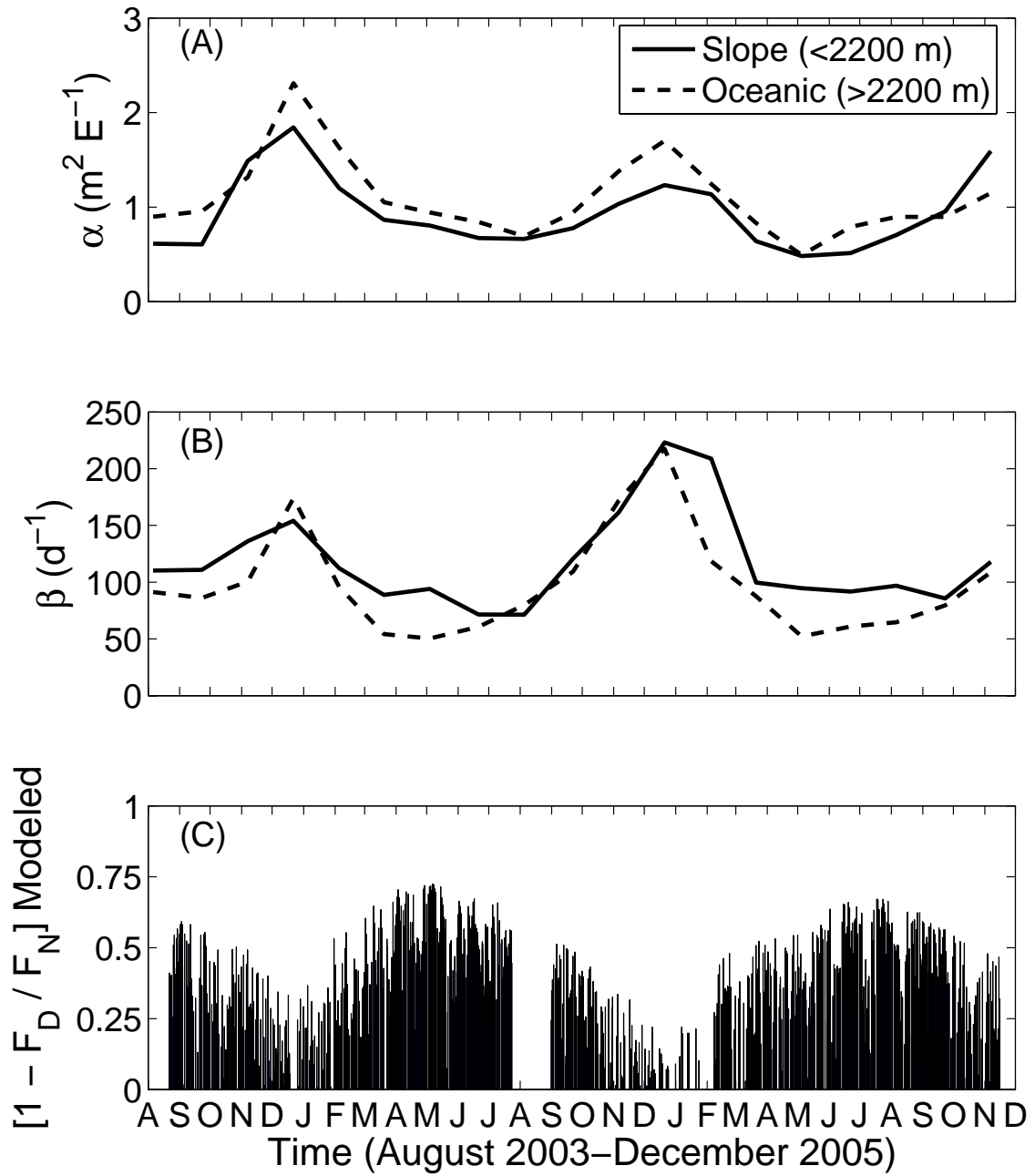
$$\frac{f(\mathbf{x}, t)}{f^0(\mathbf{x})} = e^{-\alpha S(\mathbf{x}, t) - \beta t} [1 + \beta \int_0^t e^{\alpha S(\mathbf{x}, u) + \beta u} du] \approx \frac{F_D}{F_N}. \quad \text{Equation B.2}$$

where $S(\mathbf{x}, u) = \int_0^u s(\mathbf{x}, v) dv$. Using estimates iPAR from SeaWiFS and $F_D:F_N$ from

Seaglider a non-linear, least-squares minimization technique (unconstrained Nelder-Mead method) was used to solve Equation B.2 and obtain estimates for α and β (Fig. B.1).

To explore patterns of variability in the estimates of α and β data were binned in both space and time. The area of interest was divided into two spatial subregions, ‘Slope’ and ‘Oceanic’, using the 2200 m isobath to separate the two regions (Sackmann *et al.*, 2004). Temporally the data were binned using half-overlapping 90-day bins. When constructing model estimates of $1-F_D:F_N$ only the nearest estimates of α and β were used (Fig. B.1C, B.2). Correlations between modeled and observed values of $1-F_D:F_N$ were used to assess overall model performance and the strength and statistical significance (* $p < 0.05$) of a linear relationship between the datasets (Fig. B.2). To compare model results from different locations observed combinations of α and β were used to simulate $1-F_D:F_N$ for a hypothetical 12-hr day with daily-PAR = 30 mol/m²/day (Fig. B.3).

Figure B.1 **Model estimates of $1-F_D:F_N$.** Rates of fluorescence quenching (α) and recovery (β) calculated from subsets of the Seaglider dataset binned in space and time from August 2003 – December 2005 (A-B). The 2200 m isobath was used to divide the region into ‘Slope’ and ‘Oceanic’ subregions. Temporally, data were binned using half-overlapping 90-day bins. When constructing model estimates of $1-F_D:F_N$ only the nearest estimates of α and β were used (C).



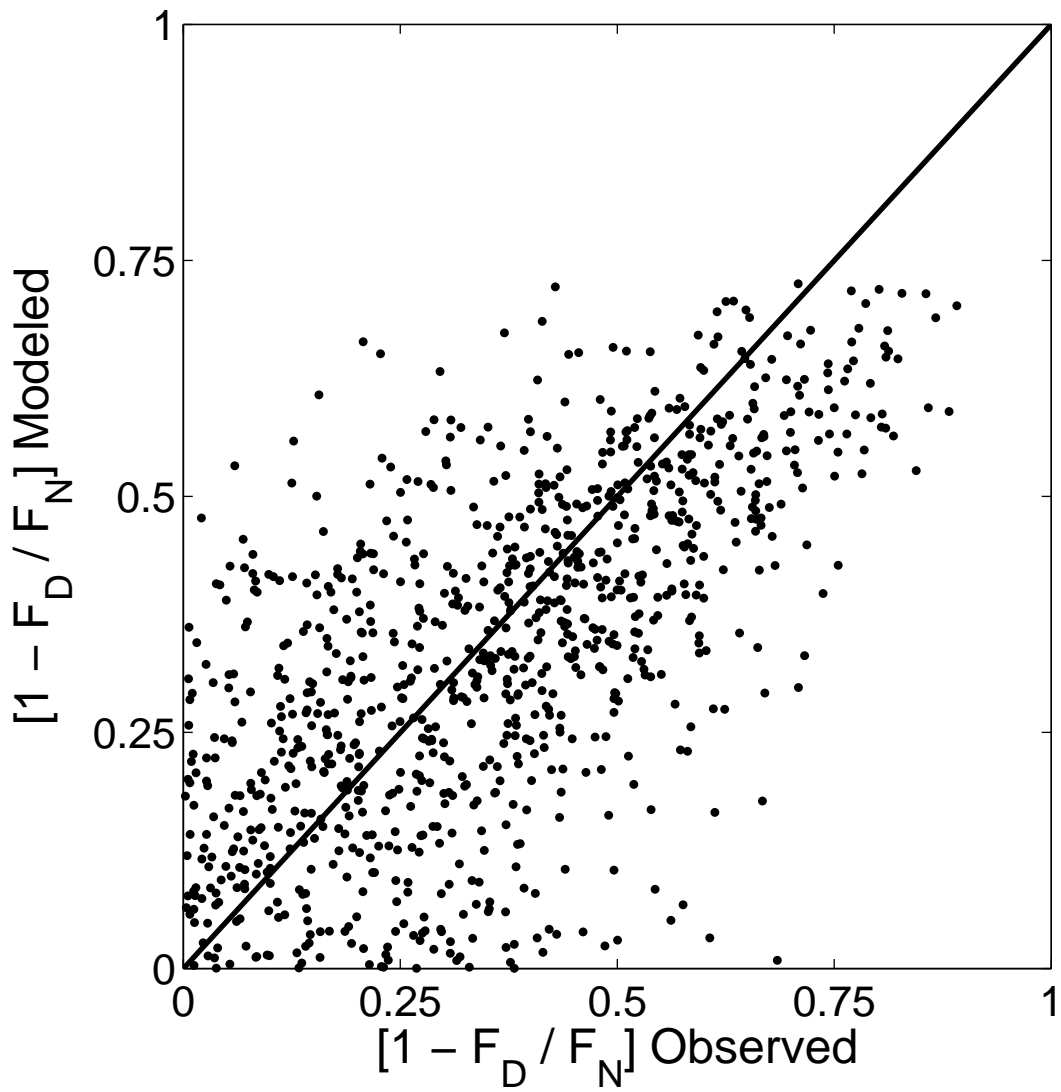


Figure B.2 **Modeled versus observed estimates of $1-F_D:F_N$.** Heavy solid line represents the 1:1 line. The model explained 41% of the variance in the dataset ($r = 0.64^*$) and achieved a median absolute deviation (MAD) between observed and modeled values of $1-F_D:F_N$ of 0.11.

A final predictive model for fluorescence quenching off the Washington coast (without sub-region or temporal specificity) was developed by first deriving estimates for α and β using half of the dataset chosen at random. These values of α and β were then used to predict $1-F_D:F_N$ for the second half of the dataset previously set aside. This model was chosen for its simplicity and to determine to what extent mid-day quenching is affected only by changes in iPAR and was not designed to be a full characterization of all processes known to influence mid-day fluorescence quenching.

Statistical Model Results and Interpretation

Fitting observed values of $1-F_D:F_N$ using a simple 2-parameter differential equation model which used iPAR as input allowed us to quantitatively assess spatial and temporal changes in mid-day fluorescence quenching and to determine how much of the variability in $1-F_D:F_N$ could be ascribed to changes in iPAR and how much remained unexplained. The two fitting parameters $\alpha > 0$ and $\beta > 0$ used in the model represent the rates of quenching and recovery, respectively. In general α and β covaried as a function of time with higher values observed during winter months. In ‘Oceanic’ waters α tended to be higher, and β somewhat lower, when compared to ‘Slope’ waters. This confirmed initial observations that suggested that the effects of mid-day quenching were proportionally more pronounced in ‘Oceanic’ waters; likely the result of higher subsurface irradiances and/or increased nutrient stress for phytoplankton in this more oligotrophic environment (Fig. B.1A-B).

Using this model, and fitting only small subsets of the data at any one time (effectively allowing α and β to vary regionally and with time), we were able to explain

41% of the variance in our dataset ($r = 0.64^*$) and achieve a median absolute deviation (MAD) between observed and modeled values of $1-F_D:F_N$ of 0.11 (Figs. B.1C, B.2). To determine whether a more general predictive model could be developed for the entire dataset (i.e., with a single value for α and β) we determined estimates of α and β using half of the dataset (chosen at random) and then used these estimates to predict $1-F_D:F_N$ for the second half of the dataset (previously set aside). With $\alpha = 0.8543 \text{ m}^{-2} \text{ E}^{-1}$ and $\beta = 68.4643 \text{ d}^{-1}$ this more general model explained 37% ($r = 0.61^*$) of the total variance and the MAD increased to only 0.12. The implications for the various combinations α and β were assessed by modeling $1-F_D:F_N$ for a hypothetical 12-hr day with daily-PAR = 30 mol/m²/day. As noted above, mid-day quenching was more pronounced and recovery was more delayed in ‘Oceanic’ waters, as compared to what was observed in ‘Slope’ waters (Fig. B.3).

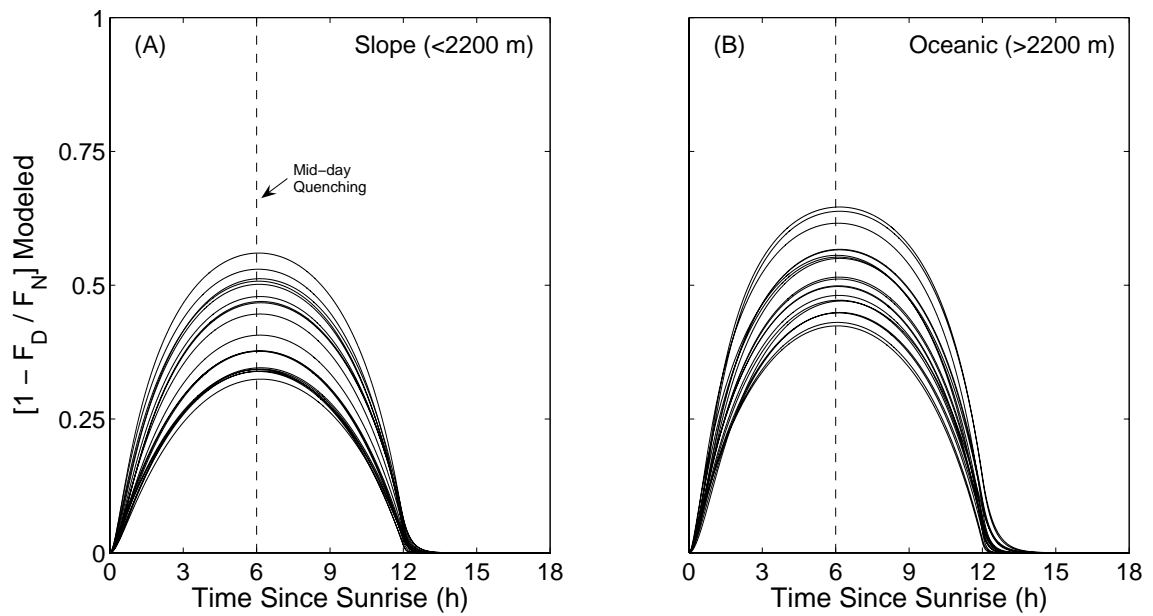


Figure B.3 **Model estimates of $1-F_D:F_N$ for a hypothetical 12-hr day.** Model estimates of $1-F_D:F_N$ for a hypothetical 12-hr day with daily-PAR = 30 mol/m²/day derived using observed combinations of α and β for ‘Slope’ (A) and ‘Oceanic’ (B) subregions.

BIOGRAPHY OF THE AUTHOR

Brandon Steven Sackmann was born in Othello, Washington on April 11, 1978. After growing up in rural eastern Washington, surrounded by sagebrush and desert, he graduated as valedictorian from Othello High School in 1996. Since he was a young boy Brandon's parents have kept a boat in western Washington or lower British Columbia, Canada, which may have indirectly fostered his desire to pursue ocean studies. Despite the three to six hour drive that preceded each vacation he always looked forward to spending time on the water.

Brandon was admitted to the University of Washington in the fall of 1996. As an elective he chose to take a course in Physical Oceanography. Despite its challenges (or perhaps because of them), the course succeeded in sparking his interest and he found himself registering for more and more Oceanography 'electives' until he ultimately declared Oceanography as his major.

As a college sophomore he was given the opportunity to work in the lab of Dr. Mary Jane Perry, a bio-optical oceanographer then at the University of Washington. He was able to apprentice under a Masters student, Ms. Lisa Mack, who was working with daily 1-km ocean color satellite data from the Sea-viewing Wide Field-of-view Sensor (SeaWiFS) for the Washington coast. Dr. Perry's early support of Brandon's work gave him the confidence necessary to consider graduate studies in Oceanography.

While attending the University of Washington Brandon's interests were not entirely academic. This is also where he met and married his wife Katherine. Brandon

graduated from the University of Washington with a B.S. in Oceanography and a minor in Applied Mathematics in 2001.

Brandon chose to pursue a Ph.D. in Oceanography at the University of Maine under the continued mentorship of Dr. Perry, who moved to Maine in 2000. While at the University of Maine he helped develop methods to combine in-water measurements from Seaglider, an autonomous underwater glider, with satellite ocean color measurements in order to create 4-dimensional representations of phytoplankton in the ocean. Brandon obtained graduate certification in Geographic Information Systems and was awarded fellowships from the National Science Foundation and the University of Maine which helped to fund his studies.

While in Maine, Brandon and Katherine also took the opportunity to start a family. They now have two boys, Aidan (born on March 31, 2003) and Ian (born on March 19, 2006). Brandon and his family will be moving to California in February 2007 as Brandon has accepted a Postdoctoral position at the Monterey Bay Aquarium Research Institute where he will be working with Dr. John Ryan and Dr. Zbigniew Kolber. Brandon is a candidate for the Doctor of Philosophy degree in Oceanography from the University of Maine in May 2007.